THE INFLUENCE OF LOCAL SEA ICE AND REMOTE NORTHERN HEMISPHERE TELECONNECTIONS ON CYCLONES IN BAFFIN BAY, DAVIS STRAIT, AND LABRADOR SEA

A Thesis

by

BRADLEY ALLEN BARGER

Submitted to the Office of Graduate and Professional Studies of
Texas A&M University
in partial fulfillment of the requirements for the degree of

MASTER OF SCIENCE

Chair of Committee,	Oliver Frauenfeld
Committee Members,	Andrew Klein
	Andrew Dessler
Head of Department,	David Cairns

May 2020

Major Subject: Geography

ABSTRACT

Cyclones are a primary mode of energy transport between the midlatitudes and the polar region in the Northern Hemisphere (NH). Due to the North Atlantic experiencing some of the highest frequencies of cyclones, this region has been extensively researched. However, Baffin Bay (BB), Davis Strait (DS), and Labrador Sea (LS) are also part of the North Atlantic, yet limited literature exists regarding cyclones and the influences of local and remote drivers on their variability in these subregions. This thesis focuses on determining the influence of local sea ice cover and remote NH teleconnections on cyclone variability in BB, DS, and LS from 1980-2015.

To represent the local sea ice area driver, the NH's monthly sea ice cover was subsetted for each subregion. To establish the remote atmospheric driver, the North Atlantic Oscillation (NAO), Arctic Oscillation (AO), Pacific Decadal Oscillation, Pacific North American Pattern, Polar Eurasian Pattern, and East Atlantic/West Russia Pattern's monthly indices were obtained for 1980-2015. Cyclone variability was represented with the annual count, central pressure, cyclogenesis and cyclolysis events, local laplacian, latitude, and longitude from NSIDC's NH Cyclone Locations and Characteristics record. Local drivers, remote drivers, and cyclone variables were analyzed using linear least-squares regression trends, compared using correlations (95% confidence interval), and all were seasonally standardized and detrended before each cyclone variable was compared with each local and remote driver at the long-term and individual monthly timescales.

Results indicate that sea ice area in BB, DS, and LS decreased significantly, but at lower rates than the NH. Furthermore, each subregion's sea ice variability is unique from the NH's and from the other subregions, however periods of similar sea ice area deviation occurs across all

subregions. The overall study area's (BB-DS-LS) total number of cyclogenesis events had the only significant trend (positive) out of all cyclone variables. Comparing subregions, cyclone variability was noticeably different (especially between BB and LS). At the long-term and individual monthly timescales, local drivers had the most significant correlations mainly with the longitudinal position and cyclolysis stage of cyclones while the remote drivers had the most with their central pressures in all subregions. Overall, the NAO and AO had the most frequent and strongest correlations. While local sea ice area was significantly related with certain cyclone variables, these associations were typically weaker and less frequent. Therefore, overall cyclone variability in BB, DS, and LS is influenced more by remote atmospheric forcing than by local sea ice cover. Comparing BB, DS, and LS, it appears that, although they are geographically connected, each experiences unique cyclone variability. Finally, because each subregion's cyclone variability is significantly related with local sea ice cover and remote teleconnections at different magnitudes and times, these subregions should be considered independently from one another and from the North Atlantic, to better capture atmospheric variability and interactions with the local environment.

CONTRIBUTORS AND FUNDING SOURCES

Contributors

This work was supervised by a thesis committee consisting of Professor Oliver Frauenfeld (advisor) and Professor Andrew Klein of the Department of Geography and Professor Andrew Dessler of the Department of Atmospheric Sciences.

All work conducted for the thesis was completed by the student independently.

Funding Sources

Graduate study was supported by an assistantship from Texas A&M University and scholarships from the M.T. Halbouty ‘30/AAPG and APSG Foundations through the College of Geosciences.

ACKNOWLEDGEMENTS

I would like to thank my committee chair, Dr. Oliver Frauenfeld, for his guidance on developing the methodology and his support over the course of this research. Additionally, I thank my committee members, Dr. Klein and Dr. Dessler for taking the time to review this thesis. Furthermore, I extent my gratitude to the Office of Graduate and Professional Studies for their contributions in reviewing the final version of this thesis.

An extended thanks goes out to my fellow classmates and professors, who have made my time at Texas A&M University an unforgettable experience. I also extend my gratitude to the Climate Science Lab research group for their assistance in preparing for my defense and past presentations related to this thesis.

Most of all, I would like to thank my girlfriend Kate and my family for their never-ending love, encouragement, and support throughout my time at Texas A&M University.

TABLE OF CONTENTS

Page

LIST OF FIGURES

Page

Page

LIST OF TABLES

1. INTRODUCTION AND LITERATURE REVIEW

1.1: Introduction

Atmospheric cyclones are a primary mode of energy transport between the midlatitudes and the Arctic (Overland et al. 1996; Porter et al. 2010; Fan et al. 2015). Influenced by Earth's atmospheric and oceanic flow regimes, long-term trends of atmospheric cyclones have been used to monitor and identify monthly, yearly, and decadal shifts in climate across North America, Eurasia, the Pacific and Atlantic Oceans, and the Arctic (e.g., Keegan, 1958; Gyakum et al. 1989; Chen et al. 1992; Hanson et al. 2004; Simmonds et al. 2008). Trends in cyclone variability have been of general interest in climate research for the last three decades (e.g., Bosart, 1981; Grønas, 1995; Kristjánsson and Thorsteinsson, 1995; Serreze et al. 1997; Tsukernik et al. 2007; Serreze and Barry, 2014). The focus on atmospheric cyclones has also included their effect on the cryosphere, due to the growing concern of declining sea ice coverage, changes in the thermohaline circulation, and influences of teleconnection patterns like the El Niño Southern Oscillation (ENSO) and the North Atlantic Oscillation (NAO) (e.g., Namias, 1958; Overland and Pease, 1982; Serreze et al. 1997).

In the Northern Hemisphere (NH), the highest number of cyclones occurs over different regions due to shifts in temperature, pressure, and moisture gradients in the troposphere. Over the Atlantic, the highest frequency occurs in winter, offshore along the East Coast of the North American continent, then tracking eastward usually remaining south of Greenland, then veering north, east of Greenland towards Svalbard. Due to the high frequency of cyclones and baroclinicity associated with this region, it has been referred to as the "North Atlantic storm track" (e.g., Tsukernik et al. 2007; Brayshaw et al. 2009; Serreze and Barry, 2014). Cyclones enter the North Atlantic either from the North American continent (Roebber, 1984; Sanders,

1986) or from the lower latitudes of the Atlantic (Sanders, 1986; Hart and Evans, 2001; Jones et al. 2003). In the Arctic, the distribution of cyclones is influenced by factors including land/ocean mass relationships, topography, sea ice extent/concentration, surface temperature gradients, and the position and orientation of baroclinic zones (Tsukernik et al. 2007; Simmonds et al. 2008).

Cyclones vary in size, strength, and duration depending on the location, central pressure, and time of year (Serreze and Barry, 2014). Depending on atmospheric conditions, cyclones can persist between a few hours to over a week (Rasmussen and Turner, 2003; Mallet et al. 2013; Serreze and Barry, 2014).When formed in the midlatitudes, they are typically classified as extratropical cyclones, characterized with a unique comma appearance when fully developed (Raible et al. 2008; Catto, 2016; Kar-Man Chang, 2018). Cyclones that form in the high-latitudes (north of 60° N) are referred to as polar lows, which can take on the appearance of either extratropical cyclones (comma shape) or tropical cyclones (cloud-free eye) depending on the magnitude of baroclinicity (Rasmussen, 1981; Forbes and Lottes, 1985; Reed and Duncan, 1987). Although these are the two main types of cyclones found in the North Atlantic, there are various approaches and levels of cyclone classification (Catto, 2016), however, all cyclones have the same life cycle.

In the North Atlantic, most cyclones begin their life spawning from baroclinic instability initiated mainly by large meridional temperature and wind gradients at the surface and upper-troposphere associated with two propagating Rossby waves at different altitudes (Catto, 2016). These gradients initiate a baroclinic environment promoting uplifting of air at the surface. If uplifting is maintained, pressure will continue to decrease at the surface and baroclinicity will continue, causing the system to develop (deepen) and maintain its structure. Cyclogenesis, the process of cyclone formation, must be initiated by a lifting mechanism (Petterssen and Smebye,

1971; Deveson et al. 2002; Gray and Dacre, 2006). Lifting mechanisms can vary depending on the location of cyclogenesis (Petterssen et al. 1955; Catto, 2016). The primary mechanisms for lifting are orographic uplifting from the terrain (Campins et al. 2000; Jung and Rhines, 2007; Romero, 2008), convection resulting from warmer (unstable) air at the surface rising (Businger, 1985; Serreze et al. 1997; Rasmussen and Turner, 2003), air mass collision along the frontal boundary where warmer, unstable air is uplifted by colder, stable air (Miller, 1946; Sawyer, 1950; Parker, 1998; Hewson and Titley, 2010), and convergence (Harrold and Browning, 1969; Wang and Rogers, 2001).

In the North Atlantic (especially during winter), large contrasts in ocean temperature and salinity as well as air temperature and humidity exist from large amounts of poleward energy transport occurring in this region (Overland and Turet, 1994; Overland et al. 1996; Serreze et al. 2007a). In the upper levels of the ocean, warm, saltier water from the lower latitudes is transported poleward via the Gulf Stream and North Atlantic Current (Mann, 1967; Shaffrey and Sutton, 2004). Once this warmer saline water approaches the North Atlantic it meets colder fresher waters from the Arctic, thus forming large horizontal thermal and thermohaline gradients (Belkin et al. 1998; Zweng and Münchow, 2006; Serreze and Barry, 2014). Due to the density of salt water being greater than fresh water, it descends and becomes North Atlantic deep water mainly between Greenland and Norway (Lazier, 1994; Belkin et al. 1998). Additionally, the atmosphere transports warm moist air poleward through wind patterns comprised within the global circulation (e.g., jet streams, fronts, and air masses; Palmén, 1951; Defant and Taba, 1957; Palmén and Newton, 1969). Once warm moist from the tropics reaches the North Atlantic, it collides with colder drier air from the Arctic, forming large vertical and horizontal temperature gradients. The boundary of where these conflicting air masses meet is known as the Polar Front,

consisting of fast-moving winds at the top of the troposphere known as the Polar Jet (Dzerdzeevskii, 1945; Reed and Kunkel, 1960). These strong winds over the North Atlantic are generally positioned near areas of the ocean surface experiencing the largest horizontal temperature gradients (e.g., open water/sea ice margin; Serreze and Barry, 2014). These gradients are a critical component in cyclogenesis and the overall life span of a cyclone due to the baroclinicity in this environment initiating and maintaining uplift in the cyclone's center (Hoskins and Valdes, 1990). As the seasons change the strength and position of these upper-level winds fluctuate, modifying the location, strength, and frequency of atmospheric cyclones throughout the year (Cullather and Lynch, 2003; Serreze and Barry, 2014).

Although trends of cyclone variability have been well-documented in the North Atlantic Ocean (e.g., Sanders, 1986; Brümmer et al. 2000; Jung and Rhines, 2007; Simmonds et al. 2008), no studies have investigated variability of cyclones within Baffin Bay (BB), Davis Strait (DS), and Labrador Sea (LS) in detail. These subregions are characterized by their connection to the North Atlantic and Arctic Ocean between eastern Canada and Greenland, near the northern boundary North Atlantic storm track (Tang et al. 2004; Tsukernik et al. 2007; Schuenemann et al. 2009). Due to this, BB, DS, and LS can potentially experience the highest frequencies of cyclones in the NH between autumn-spring (Serreze, 1995; Serreze and Barry, 2014). However, most research conducted in these subregions has been related to the oceanic current structure (e.g., Melling et al. 2001; Tang et al. 2004), local sea ice export trends (e.g., Wang et al. 1994; Parkinson et al. 1999; Onarheim et al. 2018; Bi et al. 2019), and freshwater fluxes relating to LS's deep water overturning cell (e.g., Bourke et al. 1989; Zweng and Münchow, 2006; Azetsu-Scott et al. 2012). Knowing that certain characteristics of cyclones across the NH are potentially coupled to sea ice extent fluctuations (e.g., Murray and Simmonds, 1995; Maslanik et al. 1996;

Yang et al. 2004) and atmospheric circulation patterns (e.g., Serreze et al. 1997; Luo at al. 2007), this thesis will identify the influence these local sea ice versus remote atmospheric drivers have on cyclones in BB, DS, and LS subregions of the North Atlantic.

Further knowledge on the effects of certain drivers on cyclones in BB, DS, and LS could provide an enhanced understanding of local climate change in these subpolar/polar environments.

1.2: Cyclone Research Over the Past Century

The North Atlantic experiences one of the highest frequencies of cyclones annually in the NH (Serreze and Barry, 2014). Different types of cyclones migrate through this region depending on the season. During fall, winter, and spring, extratropical cyclones enter this region from the North American continent following the Polar Front (Catto, 2016), often deepening and continuing into the high-latitudes or northern Europe over the course of several days to a week. North of the Polar Front, cyclones known as polar lows develop in maritime environments where warm open ocean meets colder land masses and along the sea ice margin (Businger and Reed, 1989; Montgomery and Farrell, 1992; Rasmussen and Turner, 2003). These cyclones are typically smaller than extratropical cyclones and last from few hours to a couple of days (Renfrew, 2003; Serreze and Barry, 2014). Polar lows can bring mild to severe winds and precipitation depending on the magnitude of baroclinicity and can resemble both tropical and extratropical cyclones (Rasmussen, 1981; Reed and Duncan, 1987; Catto, 2016). During summer and fall, tropical cyclones migrating into the midlatitudes may undergo extratropical transition into an extratropical cyclone then continue northward into the North Atlantic (Hart and Evans, 2001; Jones et al. 2003). These transition events often pose significant risks to maritime shipping

and coastal communities with high swells, strong force winds, and widespread precipitation (e.g., DiMego and Bosart, 1982; Atallah and Bosart, 2003; Evans and Hart, 2008; Blake et al. 2013). Due to high cyclone activity in the North Atlantic, the environments and mechanisms that promote cyclogenesis and deepening here have been extensively covered in the literature over the previous century.

The life cycle of cyclones has been well-understood for decades (Parsons and Smith, 2004). Prior to the twentieth century, the structure of a developed cyclone was known, yet the formation of these systems was left open to debate until the Thermal Theory of Cyclogenesis was developed in the nineteenth-century (Kutzbach, 2016); however this theory was only able to explain tropical cyclogenesis through convection, not the genesis and deepening of extratropical cyclones over land from frontal convergence. Bjerknes (1919) described the structure of these cyclones and stated that his findings supported the older theories of Dove (1837), Ferrel (1859), and Milham (1912) (refer to Lorenz, 1983). However, this theory only explained one part of extratropical cyclone development. A few years later, based on surface observations, Bjerknes and Solberg (1922) developed the Polar Front Theory describing cyclogenesis and deepening occurs along a kink in the Polar Front. Their theory became known as the Norwegian Model and led to the creation of the Bergen School of Meteorology (Catto, 2016).

Subsequent studies of cyclone characteristics led to empirical approaches to confirm the subjective conclusions of this theory (Charney, 1947). Solberg (1928, 1931) developed the most successful approach explaining that two isothermal layers in parallel flow at different altitudes can exist with a “tilt”. Scherhag (1934) and Bjerknes and Godske (1936) looked at the upper-air trough independently from the surface trough and discovered cyclone deepening is attributed to the rate at which upper-level air is displaced, thus influencing the vertical wind shear, which led

to the Divergence Theory. This theory proposed that upper-level divergence of winds produces a drop in pressure lower in the atmosphere (which is necessary for cyclone development) if the rate of convergence at the surface is less (Sutcliffe, 1939). Progress in connecting the upper and surface troughs was greatly hindered by the lack of in-situ observations in the middle and high-latitudes (Charney, 1947). A breakthrough occurred when Rossby (1939) theorized zonal atmospheric motion in an incompressible atmosphere, which resulted in determining that the speed of an atmospheric wave was dependent on the strength of the zonal westerly winds and the wave's meridional length. Rossby's approach was later perfected by Bjerknes and Holmboe (1944) to represent a baroclinic atmosphere.

Halfway through the twentieth-century, the focus of understanding the cyclonic life cycle morphed into establishing wholly recognized definitions of different atmospheric features (Sutcliffe, 1939, 1947). At the same time, Charney (1947) stated that baroclinic waves and the cyclones associated with them need to be looked at in three dimensions to fully understand their structure. This interest led to the pursuit of improving forecasting by looking at specific cyclonic events and attempting to improve spatial and temporal data coverage (e.g., Miller, 1946; Petterssen et al. 1955; Wagner, 1979; Bosart 1981; Nordeng and Rasmussen, 1992). As the processing power of computers increased in the 1960s and 70s, researchers began designing models depicting various levels of the atmosphere with varying degrees of baroclinicity to determine causes of cyclogenesis from the surface to the upper-troposphere (e.g., Eliassen and Raustein, 1970; Saltzman and Tang, 1972, 1974; Shapiro, 1975). Through the 1980s, satellite imagery improved the spatial and temporal resolution of atmospheric data across the midlatitudes and especially the Arctic, allowing improved climate models and data validation methods which led to further research on cyclone development, especially 'explosive' cyclogenesis (e.g.,

Sanders and Gyakum, 1980; Anthes et al. 1983; Roebber, 1984; Sanders, 1986; Gadd et al. 1990; Hedley and Yau, 1991). By the end of the 1990s, research of cyclones transitioned into a new era where computer modeling, and publicly-available datasets enhanced the capabilities of midlatitude and Arctic cyclone research. The key focus areas of interest related to cyclone identification and prediction through computer modelling (e.g., Serreze, 1995; Simmons et al. 1995) and empirical analysis utilizing teleconnection indices (e.g., Rogers, 1997; Serreze et al. 1997; Parsons and Smith, 2004).

Current interest in North Atlantic cyclones arises from the need for improved forecasting in North America and Europe at higher temporal and spatial resolutions and understanding the relationships between cyclone storm tracks and global atmospheric/oceanic circulation (e.g., Simmonds et al. 2008; Brayshaw et al. 2009), topography (e.g., Jung and Rhines, 2007; Tsukernik et al. 2007), and reducing the degree of error with cyclone locations and intensities in models (Catto, 2016). Walsh and Chapman (1990) and Serreze et al. (1997) mention interest will grow in identifying the relationships of atmospheric dynamics/systems driving sea ice circulation, extent, concentration, and thickness in the Arctic as datasets improve. Although there is still much research needed to fully understand midlatitude and Arctic cyclones, the general process of how they form, deepen, and dissipate have been thoroughly researched.

1.3: Life Cycle of a Cyclone

1.3.1: Cyclogenesis

The first stage of a cyclone's life cycle is known as cyclogenesis. The American Meteorological Society's Glossary of Meteorology (2012) defines cyclogenesis as "any development or strengthening of cyclonic (anti-clockwise) circulation in the atmosphere. It

is commonly applied to areas with newly-developed cyclonic circulation (e.g., low or trough) as well as to the strengthening of an existing cyclonic flow." In some cases, a cyclone may undergo rapid intensification or "explosive" cyclogenesis. As stated in Sanders and Gyakum (1980), in 1918 Tor Bergeron defined that explosive cyclogenesis occurs when the central pressure of a cyclone drops at least 1 hPa per hour for at least 24 hours. Explosive cyclogenesis has been an area of active meteorological research since the 1980s due to its effects on communities along the North American east coast and Europe (Wang and Rogers, 2001). In early models, explosive cyclogenesis events were difficult to forecast and include (e.g., Silberberg and Bosart, 1982; Sanders, 1986, 1987; Sanders and Auciello, 1989). These systems are often associated with hurricane-force winds, rapid temperature and wind shifts at the surface, and heavy precipitation in the form of rain, sleet, and snow (e.g., Bosart, 1981; Grønas, 1995; Allen et al. 2010; Zhang et al. 2017). Two famous explosive cyclones are the Queen Elizabeth II storm of 1978 (Gyakum, 1983a; Kocin and Uccellini, 1985) and the Presidents' Day cyclone in 1979 (Bosart, 1981). Sanders and Gyakum (1980) and Roebber (1984) first observed the majority of cyclones undergoing explosive cyclogenesis in the NH occurred during winter months over maritime environments. It was later found explosive cyclogenesis occurs over strong baroclinic zones near the coasts of North America and Europe (Wang and Rogers, 2001; Sun et al. 2018). Although the primary locations of explosive cyclogenesis were known, several studies at the time concluded that the frequency and intensity of all cyclogenesis events were likely underestimated over these regions due to sparse data coverage at the surface (e.g., Sanders and Gyakum, 1980; Gyakum et al. 1989; Chen et al. 1992). The onset of computer models and improved satellite coverage brought a new perspective of cyclone research at the surface and in the atmosphere. For example, Overland and Pease (1982), Serreze and Barry (1988), and Serreze et al. (1993) studied the

spatial and seasonal distribution of Arctic pressure features and their storm tracks. As the temporal and spatial resolution of climate data improved through increased weather station density, satellite coverage, and improved computer models, scientists now had the capability to investigate cyclogenesis events with increased accuracy.

1.3.1.1: Cyclogenesis of Polar Lows

Atmospheric cyclones known as polar lows can rapidly develop north of the Polar Front over the Arctic, especially in winter (e.g., Rasmussen, 1979; Businger and Reed, 1989; LeDrew, 1984, 1988; Emanuel and Rotunno, 1989; Grønas and Kvamstø, 1995; Carlton, 1996; Zhang et al. 2017). Shapiro et al. (1987) and Businger and Reed (1989) have shown that open-water sections of the North Atlantic, North Pacific, and Arctic Oceans during the winter months can induce explosive cyclogenesis in polar lows. Montgomery and Farrell (1992) explain further that enhanced moisture convection and steep temperature gradients between landmasses and ocean, air masses, or along the sea ice margin can create ideal environments for cyclogenesis of polar lows. With enhanced data, polar lows have been observed forming in the Nordic Seas, Bering Sea, Gulf of Alaska, Sea of Japan, and LS (Renfrew, 2003; Serreze and Barry, 2014).

Unlike extratropical cyclones in the midlatitudes which are synoptic features, polar lows are classified as smaller meso-scale features. They span approximately 95-480 km (60-300 mi) in diameter and last from 3-36 hours (Serreze and Barry, 2014), tending to form behind a main cold frontal feature (Sardie and Warner, 1983). However, polar lows share many similarities with extratropical cyclones in how they form (Catto, 2016). Studies have shown that cyclogenesis of polar lows is dependent on the magnitude of baroclinicity, latent heat release, surface flux interactions with latent heating, and upper-atmosphere anomalies (e.g., Rasmussen, 1979;

Nordeng, 1987; Emanuel and Rotunno, 1989; Grønås and Kvamstø, 1995;Yanase and Niino, 2005, 2007; Terpstra et al. 2015). With the aid of satellite imagery (Rasmussen, 1981) observed polar lows could develop the physical traits of either a tropical cyclone (open eye in the center) or extratropical cyclone (comma shape). According to modeling results from Yanase and Niino (2005, 2007), a polar low developing in an environment with a higher magnitude of baroclinicity and convection would likely take on the structure of an extratropical cyclone, whereas weaker magnitudes of baroclinicity and convection lead to polar lows resembling a tropical cyclone. Polar lows were originally thought to form due only to thermal changes in the atmosphere (Bretagna et al. 1962). Early research and observations relating to polar lows only pertained to baroclinicity in the upper levels of the troposphere, and due to sparse data coverage and their relatively small size compared to other midlatitude cyclones, only qualitative theories were proposed to the formation and development of a polar low's internal structure (Montgomery and Farrell, 1992). As surface observations became more widespread over the latter-half of the twentieth-century, it was found that baroclinicity at the lower levels of the troposphere was also a component of polar low cyclogenesis (e.g., Harrold and Browning, 1969; Mansfield, 1974; Rasmussen, 1979; Reed and Duncan, 1987; Craig and Cho, 1988). Modelling studies (e.g., Sardie and Warner, 1985; Orlansnki 1986; Nordeng 1987, 1990; Emanuel and Rotunno, 1989) attempted to further depict the role baroclinicity plays in polar low cyclogenesis, however Montgomery and Farrell (1992) state the outputs from these models are difficult to interpret and are primitive. This led them to develop a comprehensive balanced three-dimensional model that not only included baroclinicity, but also latent heat release though convection. Rasmussen (1979) first proposed that convection in polar lows could be initiated through Conditional Instability of the Second Kind (CISK). CISK is defined as, "the process whereby low-level convergence in the

wind field produces convective cumulus formation, thereby releasing latent heat" (American Meteorological Society, 2012). The CISK theory describes polar lows originating from baroclinic disturbances utilizing Convective Available Potential Energy through cooperative feedbacks between cumulus clouds and large-scale moisture convergence (Rasmussen, 1979). It was concluded that outbreaks of cold polar air could produce the baroclinic instability needed to support the CISK theory of polar low cyclogenesis (Serreze and Barry, 2014). A second theory proposed as the mechanism for polar low cyclogenesis was Wind Induced Surface Heat Exchange (WISHE). WISHE consists of a positive feedback between atmospheric circulation and heat fluxes from the ocean surface, with increased circulation of the cyclone leading to larger surface fluxes of heat, which are quickly transported aloft through convection, thus strengthening the circulation of the cyclone (American Meteorological Society, 2012). Serreze and Barry (2014) state these theories contradict each other as to which maintains the cyclone (convection vs. surface fluxes); however, there is agreement that both environments must be preceded by an initial disturbance (e.g., katabatic winds off Greenland). Given the unrealistic conditions for either of these theories to be individually effective, neither are suitable scenarios for explaining cyclogenesis of polar lows (Terpstra et al. 2015). As these theories were being researched, a new approach was developed considering that cyclogenesis of polar lows is initiated through a "mixed-instability" between latent heat and baroclinicity (Sardie and Warner, 1983; Craig and Cho, 1988). This theory came about due to improved numerical modeling techniques attempting to pinpoint the mechanism(s) responsible for polar low cyclogenesis, the consensus was that latent heat (e.g., Bresch et al. 1997; Claud et al. 2004; McInnes et al. 2011) and baroclinicity (e.g., Nordeng and Rasmussen, 1992; Douglas et al. 1995; Claud et al. 2004; Brümmer et al. 2009; Bracegirdle and Gray, 2009; Føre et al. 2011, 2012) were the most ideal variables.

Montgomery and Farrell (1992) designed the first conceptual model of polar low cyclogenesis based on these two variables. Their conclusions stated that development of polar lows occur in two stages: (1) mutual interaction between positive upper and lower-tropospheric potential vorticity anomalies that are supported by strong ascending motion ahead of the trough, and (2) a second intensification (diabatic destabilization phase) where potential vorticity is redistributed through latent heat release in the ascending core of the cyclone (Terpstra et al. 2015). Montgomery and Farrell (1992) also concluded that the second stage over open water is the key to allow a polar low to deepen. However, modeling results from Føre et al. (2012) brought up contradictions of the magnitude latent heat plays in the cyclogenesis of polar lows, recommending that further research of the primary mechanisms and their effects on polar low development need to be conducted.

1.3.2: Deepening

After cyclogenesis, the second stage of a cyclone's life cycle is referred to as deepening. Deepening is defined as, "a decrease in the central pressure of a pressure system, usually applied to low pressure (cyclonic) systems to express its circulation strength" (American Meteorological Society, 2012). Tsukernik et al. (2007) identify three areas of preferred deepening in the North Atlantic: (1) south of Greenland (around 54° N); (2) near the locus of Icelandic Low; and (3) just south of Svalbard. Within all of these regions exists the North Atlantic storm track.

The North Atlantic storm track experiences one of the highest annual frequencies of cyclones in the world, and has the most prominent cyclone activity in the NH during the winter months (Geng and Sugi, 2001; Serreze and Barry, 2014). The cause of this is related to the variability within the global circulation over this region and its influence on the strength and

position of the Polar Front. Before the advent of satellite imagery and improved weather stations, it was thought that the area around Greenland was associated with minimal cyclone activity due to the extreme topographic gradients along its coasts (Sardie and Warner 1985; Businger and Reed 1989; Nordeng and Rasmussen, 1992). Several studies have shown that cyclones form and deepen over Greenland and its presence directly effects the tracks of some systems in the North Atlantic through bifurcation along the southern tip (e.g., Douglas et al. 1995; Chen et al. 1997; Doyle and Shapiro 1999; Kristjánsson and McInnes 1999; Petersen et al. 2003; Doyle et al. 2005; Jung and Rhines, 2007; Tsukernik et al. 2007). Even though Greenland's presence influences cyclones in the North Atlantic, the relationship between the atmosphere and upper-ocean is critical to understanding why this region is cyclonically active.

In the North Atlantic, large horizontal thermal and salinity gradients exist in this region separating the colder Labrador Current originating in LS from the warmer North Atlantic current (Serreze and Barry, 2014). During the winter months, when temperature gradients are strongest between the ocean surface and boundary layer of the atmosphere, fluxes in temperature and moisture promote baroclinicity (e.g., Sanders, 1986; Roebber, 1989; Gadd et al. 1990; Rogers, 1997; Wang and Rogers, 2001; Hanson et al. 2004; Simmonds et al. 2008; Brayshaw et al. 2009). Because of this, extratropical cyclones migrating from the North American continent and tropical cyclones from the lower latitudes often transition and deepen within this region (U.K. Meteorological Office, 1964; Whittaker and Horn, 1982; Jones et al. 2003).

By the end the twentieth-century, the variables contributing to cyclone deepening have been well documented in the literature. They are: (1) large magnitudes of upper-level forcing (e.g., Rogers and Bosart, 1986; Macdonald and Reiter, 1988; Hirschberg and Fritsch, 1991; Lupo et al. 1992), (2) intrusion of high potential vorticity stratospheric air (e.g., Bosart and Lin, 1984;

Uccellini et al. 1985; Zehnder and Keyser, 1991; Reader and Moore, 1995), (3) latent heat release (e.g., Gall, 1976; Anthes et al. 1983; Gyakum, 1983b; Emanuel et al. 1987; Mullen and Baumhefner, 1988; Kuo et al. 1991b; Whitaker and Davis, 1994), (4) surface energy fluxes from the ocean (e.g., Atlas, 1987; Davis and Emanuel, 1988; Fantini, 1990; Nuss and Kamikawa, 1990; Kuo et al. 1991a; Hedley and Yau, 1991) and (5) local baroclinicity resulting from diabatic heating (e.g., Bosart, 1981; Rogers and Bosart, 1991). Uccellini (1990) and Gyakum et al. (1995) noted that not all of these variables need to be present for deepening to occur. Furthermore, Reed et al. (1993) concluded that the magnitude of these variables significantly change from cyclone to cyclone. Wang and Rogers (2001) support this finding and mention these variables interact non-linearly, making accurate predictions of several deepening events difficult based on similar criteria. LeDrew (1984, 1988) find that local diabatic heating associated with open water areas within sea ice cover can be significant to the intensification and rejuvenation of cyclones entering the North Atlantic, making them potentially dangerous to shipping traffic (e.g., Buckley, 1983; Gyakum, 1983a). Roebber (1989) supports the results of Gyakum et al. (1989) where deepening rates between cyclones over land and ocean are significantly different. Wang and Rogers (2001) state this difference is not the result of upper-level forcing (which occurs over both land and ocean), but of the difference in moisture abundance, allowing (on average) higher deepening rates of cyclones over the ocean. With a constant source of moisture and instability, the North Atlantic primarily supports the cyclogenesis and deepening stages of cyclones. However, cyclones can experience weakening in the North Atlantic if baroclinicity is reduced.

1.3.3: Cyclolysis

The final stage of a cyclone's life cycle is known cyclolysis. Cyclolysis is defined as, "any weakening of cyclonic circulation that does not include filling (increase in atmospheric pressure), and is the opposite of cyclogenesis" (American Meteorological Society, 2012). Cyclolysis begins when the cold front overtakes the warm front leading to occlusion. This occlusion leads to a reduction in horizontal temperature gradients and convergence at the surface (Azad and Sorteberg, 2014). Carlson (1994), states that occlusion is not due to motion of the frontal structure, but of rearrangement of mass by quasi-geostrophic forcing. Furthermore, Schultz and Vaughan (2011) mention that although weakening may occur after occlusion, the structural and dynamical changes in the air within the occlusion zone is responsible for cyclolysis.

Significantly less research has focused on cyclolysis when compared to cyclogenesis and deepening (Morris and Smith, 2001; Azad and Sorteberg, 2014). The latter study goes as far as to claim that well-known cyclone life cycle models such as the Bergen model of extratropical cyclone development (Bjerknes and Solberg, 1922) and the Shapiro-Keyser marine ETC model (Shapiro and Keyser, 1990) do not provide adequate clarification on the cyclolysis stage. It is unclear when cyclone decay was first identified and researched, the first mention of it was found in a statistical study by Zishka and Smith (1980) where they investigated cyclone and anticyclone climatologies over North America and the Pacific Ocean, but were limited in data coverage. A complete history of research pertaining to cyclolysis is provided by Martin, Grauman, and Marsili (2001), with most research pertaining to the North Pacific. Rolfson and Smith's (1996) research on cyclolysis dynamics was the first to provide a weakening cyclone category in their analysis. They concluded that increased cold air advection and reduced

horizontal vorticity advection lead to an increase in pressure and reduced uplift at the surface. This conclusion was found to best explain cyclone decay for winter cyclones over North America (Morris and Smith, 2001) and over the North Atlantic (Azad and Sorteberg, 2014). However, the former study adds that rates of latent heat release and adiabatic warming also contribute to weakening. In addition, their research identified upper-level dynamics associated with cyclolysis based on events over North America. They found that weakening initiates when the distance between the upper-level and surface troughs decreases. In addition, Martin et al. (2001) state the magnitude of upper-level vorticity was not a contributing factor of weakening until the upper-level trough overtook the surface trough, resulting in a decrease of mass transport in the cyclone's core. Azad and Sorteberg (2014) also found that these dynamics change over the course of the decay period, with upper-air dynamics initiating cyclolysis followed by low-level dynamics sustaining decay. Azad and Sorteberg (2014) conclude that the mechanisms responsible for cyclolysis are far from being understood and the lack of research has led to climate models having inaccurate physics during cyclone decay. They recommend scientists to improve the estimation of low-level dynamics and associated processes to better depict cyclolysis in the later stages.

1.3.4: Cyclones Overview

Cyclones are a primary mechanism of energy transport between the midlatitudes and the Arctic in the North Atlantic region. Depending on their location in the NH, cyclones can take on different names: tropical cyclone in lower latitudes, extratropical cyclone in midlatitudes, and polar lows in high-latitudes. Each has different physical structures (e.g., "comma" shape or "open-eye"), varies in extent, and in duration. A baroclinic environment is required for

cyclogenesis to initiate. During winter, large horizontal air and water temperature gradients in the North Atlantic region allow high frequencies of cyclogenesis and deepening to occur. Since cyclones were first studied over a century ago, the ability to forecast and understand the mechanisms of cyclogenesis has been of the most interest due to the potential socioeconomic impacts, especially along the coasts of North America and Europe. For the first half of twentieth-century, research aimed at developing theories of cyclogenesis and providing universally accepted terms for each component of a cyclone's structure. Predicting when cyclogenesis and deepening would occur was restricted to populated areas with surface weather stations until satellites were implemented in the 1970s. Satellites improved spatial and temporal coverage of cyclones over the North Atlantic. With the advancement of computers in the 1980s, modelling studies attempted to determine the accuracy of the theories proposed from decades earlier were accurate utilizing specific cyclone events. Through the 1990s, modelling studies became more complex as datasets derived from satellites became available and more variables were implemented. This allowed, for the first time, long-term climatologies of cyclones across the NH and the ability to identify potential variables related to their development. Over the past two decades, models have improved in spatial resolution and processing power allowing better understanding of a cyclone's formation and deepening, particularly in the North Atlantic. However, the decaying stage of cyclones has not experienced the same level of attention and its processes have not been taken into full consideration in most climate models leading to inaccuracies. Although the processes related to the life cycle of cyclones have been documented in the literature for several decades, the primary knowledge gap that exists relates to the interconnections between cyclones and their drivers in isolated regions. One environmental

variable that affects a cyclone's life cycle is local sea ice, due to the baroclinic environment from the sea ice edge.

1.4: Arctic Sea Ice Formation

One of the most used proxies to study climate change in the Arctic is the temporal and spatial variability of sea ice due to its coupling to the atmospheric circulation (e.g., Carsey, 1982; Giovinetto and Zwally, 1995; Parkinson, 1995; Deser et al. 2004; Kwok, 2004; Serreze et al. 2007b; Ogi and Rigor, 2013; Scott and Feltham, 2010; Serreze and Barry, 2014). During the autumn and winter months, new sea ice (first-year ice) is produced in the East Siberian and Chukchi Seas due to runoff and river discharge from the Siberian interior emptying into the Arctic Ocean (Aagaard and Carmack, 1989). Fresh water inputs from precipitation events and glacial runoff in northern Canada and Greenland have also been documented to contribute to the Arctic Ocean's fresh water budget (Warren, 1983; Emile-Geay et al. 2003; Serreze and Barry, 2014). Due to this runoff having lower salinity and density (and higher freezing point) than salt water, it remains at the ocean surface, making sea ice production more favorable in this area of the Arctic Ocean (Steele and Boyd, 1998). As winter approaches, atmospheric temperature and pressure gradients between the middle and high-latitudes become stronger, causing winds to "steer" the first-year ice towards the Central Arctic Ocean and Canadian Arctic Archipelago where the thickest sea ice is located (Kwok, 2015). The direction of travel is also the result of the general flow pattern of ocean water entering the Arctic from the Bering Sea and exiting in the North Atlantic (Melling, 2000; Samelson et al. 2006). Once the new sea ice approaches this region, it may collide with much thicker fast ice (ice fastened to land) and float in place for many years or drift within the gyres of the Arctic Ocean (Parkinson and Cavalieri, 2008). If first-year

ice persists through the upcoming melt season (summer), it becomes second-year sea ice. Any sea ice that persists through two or more melting seasons becomes multiyear sea ice.

1.4.1: Arctic Multiyear Ice Pack

The multiyear sea ice pack floats constantly within the Arctic Ocean, varying in extent and thickness throughout the year (Serreze and Barry, 2014). Multiyear sea ice is an important component in stabilizing the Arctic's climate due to its high albedo which reflects 80% of sunlight, acting as buffer between oceanic/atmospheric heat exchange (Ogi and Rigor, 2013) whereas open ocean water absorbs 90% of incoming solar insolation (Kellog, 1975, Serreze and Barry, 2014). When multiyear ice is exported out of the Arctic it is replaced with first-year ice that is more susceptible to melting due to being thinner. The decrease of multiyear sea ice allows for increased rates of warming in the Arctic Ocean, through creating melt ponds and polynyas (Serreze and Barry, 2014). These open water areas within the sea ice pack allow incoming solar insolation to be absorbed into the upper-levels of the Arctic Ocean leading to an increase of sea ice loss (Kellogg, 1975; Curry et al. 1996; Serreze and Barry, 2014). This process known as the Ice Albedo Feedback (Scott and Feltham, 2010). Aiding this process are the strong surface winds breaking apart the ice and temperature/salinity increases at the base of the sea ice, promoting melting from the bottom-up (Langehaug et al. 2013). Once the multiyear ice pack begins to break apart it can be exported through gateways connecting the Arctic Ocean to the Pacific (Bering Strait) and Atlantic Oceans (Fram Strait; Melling, 2000).

1.4.2: Sea Ice Export

The Fram Strait exports the highest amount of sea ice; around 10% (880,000 km^2) of the Arctic's total sea ice area per year (Kwok, 2009) or 25% of the Arctic's total fresh water (Lique et al. 2009; Ricker et al. 2018). Sea ice export through the Fram Strait has been of the most interest due to it being the largest gateway and its proximity to the North Atlantic deep water formation cells (Aagaard and Carmack, 1989; Ricker et al. 2018). The numerous channels in the Canadian Archipelago and Nares Strait in northern BB are the two other smaller gateways to the Atlantic, and export significantly less sea ice from the Arctic Ocean (Melling, 2000; Serreze et al. 2006; Melling et al. 2008). The amount of sea ice exported can have significant influences on the local and global thermohaline circulation, especially in the North Atlantic (Dickson et al. 1988). Studies have found that changes in the atmospheric circulation (especially in winter) can significantly affect the rate of sea ice export through the Fram Strait (Ionita et al. 2016) and Nares Strait (Samelson et al. 2006), causing abrupt shifts in the North Atlantic deep water formation cells. Even though the majority of deep water forms between Greenland and Scandinavia, one recently discovered cell located in LS (Smethie et al. 2000) to the south/west of Greenland is dependent on the flux of freshwater (including sea ice) from the Arctic through BB/DS (Talley and McCartney, 1982; Goosse et al. 1997; Khatiwala et al. 1999; Münchow et al. 2006; Kwok, 2007).

1.4.2.1: Nares Strait

It has been found that fresh water fluxes through Nares Strait and the Canadian Archipelago may reflect the impacts of diminishing sea ice in the Arctic (Parkinson and Cavalieri, 2008), disintegrating ice shelves of northern Canada (Nutt, 1966; Copland et al. 2007),

and potentially surging glaciers of northern Greenland (Rignot and Steffen, 2008). Fresh water inputs from the Canadian Archipelago/Nares Strait can influence the current structure and deep water production in LS (e.g., Bourke et al. 1989; Lazier, 1995; Dickson et al. 2003; Jones et al. 2003; White et al. 2007; Melling et al. 2008). At the northern boundary of BB is a narrow channel known as the Nares Strait, separating northern Greenland from the Canadian Archipelago. Nares Strait is over 500 km (310 mi) in length and varies from 20-50 km (13-31 mi) in width (Münchow et al. 2006). Due to Nares Strait being frozen over in winter, multiyear ice is exported during spring and summer (Dunbar, 1973; Kwok, 2005). Jones et al. (2003) and Woodgate and Aagaard (2005) observed that water entering BB from the north originates from the Pacific Ocean. Increasing inputs of fresh water into BB through Nares Strait from the Arctic has been found to promote desalinization of the upper ocean, stabilizing of the water column, and potentially reducing the rate of deep water formation in LS (Kwok, 2007). Zweng and Münchow (2006) reported northern and western BB have become fresher from increased fresh water inputs from Nares Strait and increased warming along the west coast of Greenland when looking at sea ice observations from 1928-2003.

Sea ice thickness and export in BB have become an increasing topic of interest. The most detailed description is provided by Kwok (2007) who calculated an average thickness of 1.2 m for first-year sea ice in BB from 2002-2007. However, multiyear sea ice originating from Nares Strait and the Canadian Archipelago can have an average thickness between 2.5-6 m (e.g., Dunbar, 1973; Sadler, 1976; Dey, 1981; Agnew, 1998; Haas et al. 2006). Recently, Bi et al. (2019) conducted 40-year sea ice thickness approximations in BB are in general agreement with the previous literature. From the limited literature, it is known that a sea ice thickness gradient exists across BB/DS with the thickest sea ice values located along the western shore (1-2 m) due

to rough hummocky multiyear floes, then gradually decreasing eastward based upon limited data over different years (Kwok, 2007). Sea ice drift characteristics within BB and DS have been more thoroughly researched. Annual drift tracks of sea ice in BB suggest most motion occurs in the western part and dominates the local oceanic circulation patterns during winter (Heide-Jørgensen et al. 2007; Kwok, 2007).

1.4.3: Sea Ice in Baffin Bay, Davis Strait, and Labrador Sea

The discovery of BB and DS was the result of attempting to locate a "Northwest Passage" between the Atlantic and Pacific Oceans (Dunbar and Dunbar, 1972). DS was identified first in 1586 by John Davis while BB was identified in 1616 by William Baffin, yet these subregions was not included on maps until the early nineteenth-century (Serreze and Berry, 2014). Even though BB and DS's sea ice characteristics were observed during the 1882-83 International Polar Year, sea ice from these regions first became a modern concern after the sinking of the Titanic in 1912 (Serreze and Barry, 2014). However, the first expedition to document sea ice conditions in this region was not carried out until 1928 by the U.S. Coast Guard (Smith et al. 1937). BB's width varies between 110-650 km (68-404 mi) and is bounded by Baffin Island to the west, Greenland to the east, and Ellesmere Island to the north. To the south, it meets LS/North Atlantic at DS. Between BB and LS, DS spans 650 km (400 mi) from south to north and between 125-250 km (200-400 mi) wide (Encyclopedia Britannica, 2018). LS is an extension of the North Atlantic, connecting BB and DS to the Atlantic Ocean. Each winter, sea ice and fresh water migrate from the Arctic Ocean through Nares Strait/Smith Sound (Münchow et al. 2006; Melling et al. 2001), Jones Sound (Melling, 2000), and Lancaster Sound

(Sanderson and LeBlond, 1984; Fissel et al. 1982) in northern BB reaching maximum extent typically in March (Zweng and Münchow, 2006).

Over the past few decades, several studies have found that the freshwater intake and sea ice extent have been increasing in this region (e.g., Parkinson, 1995; Münchow et al. 2006; Zweng and Münchow, 2006). Cold, fresh Arctic waters flow through which channels and travel along the base of the Baffin Island shelf, forming the Labrador Current (Fissel et al. 1982). On the eastern shore along Greenland's western shelf, warm saline water travels northward, gradually mixing throughout the bay, becoming the West Greenland Current (Reverdin et al. 2003; Zweng and Münchow, 2006). Due to this temperature/salinity gradient across the region, sea ice first forms in the north along the western side following the Labrador Current. Over the winter months, sea ice advances southward into the DS and LS and eastward towards Greenland (Parkinson, 1995; Heide-Jørgensen et al. 2007; Kwok, 2007). When BB is covered in sea ice, an area of open water known as the North Water (76° N to 79° N and 70° W to 80° W) exists due to upwelling of the West Greenland Current along the southern border of Nares Strait and from persistent strong northerly winds (Loder et al. 1998; Heide-Jørgensen et al. 2013). This polynya is the primary mechanism of sea ice formation and advection (e.g., Mysak and Huang, 1992; Darby et al. 1994; Willmott et al. 1997; Bi et al. 2019) and serves as a vital sustenance resource for local land and marine wildlife (Stirling, 1980; Stirling and Cleator, 1981; Born, 1987; Heide-Jørgensen et al. 2013). Since its discovery, the North Water has been of recurring interest since in-situ observations have been limited, especially during the winter (Tang et al. 2004). Kwok (2006) found that very little sea ice drifts from the Arctic Ocean into BB through the Canadian Archipelago, and suggested that sea ice is rather produced in the various narrow channels. Early, coarse satellite imagery of sea ice motion in the region from Dey (1981) concluded that sea ice

entering BB from these channels accounts for up to one-third of the total sea ice area in BB. Wilson et al. (2001) claim that the North Water produces the majority of sea ice in BB due to its connection with the atmospheric and oceanic structure of the region. Looking at a short-term five-year period (2002-2007) of sea ice drift in BB, Kwok (2007) concluded that the North Water produced approximately two-thirds of the sea ice in BB/DS. Lower sea ice coverage occurs in eastern BB due to the cyclonic drift pattern of sea ice and the warm West Greenland Current impeding advancement (Kwok, 2007). This study also estimated sea ice drift in DS can reach speeds of up to 20 km/day when coupled with strong northerly winds. From these northerly winds, Kwok (2007) found the annual average sea ice export volume in BB to be between 530-800 km^3, which is higher than the results of Cuny et al. (2005), who gave an estimate of 500 km^3 using coarser Special Sensor Microwave Imager (SSMI) ice drift imagery instead of Envisat ice motion. Of this total volume, up to 100 km^3 could be related to multiyear ice inflow from the Nares Strait identified in Kwok, (2005). In DS, the mean speed of winter sea ice export was calculated at 6 km/day in the lowest year and 8.6 km/day in the highest year, with the largest export being in the month of February (Kwok, 2007). The recent study of Bi et al. (2019) found large year-to-year fluctuations at Nares Strait and Lancaster Sound inlets, with increasing positive significant trends of sea ice at these inlets. Across the 40-year period, they estimated the annual sea ice inflows through Nares Strait and Lancaster Sound to be 200 x $10^3 km^2$ and 55 x $10^3 km^2$, with positive decadal trends of 39 x $10^3 km^2$ and 7.5 x $10^3 km^2$. Annual sea ice export into DS was estimated at 395 x $10^3 km^2$ with a positive decadal trend of 82 x $10^3 km^2$. Additionally, Bi et al. (2019) found during winter months, the amount of sea ice exported is greater than the inflow from these two inlets, while summer months have much smaller inflow/outflow fluxes. They also state that the North Water formed 75-85% of the sea ice within

BB across their 40-year period. Their final observations showed sea ice motion and surface air temperatures have been increasing in BB over the past four decades due to decreasing sea ice thickness and increasing surface warming. Even though the contribution of sea ice from the Canadian Archipelago and Nares Strait are relatively small, they are still very important in the freshwater budget of BB, DS, and LS.

1.4.4: Sea Ice Measurement (Pre-Satellite) Methods

Prior to the nineteenth-century, voyages to the North Atlantic side of the Arctic were based solely upon identifying 'unknown geography,' the Northwest Passage, and document suitable locations for the whaling and fishing industries; however there has been documentation regarding sea ice drift and ocean surface characteristics (Dunbar, 1951; Tang et al. 2004). By the end of the nineteenth-century, the works of Hayes (1867), Petermann (1867), and Petterson, (1900) led to the understanding of the general circulation of BB/DS. However, the sinking of the Titanic in 1912 further drew attention to sea ice variability in the North Atlantic. Most observations of sea-ice distribution in BB for the first half of the twentieth-century were made mainly by ships and reconnaissance flights (Tang et al. 2004). By the end of the 1920s, the Marion and General Greene expeditions led by International Ice Patrol of the U.S. Coast Guard in 1928 was the first attempt to illustrate the geostrophic flow within DS (Smith et al. 1937). That same year, the Danish Godthaab Expedition (Riis-Carstenson, 1931) provided the first extensive data coverage of BB which Kiilerich (1939) first used to describe the Labrador and West Greenland Currents in the region. After the start of the Cold War, militaries from both the U.S. and the U.S.S.R. began looking for new strategic locations for submarines, countries whose boundaries extend into the Arctic (Canada and Greenland) faced sovereignty issues, and the

increased prospecting of oil further sparked interest in researching BB and the Arctic (Tang et al. 2004). In the 1960s, icebreakers from Canada and the U.S. partook in expeditions in northern BB observing sea ice and ocean currents which were described in the works of Collin and Dunbar (1964) and Muench (1971). However, southward toward DS much more hydrospheric, cryospheric, and atmospheric data were collected by several groups (e.g., Greenland Technical Organization from 1975-1978 and the petroleum industry in 1976 and 1977; Danish Hydraulic Institute, 1979). Due to the lack of sea ice in the eastern part of BB/DS along Greenland, more research on the physical environment in this area was conducted, which produced additional in-situ datasets used in studies such as: Valeur et al. (1996); Zweng and Münchow (2006); and Heide-Jørgensen et al. (2007a-b). A breakthrough of identifying the currents of BB being connected to the Arctic Ocean was first identified by Sadler (1976) using monthly measurements of ocean currents collected near Nares Strait. Similarly, Prinsenberg and Bennett (1987) analyzed an 8-month mooring collection in the Canadian Archipelago which indicated a net transport of water from the Arctic Ocean into BB. At the dawn of environmental interest at the end of the 1970s, expeditions funded by petroleum companies to identify suitable sites for drilling in northwest BB required understanding both above and below the ocean surface (Tang et al. 2004). Measurements included conductivity, temperature, and depth at stations in summer (Fissel et al. 1982), moorings (Fissel, 1982), and tracking sea ice both visually and remotely (deLange Boom et al. 1982). Their results confirmed the theory that the oceanic and sea ice circulation in BB is cyclonic with a major southward flowing current along the western shores of BB/DS (Tang et al. 2004). Starting in 1983, a project initiated by the Canadian-based Bedford Institute of Oceanography recorded annual current dynamics with moorings in BB. A different region was selected each year to improve the record for the entire region (Ross, 1990a-b, 1991, and 1993).

For a period of three years (1987-1990), an array of five moorings was established across DS (Tang et al. 2004). Today, the primary platforms of surface data acquisition in BB/DS and the Arctic are aircraft (Steffen, 1985), satellite/spacecraft (Press and Blais, 1993), and ships (Barber et al. 2001). While these methods were applied in early trend analysis studies, Dey (1981) mentions their results were founded on high subjectivity and that uncertainties were typically not quantified. Even though limitations exist with satellite imagery, this fast and relatively cheap data collection method has provided the longest record of temporal and spatial data for the North Atlantic and Arctic.

1.4.5: Visible, Infrared, and Microwave Sensors

Consistent satellite coverage of the Arctic began in the early 1970s with the polar-orbiting U.S. Air Force Defense Meteorological Satellite Program (DMSP) and NOAA's Television Infrared Observation Satellite (TIROS) equipped with the Very High Resolution Radiometer sensor. The first series of continually updated sensors began on TIROS-N with the implementation of the Optional Vertical Spectrometer and Advanced Very High Resolution Radiometer. Since 1999, the Moderate Resolution Imaging Spectro-Radiometer (has been part of NASA's Earth Observing System. Even though these satellites were ground-breaking with their ability to capture large areas of the Arctic in relatively short periods of time, they were limited in surface measurements by their visible and infrared bandwidths which were unable to penetrate cloud cover, in addition, visible bandwidths were unable to operate at night (Carsey, 1992). However, the microwave spectrum would prove to overcome these limitations and usher in a whole new series of Arctic datasets.

The microwave spectrum was first used by NASA in 1973 with the Electronically Scanning Microwave Radiometer (ESMR) which passively measured Earth's naturally emitted microwave energy (Carsey, 1992). This sensor became the first to continually measure sea ice conditions through polar night and cloud cover (Serreze and Barry, 2014). ESMR was succeeded by the Scanning Multichannel Microwave Radiometer in 1978 and lasted until 1987 when the DMSP F8 satellite carried the first of the Special Sensor Microwave Imager sensors (SSMI). Being used for almost two decades, SSMI was replaced in 2005 by the Special Sensor Microwave Imager/Sounder (SSMIS). Through the 1990s, Europe and Japan fitted synthetic aperture radar sensor to several research satellites providing high-resolution sea ice data, while Canada launched Radarsat. In 2002, the Advanced Microwave Sounding Radiometer E from NASA provided higher spatial resolution of sea ice concentration than the SSMI and SSMIS sensors, however it failed in 2011. Japan successfully launched an equally capable sensor named "AMSR2" in 2012. From 2003-2009 NASA used a laser altimeter system with the capability to measure changes in height at the surface, thickness in sea ice, and ice sheet mass balance over time with the Ice, Cloud, and Land Elevation Satellite (ICESat). In 2017, ICESat-2 was launched with advanced capabilities compared to its predecessor. The European Space Agency launched CryoSat-2 in 2010 which uses the same technology as ICESat to measure different variables of sea ice. Once of the most successful sensors to come from of NASA was Gravity Recovery and Climate Experiment in 2002, which uses Earth's gravitational field to monitor changes in ice sheet mass balance in Greenland and Antarctica. For a more thorough overview of these sensors, refer to Serreze and Barry (2014).

1.4.6: Sea Ice Overview

Over the past century, the interests and methods of measuring sea ice in the Arctic have advanced from simple qualitative descriptions from expeditions using ships and planes to complex satellite sensors which can measure different variables of sea ice at a variety of temporal and spatial resolutions. The monthly and annual trends of sea ice in the Arctic have been well-documented over several decades due to the improvements of satellite sensors. First-year sea ice forms near the Siberian coast due to fresh water discharge from river systems in the Siberian Interior and, once it forms, strong winds steer the sea ice towards the Canadian Archipelago or the ice pack over the central Arctic Ocean where it collides with much thicker multiyear sea ice. Sea ice can remain drifting in the Arctic Ocean for many years before it is exported through the Fram Strait in the North Atlantic. Since records have been kept, the overall extent of multiyear sea ice in the Arctic Ocean has been decreasing in all months and being replaced with first-year ice. Although BB, DS, and LS were explored prior to the Arctic Ocean and closer to populated areas, quantitative scientific studies on sea ice trends in these subregions have only been attempted within the last couple decades, with most covering only winter months over less than a decade. This results in several knowledge gaps relating to the connection between local currents and sea ice formation and export as well as the relationship between sea ice extent and local atmospheric structure. What has been found in the literature is that in the northern section of the bay, the North Water Polynya creates a majority of the sea ice which follows the Labrador Current along the Canadian shoreline and then exits into LS. As winter progresses, sea ice reaches further south and east towards Greenland, however the warmer West Greenland Current prevents this region from completely freezing over. Although high-resolution currents and sea ice measurements in the Canadian Archipelago and Nares Strait confirm that BB

receives fresh water from the Arctic Ocean, it only contributes up to one-third of the total sea ice production in BB/DS. Sea ice exported from both the Arctic Ocean and BB/DS can significantly influence the deep water formation in the North Atlantic through changes in the local fresh water fluxes. Due to the potential impacts sea ice can have on the global oceanic circulation, large-scale atmospheric patterns known as teleconnections are coupled with this system could potentially be affected and influence the atmospheric structure and sea ice extent within the Arctic and BB/DS.

1.5: Teleconnections

Atmospheric teleconnections are crucial in predicting climate variability across the NH by representing the atmosphere's variable frequency across various temporal ranges (Wang and Zhang, 2015; Zhang et al. 2016). The definition of what an atmospheric teleconnection is has evolved in the literature, yet there currently lacks a single universally accepted definition. For example, Wallace and Gutzler (1981) define atmospheric teleconnections as "significant simultaneous correlations in geopotential height occurring at specific temporal periods at distant locations." Barnston and Livezey (1987) further explain that teleconnections are typically made up of two to four centers of action in the global circulation separated by great distances and experience high changes in horizontal amplitude resulting from negative correlations between these centers. However, they emphasized that this criterion may not represent all teleconnections, and does not dictate their importance and temporal variability. Rogers (1997) defines these features as "slowly varying circulation features that retain their identities on temporal charts, each having specific spatial centers of action." van den Dool (2007) states atmospheric teleconnections are "a simultaneous significant temporal correlation in the geopotential height

field between two widely separated locations." Finally, the definitions according to American Meteorological Society (2012) relate to linkages between weather events in different regions of the world and significant correlations within a field defined by widely separated points. Atmospheric teleconnections are composed of centers of action which identify the fluctuating pressure systems that migrate in location. These changes are referred to as positive, neutral, or negative phases. The magnitude and strength in position of an atmospheric teleconnection's centers of action can shift over weekly to decadal timescales (Kutzbach, 1970). Extreme phase shifts can potentially impact Arctic sea ice (Kwok and Rothruck, 1999; Jung and Hilmer, 2000; Rigor et al. 2002; Rigor and Wallace, 2004; Serreze and Barry, 2014; Bushuk et al. 2015), regional warming (Hurrell, 1995, 1996; Thompson and Wallace, 1998; Dickson et al. 2000;), and cyclone characteristics (e.g., Blackmon et al. 1976; Cai and Van den Pool, 1991; Rogers and Mosley-Thompson, 1995; Serreze et al. 1997; Ulbrich and Christoph, 1999; Serreze et al. 2006; Serreze and Barry, 2014; Wei et al. 2017). Due to the Atlantic side of the Arctic experiencing large temperature and pressure variations, the influences of certain NH teleconnections can be amplified in this region.

1.5.1: North Atlantic Oscillation (NAO)

One of the most dominant teleconnections in the NH is the NAO. The NAO was first "officially" documented by Exner (1913) and Walker (1923) and has been recognized as one on of the primary Northern Hemispheric teleconnections since the 1930s, especially during winter (van Loon and Rogers, 1978; Serreze and Barry, 2014). The NAO is composed of the Bermuda (Azores) High in the mid-Atlantic and the Icelandic Low in the North Atlantic and these centers of action fluctuate or "seesaw" back and forth in pressure and migrate to different areas of the

Atlantic depending on the phase and time of year (Lorenz 1951; Lamb and Peppler, 1987). Throughout the twentieth-century, several multidecadal shifts in the NAO have been observed (Serreze and Barry, 2014). For the first half of the century, the NAO experienced a positive phase, then between the 1950s-1960s, it transitioned into a negative phase lasting until 1980. From then until around 2000, the NAO remained in another positive phase. Currently, many forecast the NAO to shift into another negative phase, however over the past decade several extreme positive (2011/2012) and negative (2009/2010, 2010/2011) events during winter have been observed (Serreze and Barry, 2014). When the NAO is in a positive phase, larger pressure gradients exist between the two centers of action, and vice versa during the negative phase.

During positive phases, the Icelandic Low will transport cold polar air from the Canadian and Greenland Interior, promoting baroclinicity in the North Atlantic (Serreze and Barry, 2014). During the negative phase, the Icelandic Low migrates towards Greenland, a migration that is attributed to shifts in low-level North Atlantic air masses and ocean surface temperature patterns decreasing cyclone activity, moisture transport, and precipitation along the North Atlantic storm track (e.g., Rogers, 1997; Serreze et al. 1997; Belkin et al. 1998; Ulbrich and Christoph, 1999; Tsukernik et al. 2007; Vihma et al. 2012; Serreze and Barry, 2014; Wei et al. 2017). Rogers (1990) found that during extreme NAO phases, cyclone tracks over the central North Atlantic and Europe exhibited large latitudinal variation. Rogers (1997) followed up concluding that NAO positive phases exhibit maximum cyclone frequencies in the eastern North Atlantic and decreasing frequencies near Iceland and BB. Similarly, the study of Serreze et al. (1997) investigated NAO extremes and cyclone tracks in the winter months from 1966-1993 within the North Atlantic. Their results found that positive phases result in northward shifts of storm tracks while negative phases shift tracks southward. In addition, they observed cyclone frequencies

double, with significantly deeper centers in close proximity to the Icelandic Low during extreme positive phases. These results were also found by the comprehensive study of Wei et al. (2017). Recent studies by Serreze and Barry (2014) and Wei et al. (2017) emphasize that atmospheric teleconnections affect both the monthly and seasonal trends of cyclones, however they also emphasize the importance of sea ice in cyclone behavior and linkages to the NAO. Modelling studies conducted by Alexander et al. (2004) and Deser et al. (2004) observed northward shifts in the storm track during periods of sea ice retreat, yet the NAO had little input to the retreat periods. Serreze and Barry (2014) further mention that sea ice acts as a barrier between the ocean and atmosphere fluxes, which can lead to immediate and delayed effects towards the strength of Icelandic Low. Francis et al. (2009) and Overland and Wang (2010) investigated the delayed effects of the summer Arctic Sea ice on the following winter's NAO behavior. They found summers with below-average sea ice extent often led to more neutral or negative phases later in the year due to increased heat fluxes weakening the Polar Jet and diminishing the north-south temperature gradient. Due to pressure gradients being highest during the winter months, most research regarding the NAO's behavior has been focused on this time period (e.g., Trenberth and Paolino, 1980; Wallace and Gutzler, 1981; Hurrell 1996; Rogers, 1997; Thompson and Wallace, 1998; Portis et al. 2001).The study of Trenberth and Paolino (1980) found that the NAO accounted for up to one-third of the sea level pressure variability in the NH during winter months between 1899-1977. In addition, Hurrell (1996) found that from 1935-1994, the NAO contributed to nearly one-third of the temperature variation across the extratropical regions in the NH, nearly twice as much as the ENSO pattern. Due to both centers of action existing in the lower troposphere over the Atlantic, the phases of the NAO have since been found to influence climatological and oceanographic processes over the Atlantic, Europe, and the Arctic regions

(e.g., van Loon and Rogers 1978; Lamb and Peppler 1987; Moses et al. 1987; Mann and Drinkwater, 1994; Hurrell, 1995). These processes are associated with local/distant sea level pressure gradient variability, strength of the westerly wind pattern, and ocean surface temperature (Serreze and Barry, 2014).

Walker and Bliss (1932) developed the first NAO index using a combination of station-based air temperature, sea level pressure, and precipitation datasets over the United States and Europe. They identified the existence of the NAO through observing anomalies in low pressure over Iceland while higher pressure exists over the mid-Atlantic, concluding that the strongest gradients exist during the winter months (Serreze and Barry, 2014). Later studies continued to implement the station-based approach (Wallace and Gutzler, 1981) using sea level pressure standardization across several regions (e.g., Rogers, 1984; Hurrell, 1995 and 1996) and latitudinal sea level pressure variation (e.g., van Loon and Rogers, 1978). However, this straight-forward method fails to accurately measure the pressure gradients between the migrating centers of action due to each station's location being static. Portis et al. (2001) attempted to overcome this limitation by creating a "shifting" station-based NAO index. However, the use of empirical orthogonal functions (EOFs) or rotated principal component analysis (PC) using gridded domains of pressure and height have been developed (e.g., Trenberth and Paolino, 1980; Wallace and Gutzler, 1981; Barnston and Livezy, 1987; Thompson and Wallace, 1998, 2000a-b; Hurrell et al. 2003). According to Serreze and Barry (2014), EOF and PC methods are more robust than station-based data by using multiple variables; yet station-based data have longer records which can better track the long-term variability of the NAO's behavior.

When it comes to the NAO's long-term variability, observed shifts have been identified occurring from every few years to several decades in the studies of Hurrell and van Loon (1997)

and Cook et al. (1998); yet other studies (e.g., Hurrell et al. 2003) have argued that there are no significant maximums/minimums in the NAO's trend. Between these opposing viewpoints, the study of Hoerling et al. (2001) highlighted an even more major issue regarding the inability of climate models to duplicate the observed NAO trends. Just prior, the study of Rodewell et al. (1999) recommended incorporating sea surface temperature data from the North Atlantic to improve a majority of the NAO's observed trend. Due to these inconsistencies, there has been an increasing concern that sea surface temperatures affect the NAO more than previously thought (Serreze and Barry, 2014). However, some studies (e.g., Hoerling et al. 2001; Alexander et al. 2004; Deser et al. 2004) claim heat fluxes between the atmosphere and ocean surface in the Atlantic are insignificant, rather the overlooked gradual subtropical warming contributes to the NAO's decadal trend. However, there is a growing interest in the relationships between the freshwater flux from the Arctic to the North Atlantic (Serreze and Barry, 2014). The study of Dukhovskoy et al. (2004) is one of the first to attempt a calculation of the freshwater flux between Greenland and Norway and found that less fresh water entering the North Atlantic promotes deep water formation and widespread local heat fluxes in the lower troposphere, promoting baroclinicity, thus deepening the Icelandic Low. Harold et al. (1999) investigated polar low activity from infrared satellite imagery associated with the NAO over a two-year period. Their results found that during positive phases, more mid-size polar lows 200-600 km (125-375 mi) were observed in the eastern North Atlantic due to the enhanced baroclinicity in the Nordic Seas and a weakened Polar Front. Kolstad (2006) found relationships between the NAO and reverse shear polar lows (Duncan, 1977) where low level winds are not parallel to the thermal wind in adjoining layers. Although the NAO is the prominent atmospheric

teleconnection in the NH, has been seen proposed by some that it may be actually a local component of a larger pattern known as the Arctic Oscillation (AO) (Serreze and Barry, 2014).

1.5.2: Arctic Oscillation (AO)

The existence of the AO was first proposed in the studies of Lorenz (1951), Kutzbach (1970), and Wallace and Gutzler (1981), who argued that the NAO was actually a regional manifestation of a larger-scale atmospheric teleconnection over the high-latitudes. The major center of action of the AO is the Icelandic Low over the Atlantic-side of the Arctic, with several smaller high-pressure systems in the Atlantic and North Pacific. Yet, studies like Deser (2000) argued that the correlations between the smaller centers of action are insignificant, thus rejecting the AO as a broad teleconnection linking the Atlantic and Pacific. Another study by Ambaum et al. (2001) came to similar conclusions stating that the AO simply depicts similar variability in the Pacific and Atlantic sectors. Interestingly, prior to these arguments, Thompson and Wallace (1998) identified the AO based upon EOF-based climate analysis results from 1900-1997, which depicted the AO as the leading sea level pressure pattern in the NH during the winter months. In addition, they concluded the index of the AO reflects the variability of the stratospheric polar vortex, tropospheric flow, and surface pressure as one-single mode (zonal flow pattern) in the Arctic, unlike the NAO's index that is based on separate tropospheric and surface pressure (meridional flow pattern) in the North Atlantic. Only general characteristics of this "one mode" relationship between the atmosphere and surface have been discussed in the literature, however Serreze and Barry (2014) mention that much of the AO's structure is still unknown. They specify that stratospheric cooling associated with ozone levels and greenhouse gases are the primary topics of interest associated with the AO due to their potential effects on stratospheric motion.

The study of Ogi et al. (2004) conducted EOF analysis on geopotential heights in the troposphere of 40° N and found the size of the AO is smaller than in winter. Serreze and Barry (2014) mention that the AO's variability (primarily the Icelandic Low) is driven by the distribution of landmasses and orography of Greenland. The variability of the AO has been found to strongly influence atmospheric flow patterns over the midlatitudes and the Arctic, especially over the North Atlantic and North Pacific Oceans (Thompson and Wallace, 2000a-b). Serreze and Barry (2014) describe positive phases of the AO are associated with positive height anomalies over the Arctic (vice-versa in in the midlatitudes), thus a stronger pressure gradient exists. The opposite occurs during negative phases. Additionally, Serreze and Barry (2014) state when looking at spatial trends of the NAO and AO based on air temperature, especially in winter, they are highly-correlated; but the AO has a stronger positive signal over northern Eurasia and negative signal over the North Pacific. Due to this "connectivity" between the Atlantic and Pacific, the AO shares centers of actions with not only the NAO but a mode known as the Pacific Decadal Oscillation (PDO).

1.5.3: Pacific Decadal Oscillation (PDO)

The PDO is located over the North Pacific Ocean and regarded as the most important ENSO-like pattern in the NH (Serreze and Barry, 2014). Located north of the ENSO pattern, the PDO's sea surface temperature anomalies have been observed to be coupled with sea surface temperature anomalies of its neighboring mode over the South Pacific, but on magnitudes of decades instead of multiyear (Zhang et al. 1997; Mantua and Hare, 2002). Due to this coupling, scientists believe that the PDO amplifies the ENSO pattern's climate effects over the North American continent (Gershunov and Barnett, 1998). The PDO was first identified by Steven

Hare in 1996 while researching relationships between salmon production and climate in the North Pacific (Mantua et al. 1997). Unlike most other teleconnections in the NH, the PDO only has one center of action, the Aleutian Low. The PDO's variation is observed based upon changes in the Aleutian Low (resulting in air temperature anomalies over Alaska) and sea surface temperatures in different regions of the North Pacific with phases either being warm or cold (Hartmann and Wendler, 2003). Warm phases of the PDO are represented by abnormally high sea surface temperatures along the Pacific Coast of North America and abnormally low temperatures in the North Pacific interior accompanied by deeper central pressure values of the Aleutian Low (Serreze and Barry, 2014). In addition, Hartmann and Wendler (2003) found warm phases can result in trends of increased cloud cover, wind speed, and precipitation events over the North Pacific (opposite occurs during cold phases). Through the twentieth-century, phases of the PDO have lasted between two to three decades with cold phases occurring in the first and third quarters and warm phases occurring in the second and fourth quarters of the century. Serreze and Barry (2014) mention that the difference in average and seasonal temperatures between phases is over 3° C. The PDO's index is calculated using the leading PC of monthly sea surface temperature variability north of 20° N latitude (Serreze and Barry, 2014). During phase shifts the Aleutian Low can cause atmospheric 'blocking' of midlatitude and subpolar circulation. The behavior of the Aleutian Low is also strongly dependent on another teleconnection over the Pacific, the Pacific North American Oscillation (PNA). In regards to the PDO's influence on the Arctic, Screen and Francis (2016) found that due to sea ice loss in BB and LS, the negative phase of the PDO exhibits southerly and westerly winds which transport air from these subregions to the central Arctic. Furthermore, they claim the negative phase of the PDO is more effective than its positive phase at transporting sea ice driven surface temperature

anomalies within subregion outside the Arctic Ocean. However, they state that the PDO is not directly connected with Arctic warming, but by a weak indirect modulation of this pattern on the atmospheric response (primarily winds) to decreasing sea ice cover. Overall, they found the PDO has a weak direct relationship with the Arctic. Additionally, the results of Yu et al. (2017) provide an initial comprehensive overview of the long proposed theory that the opposite sea ice area trends in the Polar Regions may be related to low-frequency patterns. They found the positive PDO has a statistically significant relationship with decreasing Arctic sea ice, however they emphasized that a longer, high-resolution sea ice dataset needs to be implemented for improved confidence.

1.5.4: Pacific North American Pattern (PNA)

Similar to the PDO, the PNA is influenced by the ENSO pattern (Serreze and Barry, 2014), however the PNA is only associated with atmospheric variability. Positioned over the North Pacific Ocean and North America, the PNA has four primary centers of action (Blackmon et al. 1984). These centers of action relate to the atmospheric "wave train" flow pattern over the subtropical northeastern Pacific, Gulf of Alaska, northwestern North America, and southeastern United States (Baxter and Nigam, 2013). During the winter months, the PNA is strongest however, it can be identified through the year. During the summer season, all centers of action shift northward, are closer to each other, and have weaker pressure gradients and vice-versa during winter. Serreze and Barry (2014) mention that positive phases area associated with the ENSO's El Nino phase bringing higher-amplitude waves across the centers of action with abnormally higher geopotential heights over Hawaii and the western United States bringing above-normal temperatures over western Canada, Alaska, and polar latitudes while lower

geopotential heights exist over the Aleutian Islands and southeastern United States. The opposite occurs during negative phases which are connected to La Nina. The PNA's index is based upon EOF analysis of geopotential heights across the four centers of action. Even though a long-term trend of the PNA has been established, it only represents the interannual variability, not the intraseasonal and interseasonal variability (Baxter and Ingram, 2013). With this knowledge gap, much of the PNA's short-term effects and relationships with other teleconnections and regions is unknown.

The PNA is regarded as one of the most influential NH teleconnections affecting North American climate (Wallace and Gutzler, 1981); primarily impacting the hydroclimate variability over North America in winter (Baxter and Nigam, 2013). Baxter and Nigam (2013) found the PNA to be the fourth leading mode in the NH based upon EOF analysis. Due to the PNA being associated in part by the Aleutian Low, there have been theories relating to the interconnectedness of the PNA with the PDO, AO, and NAO. For example, Serreze and Barrett (2011) investigated the behavior of the Beaufort High in the Arctic and noticed its location was relatively similar during positive phases of the PNA and PDO and negative phases of the AO during the summer season. Baxter and Nigam (2013) concluded the PNA and the NAO have a lagged connection on the intraseasonal timescale and that the NAO's effect on the East Asian Jet Stream and its propagation could possibly dictate the "wave train" system over the Pacific thus influencing the PNA. Their results expanded upon and agreed with the work of Hoskins and Ambrizzi (1993). Another interest has been understanding the role tropical convection plays with the PNA's phases and structure. Franzke et al. (2011) found that intraseasonal convection in the tropics can weakly contribute to the PNA's wavelengths. Higgins and Mo, (1997) have found interannual tropical convection related to the Madden-Julian oscillation (Madden and Julian,

1971, 1972) can contribute to PNA development. Baxter and Nigam (2013) claim another important knowledge gap is the lack of measuring monthly changes in the PNA's behavior. Their justification for this claim is that the importance of accurately measuring monthly changes in the PNA could help extend the long-term accuracy of numerical weather models. It is worth mentioning that over a decade earlier, the results of Feldstein (2000) and Cash and Lee (2001) found the PNA's growth and decay life cycle occurs on average within two weeks. Feldstein (2000) utilized a daily, unfiltered PC time series of geopotential heights to come to their conclusion, whereas Cash and Lee (2001) used a linear multivariate stochastic model. According to Feldstein (2002), the idealized modelling study by Franzke et al. (2001) also came to the same temporal estimation. Feldstein (2002) also mentioned that several theories have been proposed as to what mechanisms account for the PNA's behavior. They are: (1) barotropic growth resulting from zonal asymmetry of the tropospheric circulation (e.g., Frederickson, 1983; Simmons et al. 1983; Branstator, 1990, 1992), (2) linear dispersion from a source of topographic or diabatic heating (e.g., Hoskins and Karoly, 1981), (3) combined baroclinic/barotropic instability (initial-value development) (e.g., Dole and Black 1990; Black and Dole, 1993), (4) changes in quasi-stationary eddies from zonal flow fluctuations (e.g., Branstator 1984; Nigam and Lindzen, 1989; Kang, 1990), and (5) feedback from high-frequency transient eddy fluxes (e.g., Egger and Schilling, 1983; Lau, 1988; Branstator, 1992; Ting and Lau, 1993). Based upon the results of Feldstein (2002), the two westward centers of action of the PNA grow by the first mechanism listed above and are positioned in favorable locations near the East Asia Jet exit. Dispersion then transfers the energy downstream to the other two centers of action causing them to strengthen. They also mention that divergence and Ekman pumping contribute to weakening of the PNA, but claim baroclinic processes could have an effect based upon modelling results from (Borges and

Sardeshmukh, 1995; Bladé, 1996; Sardeshmukh et al. 1997; Newman et al. 1997). Although the literature provides many suggestions as to what the physical contributors towards PNA development are, it remains difficult to determine what the most/least important factors are.

The relationships between the PNA and other features has been limited primarily just to other teleconnections: ENSO, PDO, AO, and NAO. However, the studies by Notaro et al. (2006), Wang et al. (2006), and Wei et al. (2017) compare the influence of the PNA to cyclones within the Arctic. All of these studies conclude the PNA is an important teleconnection regarding cyclone activity in the Arctic, specifically dominating the region around Newfoundland. The results of Wei et al. (2017) depict the PNA having the opposite effect on cyclone activity in the Chukchi/East Siberian Seas and the polar regions of the North American continent compared to the NAO and AO. The same study also examined the relationship between Arctic sea ice trends, cyclone track density, and the PNA's trends. Their conclusions found that cyclone track density and sea ice coverage in the Arctic were highly correlated; but only the AO and NAO contributed to Arctic sea ice changes. The AO, NAO, PDO, and PNA are teleconnections whose centers of action and effects comprise a large portion of the NH, thus affecting highly populated regions throughout the year. However, there are more small/seasonal teleconnections over remote areas which have not been researched as thoroughly. One example is the Polar/Eurasian Pattern (PEP).

1.5.5: Polar/Eurasian Pattern (PEP)

The PEP is one of the most prominent low-frequency wavelike teleconnections during the winter months (Liu et al. 2014; Wang and Zhang, 2015). It was first identified by Wallace and Gutzler (1981) who classified it as a mid-level, latitudinally oriented "wave train" over Europe and Asia, similar to the PNA. According to Liu et al. (2014), the PEP consists of three centers of

action in the troposphere: a dominant center over Siberia and two negatively correlated centers over northern Europe and Japan, having little interaction with the stratosphere. Positive phases of the PEP reflect below-normal heights over the North Atlantic, western Europe, and Japan strengthening the circumpolar vortex (East Asia Jet), with above-average heights over Siberia. In addition, positive phases can initiate substantial warming over northern Eurasia, the contiguous Arctic Ocean, and western North America (Liu et al. 2014). Negative phases depict the opposite. In either phase, the PEP always shows similar temporal and structural evolution rates of around one week (Wang and Zhang, 2015).

Variability of the PEP has been linked to major changes in the strength of the circumpolar circulation and associated with temperature and precipitation anomalies over Eurasia. For example, Park et al. (2010, 2011) found cold surges over Asia related to atmospheric "blocking" by the AO and PEP. Liu et al. (2014) found that winter sea surface temperature anomalies over the North Atlantic show significant coupling with the PEP's autumn to spring index values, suggesting forcing from North Atlantic sea surface temperatures on the PEP. They further highlight that the rate of transient eddies in the North Atlantic is very important to this forcing. Furthermore, Claud et al. (2007) found that positive phases of the PEP can produce strong northerly winds over BB and DS during winter, and high correlations in December of reverse shear polar lows near Greenland. In addition, they found correlation between the PEP and sea surface temperatures in the North Atlantic in January and February. Other studies propose that the PEP is a key process in the NH decadal geopotential height shift (Watanabe and Nitta, 1999; Ohhashi and Yamazaki, 1999). Most studies however, focus on the PEP's influences on China, Korea, and Japan's climate (e.g., Gong et al. 2002; Tachibana et al. 2008; Sung et al. 2009; Liu and Chen, 2012). From 1948-2008, Liu et al. (2014) found that the

PEP accounts for up to twenty percent of the temperature variance over East Asia, higher than any other major teleconnection.

Wang and Zhang (2015) state another knowledge gap associated with the PEP relates to both local/remote climate anomalies and the PEP's evolution. They describe the PEP as having four centers of action during its development period, then becoming three during the maintenance and decaying periods. Furthermore, they find that the development of the four centers of action occur starting about a week before the PEP's maximum amplitude is reached. They proposed that baroclinic instability may influence the behavior of the four anomalies during their initial formation, but barotropic instability maintains them. Once the decaying stage starts, the anomaly over Scandinavia dissipates. As far as how the PEP spawns and decays, Wang and Zhang (2015) conclude that advection and the magnitude of vorticity of transient eddies plays a critical role, with advection and divergence also contributing. Nowhere else in the literature is there mention of cyclone-related processes related to the PEP. Liu et al. (2014) explains the PEP is unique compared to the other dominant winter patterns in the NH. Nakamura et al. (1987) found the seesaw structure of the PEP is not as evident as other modes like the PNA. Due to this, it has been theorized that the PEP is driven by baroclinicity due to its weaker structure, unable to obtain the kinetic energy affiliated with larger teleconnections.

One of the largest arguments regarding the PEP is its similarity and uniqueness to other regional teleconnections. This started with the discovery of Barnston and Livezey (1987) who found two different variations of the PEP's centers of action over the same regions. Due to this find, these PEP variations were classified as the Scandinavia pattern (SCAND) and the East Atlantic/Western Russia pattern (EAWR). Liu et al. (2014) state these two variants still resemble the original PEP's structure. With the identification of the SCAND and EAWR, studies of the

original PEP have been sparse over the past three decades (e.g., Hongbao, 1993; Haishan and Zhaobo, 2003; Sung et al. 2009). Liu et al. (2014) claim the reason for this relates to the two variants of the PEP closely resembling the original pattern's centers of action. Interestingly, the literature claims the SCAND and EAWR patterns have different climatic impacts (e.g., Zveryaev, 2006; Casado et al. 2009; Hongbao, 1993; Haishan and Zhaobo, 2003) between each other and the original PEP. The study by Liu et al. (2014) was the first attempt to clarify the similarities and differences between these variants and the PEP. Their results found that all three modes can be found using a rotated empirical orthogonal function analysis on 500 hPa mean geopotential height data, and that all are characterized by inter-annual variability. However, the rate of variability differs between two to four years for the SCAND and four to eight years for the PEP and EAWR. Liu et al. (2014) also mention that the EAWR has no identifiable relationship with sea ice in the Arctic. They further discuss the EAWR could be potentially driven in part by the snow cover in North America; however the PEP and SCAND appear to only have external forcing originating in the tropics. Even though the results of Liu et al. (2014) provide clarity between these three teleconnections, they emphasize the need to further investigate the similarities primarily between the EAWR and PEP patterns due their contrasts in location and possible external forcing variables. Their final remarks relate to the need of data-dependent results to further find relationships between them and possible external forcing factors.

1.5.6: East Atlantic/West Russia Pattern (EAWR)

The EAWR pattern, as mentioned above, is a variation of the PEP first depicted by Gutzler and Liveley (1987). Similar to the PEP, this feature is prominent from mid-winter

through late spring. According to Ionita (2014) the EAWR is seen as the second most prominent teleconnection over the North Atlantic region during winter behind the NAO. The EAWR consists of four centers of action concentrated over Eurasia, forming a "wavetrain" from the east coast of the United States to eastern China/Siberia (Liu et al. 2014). Negative phases are associated with lower than normal pressure and polar air over the eastern North Atlantic (Claud et al. 2007). Above normal precipitation occurs over China, while drier conditions are apparent over Europe (Ionita, 2014). Surface temperature trends depict above normal values over east Asia and below normal temperatures over western and northeastern Russia (Barnston and Livezy, 1987). In addition, analysis of the EAWR's positive phases show decreasing frequency of cyclone events over the Mediterranean. In addition, Liu et al. (2014) found that the EAWR pattern contributes to significant surface cooling (exceeding -0.6° C) near Newfoundland and Labrador.

The literature review in Ionita (2014) mentions most studies relating to the EAWR pattern relate to cyclonic activities around the Mediterranean region. Although their study was centered toward the EAWR's effects on Europe's hydroclimatology, they point out that even with their results there is high uncertainty of whether this teleconnection is influenced by either local or distant climate change events. Claud et al. (2007) discuss possible linkages of the EAWR to polar low development in the North Atlantic. They state that negative phases lead to intensification of the North Atlantic storm track and cyclogenesis in its southeastern region. In addition, they found the EAWR pattern to have no correlation with sea surface temperatures in the North Atlantic. However, their conclusions for the EAWR index is that it is primarily associated with the 300 hPa easterly winds over the North Atlantic in early winter, promoting a decreased likelihood of cyclones throughout the North Atlantic, with exceptions from December

to February due to strong northerly winds promoting baroclinicity. Due to the EAWR and PEP having only been known for roughly three decades, having smaller spatial scales compared to the NAO, and being situated over vast remote regions of Europe and Asia, the literature pertaining to these patterns is very limited, focusing primarily on Europe and Asia's climate.

1.5.7: Teleconnections Overview

The role of teleconnections on climate change has been an ongoing interest. Their extent, climatic impacts, and temporal variability greatly vary both intra and inter-annually. Since the early twentieth-century, teleconnections have been identified and their behavior measured. Early measurements were based upon sea level pressure measured at various weather stations in several regions over several years. As teleconnections began to gain more interest, more sophisticated methods were applied such as EOFs and PC analysis which are still implemented currently. With a growing data record available towards the end of the twentieth-century, interest expanded towards understanding the linkages between teleconnections and as well as the local and global impacts. However, there have been several arguments regarding the existence of some teleconnections like the AO and the two variations of the PEP which leads to several knowledge gaps pertaining towards their existence, behavior, and climatic impacts. The AO and NAO teleconnections have been of the most interest due to their influence on the North Atlantic and Arctic in regards to cyclone activity and sea ice export. Due to these modes being the most dominant during winter, the neighboring PEP and EAWR patterns have very little influence with the sea surface temperatures and North Atlantic climate overall. The AO has been argued to be connected to the PDO and PNA patterns over the Pacific Ocean by all containing the Aleutian Low as one of the centers of action. Due to being in the Pacific Ocean, the PDO and PNA have

been found to be linked to the ENSO pattern through the ocean and atmosphere, thus extending ENSO's effect in the middle and high-latitudes. Due to these linkages between teleconnections in the Pacific, regions along the Pacific Coast of North America and in the southeastern United States can potentially forecast general conditions in their areas based upon ENSO pattern's phase. However, this technique is more robust with certain teleconnections than others in the NH. Over previous decades, the general characteristics of the major NH teleconnections have been researched thoroughly, which brought forth new knowledge gaps relating to: understanding their behavior at the seasonal and monthly timescales to improve forecast modelling, their structures, influences on neighboring teleconnections, and identifying new proxies (e.g., sea ice, cyclones, wind patterns, precipitation, etc.) to potentially identify complex relationships between certain regions and particular teleconnections.

1.6: Objectives

The North Atlantic region is one of the most cyclonically active regions in the NH. The complexity of the local ocean currents, global atmospheric circulation patterns, teleconnections, topography, and sea ice area fluctuations in this region present several knowledge gaps, leading to a limited understanding of the interconnectedness between the atmosphere, cryosphere, and hydrosphere within the North Atlantic. The BB-DS-LS subregion has been overlooked due to its remoteness from both the Arctic and North Atlantic. However, BB, DS, and LS play an important role in sea ice and freshwater interactions between the Arctic and North Atlantic Oceans as well as marine ecosystems near the North Water and sea ice edge. These subregions are a primary route of the fresh, colder polar water to the deep water convection cell in LS which, in turn, contributes to the thermohaline circulation and meridional overturning in the

North Atlantic. The variability of this process in LS has also been of concern due to being influenced by changes in the freshwater budget and water column chemistry northward in BB and DS. Several studies have shown BB/DS's intake of freshwater increasing due to higher rates of Arctic sea ice decline and along the western shore of Greenland's ice sheet each melting season. In addition, BB, DS, and LS are some of the most cyclonically active areas in the North Atlantic due their location just north of the primary path of the midlatitude westerlies along the North Atlantic storm track. Cyclone activity in the North Atlantic is controlled by a complex mixture of inputs from teleconnections, air/water temperature gradients, and sea ice export; thus not one single variable or system is responsible for cyclone behavior in these subregions. While these systems have been extensively researched for the North Atlantic, this is not the case for BB, DS, and LS. North Atlantic cyclone research has focused primarily on storm track density, migration, and deepening events. Most studies (e.g., Rogers and Thompson, 1995; Hanson et al. 2004; Mallet et al. 2013; Kar-Man Chang, 2018) group BB, DS, and LS as part of the North Atlantic, briefly mentioning these subregions (e.g., Serreze, 1995; Serreze et al. 1997). This is especially true regarding cyclone bifurcation events along Greenland's southern tip (Tsukernik et al. 2007). Studies in the past decade have started to solely focus on these subregions (e.g., Azetsu-Scott et al. 2012; Heide-Jørgensen et al. 2013; Ortega et al. 2017; and Bi et al. 2019) but most do not pertain to cyclone behavior and what variables influence them. Just like the North Atlantic, all potentially relevant variables need to be taken into account to obtain an improved understanding of the cyclonic activity in BB, DS, and LS. These variables include considering the effects of teleconnections and sea ice. Over the past five decades, the oceanic structure of BB, DS, and LS has been the most extensively covered topic in these subregions (e.g., Muench, 1971; Fissel et al. 1982; Bourke et al. 1989; Ross, 1990a-b and 1991; Lazier, 1995; Melling et al.

2001; Tang et al. 2004; Cuny et al. 2005; Zweng and Münchow, 2006; Heide-Jørgensen et al. 2007; Azetsu-Scott et al. 2012). In addition, the role on local sea ice export has also been discussed (e.g., Wang et al. 1994; Parkinson, 1995; Valeur et al. 1996; Parkinson et al. 1999; Barber et al. 2001; Stern and Heide-Jørgensen, 2003; Tang et al. 2004; Kwok, 2005, 2007; Samelson et al. 2006; Parkinson and Cavalieri, 2008; Bi et al. 2019). However, local sea ice trends in this region across multiple decades have only been discussed in a few studies (e.g., Wang et al. 1994; Mysak et al. 1996; Parkinson et al. 1999; Stern and Heide-Jørgensen, 2003; Heide-Jørgensen et al. 2007; Cavalieri and Parkinson, 2012; Bi et al. 2019). Furthermore, the effects of certain patterns on BB, DS, and LS's climates are only minimally discussed in the literature (e.g., Lazier, 1995; Mysak et al. 1996; Serreze et al. 1997; Mallet et al. 2013; Ortega, 2017). Additional research is required investigating how cyclones in BB, DS, and LS are influenced by teleconnections and their local sea ice cover.

Due to these knowledge gaps, this thesis will identify the influence local sea ice cover and remote NH teleconnection patterns have on cyclones in BB, DS, and LS. To accomplish this goal, the following questions will be addressed:

1) *What is the sea ice area variability in Baffin Bay, Davis Strait, and Labrador Sea and how does it compare to the Northern Hemisphere's?*
2) *What is the cyclone variability in Baffin Bay, Davis Strait, and Labrador Sea?*
3) *Is cyclone variability in Baffin Bay, Davis Strait, and Labrador Sea influenced more by local sea ice area or specific remote teleconnection pattern(s)?*

2. DATA AND METHODS

2.1: Sea Ice Area

Sea ice extent data used in Objective 1's analyses was acquired from the National Snow and Ice Data Center's (NSIDC) Sea Ice Index with a resolution of 25 km x 25 km and a sea ice area cover threshold of 15% per pixel. Sea ice extent shapefiles were downloaded for each month from January 1980 to December 2015, however, December 1987 and January 1988 were excluded due to a gap in the satellite data from December 3rd to January 13th making the time period 430 months instead of 432. Monthly sea ice areas for the NH were calculated using Python within ESRI's ArcMap software. To validate the accuracy of these values, the NH's March sea ice extent anomalies values were calculated and compared with NSIDC's NH Extent Anomalies for March 1979-2019. To obtain sea ice areas for BB, DS, and LS, three polygons were drawn depicting each subregions' boundaries based on the International Hydrographic Organization's 1953 definitions in *Limits of Oceans and Seas* (Figure 1). Finally, these polygons were merged to create a single new polygon representing the overall subregion (BB-DS-LS). The areas of each polygon were 507,000 km^2 (BB), 773,000 km^2 (DS), 907,000 km^2 (LS), and 2,187,000 km^2 (BB-DS-LS). For the complete list boundary parameters, refer to pages 10-11 in International Hydrographic Organization (1953).

The four polygons were then used to extract their respective sea ice areas each month from the NH's sea ice data. The NH and each subregions' sea ice area maximums, means, minimums, and standard deviations were calculated. To qualitatively compare the NH's monthly sea ice area values to each subregion (BB-DS-LS, BB, DS, and LS), their respective 430-month

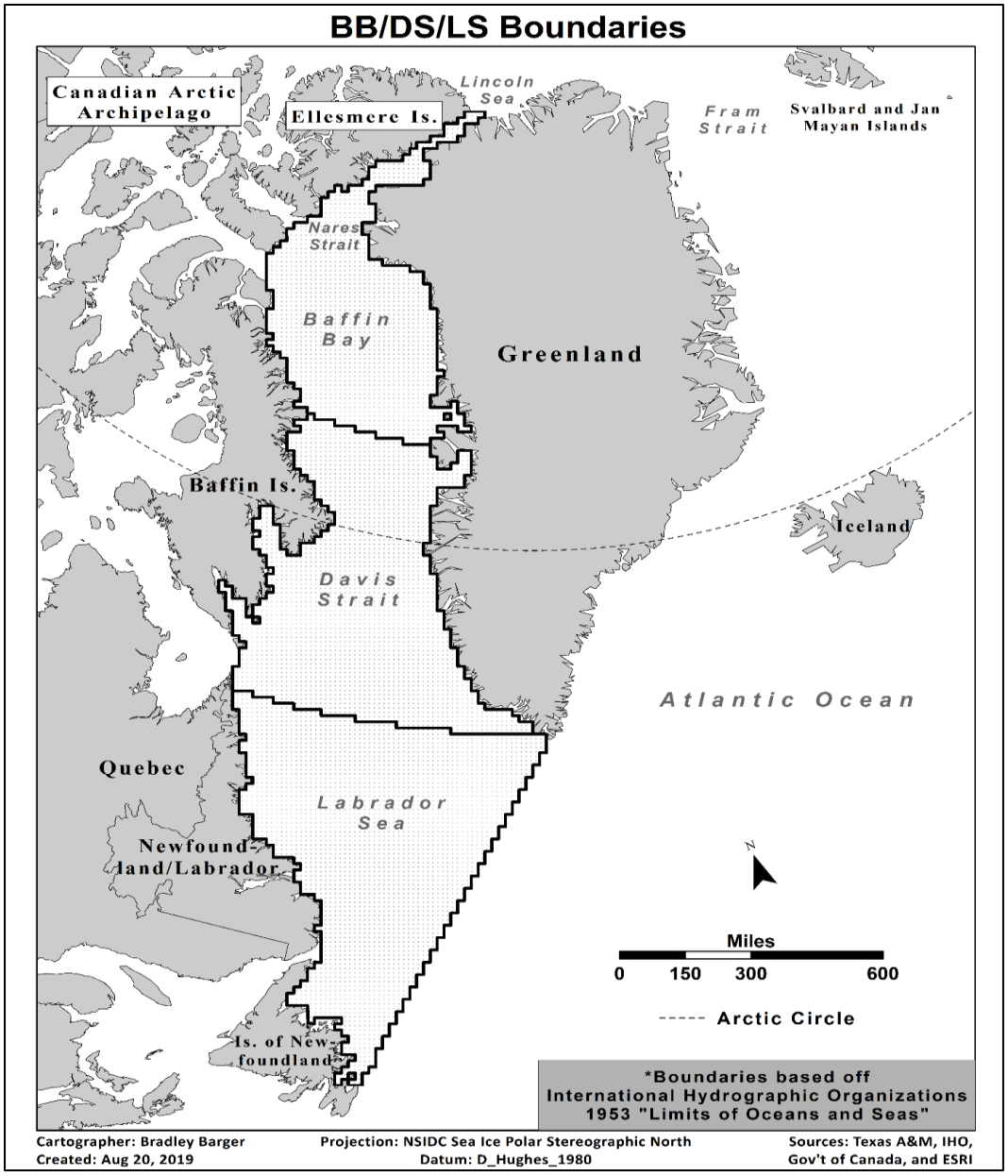

Figure 1: Boundaries of BB, DS, and LS.

(January 1980-December 2015) and individual monthly (e.g., January 1980-2015) values were plotted as time series. Additionally, their trends were calculated using linear least-squares regression and visually compared at both timescales. Using the monthly slope values, the

approximate monthly, annual (calendar year), and total sea ice area variabilities for the NH and each subregion were calculated for quantitative comparisons. To further quantitatively compare sea ice area variability and identify any relationships between the NH and each subregion, correlations and their significances (using the 95% confidence level) were calculated for the 430-month and individual monthly timescales.

In addition to analyzing the original monthly sea ice area values, due to the NH and each subregion's sea ice areas differing greatly, the five 430-month datasets were standardized for preliminary comparisons. The seasonal cycle and long-term trends were also removed. During this data pre-processing, every March and April for BB experienced complete sea ice cover and every September in LS was ice-free. Therefore, these subregions had standard deviations of zero in these months and could not be seasonally standardized. Due to this, these months were omitted from every long-term dataset, reducing the final overall temporal length to 322 months. Similar to the raw monthly values, they were plotted as time series for preliminary qualitative comparisons and correlation coefficients (using the 95% confidence interval) were calculated.

2.2: Cyclone Variables

For Objective 2, 6-hourly cyclone data were obtained from NSIDC's NH Cyclone Locations and Characteristics record derived from NCEP/NCAR Reanalysis with a spatial resolution of 250 x 250 km. Seven variables were analyzed: annual system number, central pressure, cyclogenesis event, cyclolysis event, local laplacian (a measure of cyclone intensity), latitude, and longitude. The 6-hourly NH cyclone events were downloaded and converted to annual records, then converted to shapefiles. Each shapefile's annual record was subsetted to only those having at least one time step within the BB-DS-LS polygon (Figure 2). From these

subsetted annual datasets, cyclone events with at least one time step within the BB, DS, or LS polygons were extracted for each month. A python script was then implemented to calculate the maximum, mean, and minimum values for each unique cyclone system in each month for each variable (excluding annual system number, cyclogenesis, and cyclolysis events). From these subsets, the overall monthly maximums, means, and minimums for each variable were calculated. Furthermore, the total was calculated for number of cyclone systems, cyclogenesis events, and cyclolysis events. For consistency with the sea ice datasets, December 1987 and

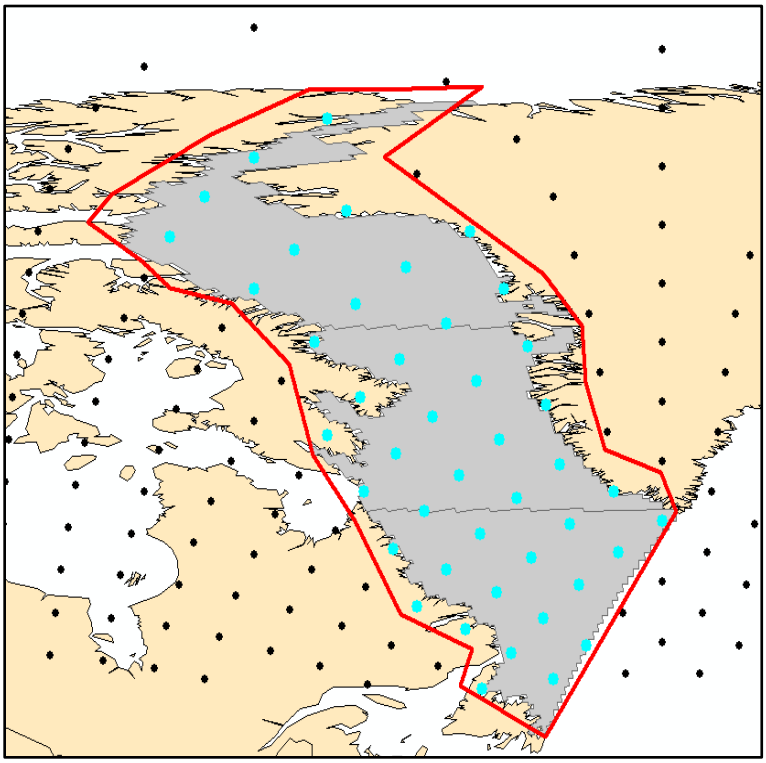

Figure 2: Polygon of the BB-DS-LS subregion (red line) used to subset cyclone time steps from the grid cell centers within (cyan circles; 44 total).

January 1988 were omitted. The 430-month and individual monthly statistics datasets were plotted as time series and trends were calculated using linear least-squares regression. Additionally, correlations (using the 95% confidence interval) were used to determine if any relationships comparing the same cyclone variable between the subregions exist. All 430-month statistics datasets were seasonally standardized and detrended, while the individual monthly datasets were only detrended. March, April, and September were also omitted from each year to obtain the same 322-month temporal length for Objective 3. Correlations (95% confidence interval) compared the same cyclone variables between the subregions. Histograms with the total number of cyclones for each month in each subregion were also created (Appendix A).

2.3: Teleconnections

For the remote driver comparison in Objective 3, monthly values for the NAO, PNA, PEP, and EAWR (obtained from NOAA's Climate Prediction Center), as well as for the AO and PDO (from NOAA's National Centers for Environmental Prediction) were used. Like the sea ice area and cyclone datasets, December 1987 and January 1988 were omitted to make the raw datasets span the same 430 months as previous analyses. The teleconnection indices did not need to be standardized. The original values were plotted as time series with trend lines (using linear least-squares regression) for preliminary comparisons. Additionally, correlations (95% confidence level) were calculated for the comparisons between each pattern to identify any relationships between them. Following the procedure of the sea ice and cyclone statistics datasets, March, April, and September were removed from each year in every teleconnection dataset before seasonally standardizing and detrending. Each pattern's time series was also compared monthly, and the detrended values compared in Objective 3.

2.4: Cyclone Variable Comparisons with Sea Ice Area and Teleconnections

For Objective 3, the 322-month and individual monthly cyclone datasets (Objective 2) were compared with the finalized sea ice area data (Objective 1) and teleconnections indices (Objective 3). Correlation (95% confidence interval) was used to identify relationships between each sea ice area and teleconnection dataset with each cyclone variable for each subregion.

3. RESULTS

3.1 Objective 1: What is the Sea Ice Variability in Baffin Bay, Davis Strait, and Labrador Sea, and how do they compare to the Northern Hemisphere?

Objective 1's goal was to identify the monthly and long-term 1980-2015 sea ice area variability for BB-DS-LS, BB, DS, and LS. Understanding sea ice variability within each subregion and their relationships with the NH can help determine if these subregions show overall similar or distinct variability with the NH. Objective 1's results present an overview of the significant observations in the 430 and 322-month, as well as the individual monthly, sea ice comparisons.

3.1.1: Long-Term and Monthly Sea Ice Area Relationships

When comparing each subregion's sea ice areas against the NH at both the 430 (original) and 322-month (seasonally standardized and detrended) timescales, all have significant, positive correlations, indicating that sea ice area in each subregion varies somewhat in-phase with the NH over the entire time period (Table 1). For every subregion, 430-month correlations were inflated by the strong seasonal cycle and long-term trends, which can be seen by the large differences between the 430 (0.82 and 0.96) and 322-month (0.11 and 0.30) correlation ranges. For the 322-month comparisons, BB-DS-LS had the strongest significant correlation with the NH (0.30) followed by DS (0.25), then BB (0.21) and finally LS (0.11). At the individual monthly scale, correlations (all positive) were also inflated, albeit to a smaller degree, by their common long-term trends. Due to these influences, only the 322-month and detrended monthly correlations will be discussed.

Region/Subregion	*Original*	*Seasonally Standardized and Detrended*
NH/BB-DS-LS	0.96*	0.30*
NH/BB	0.91*	0.21*
NH/DS	0.93*	0.25*
NH/LS	0.82*	0.11*

Table 1: Original (430-month) and seasonally standardized and detrended (322-month) sea ice area correlations. * signifies p-value < 0.05.

For the individual monthly detrended-value comparisons (right-half of Table 2), March, June-September, and November were the only months with significant correlations; with June and November having the most subregions significantly correlated with the NH. BB could not be compared with the NH in March or April due to not having any change in sea ice area during these months. Furthermore, due to the lack of sea ice in LS in September across the entire time period, LS could not be compared with the NH in this month. BB-DS-LS had the most significantly correlated months with the NH (6; March, June-September, and November). However, BB-DS-LS did not always have the highest correlation (e.g., June-September). For BB-DS-LS, November had the strongest significant correlation (0.48), whereas September had the weakest (0.33). BB's strongest significant correlation was in August (0.51), while the weakest was in September and November (0.43). DS's strongest significant correlation was in July (0.51) whereas the weakest was in March (0.33). LS was only significantly correlated with the NH in June (0.36).

The largest and smallest differences in correlation after seasonally standardizing and detrending was BB-DS-LS in July (0.82 to 0.43) and in September (0.36 to 0.33). In regards to correlation strength, the seasonally standardized and detrended analysis only had one occurrence when a correlation value was stronger than one in the original-value analysis: NH/BB in September (0.36 to 0.43).

Month	Original				Detrended			
	NH/ BB-DS-LS	NH/ BB	NH/ DS	NH/ LS	NH/ BB-DS-LS	NH/ BB	NH/ DS	NH/ LS
Jan	0.53*	0.30	0.45*	0.56*	0.13	0.08	0.10	0.15
Feb	0.55*	0.30	0.51*	0.54*	0.19	0.22	0.24	0.11
Mar	0.50*	N/A	0.44*	0.50*	0.36*	N/A	0.33*	0.33
Apr	0.45*	N/A	0.43*	0.43*	0.19	N/A	0.15	0.20
May	0.46*	0.28	0.41*	0.45*	0.18	0.02	0.09	0.22
Jun	0.75*	0.47*	0.61*	0.61*	0.38*	-0.04	0.43*	0.36*
Jul	0.82*	0.69*	0.76*	0.34*	0.43*	0.23	0.50*	-0.06
Aug	0.64*	0.60*	0.53*	0.60*	0.47*	0.51*	0.27	-0.13
Sep	0.36*	0.36*	0.14	N/A	0.33*	0.43*	-0.13	N/A
Oct	0.59*	0.58*	0.37*	0.20	0.28	0.28	0.12	0.00
Nov	0.73*	0.66*	0.72*	0.35*	0.48*	0.43*	0.46*	0.22
Dec	0.61*	0.59*	0.60*	0.53*	0.21	0.31	0.27	0.06

Table 2: Individual monthly original and detrended sea ice value correlations between the NH and each subregion from 1980-2015. * signifies p-value < 0.05.

3.1.2: Sea Ice Area Variability

Across the 430-month, annual, and monthly periods, the NH and every subregions' sea ice areas have significant negative trends, but at different magnitudes (Table 3). For each individual month (e.g., January 1980-2015), the NH shows significant negative trends (Table 4), whereas BB-DS-LS had all months but September having significant negative trends. BB had the highest number of months with not-significant trends (5; January-April, and September), whereas DS (March and September) and LS (October and November) only had 2 non-significant months. For BB-DS-LS and its subregions, the months with the largest negative trends in sea ice do not align with the months when maximum/minimum mean sea ice area coverage occurs (Table 5), but closer to months when large changes in sea ice cover occurs.

Region/Subregion	*Monthly (km^2)*	*Annual (km^2)*	*Total (km^2)*
NH	-4917*	-59,004*	-2,124,144*
BB-DS-LS	-666*	-7,992*	-287,712*
BB	-161*	-1,932*	-69,552*
DS	-276*	-3,312*	-119,232*
LS	-230*	-2760*	-99,360*

Table 3: Monthly, annual, and total sea ice area losses for the NH and each subregion. * signifies p-value < 0.05.

Month	*NH (km^2)*	*BB-DS-LS (km^2)*	*BB (km^2)*	*DS (km^2)*	*LS (km^2)*
Jan	-47,600*	-10,970*	-260	-4,670*	-6,040*
Feb	-47,500*	-9,480*	-60	-4,440*	-4,980*
Mar	-42,200*	-6,510*	0	-2,800	-3,710*
Apr	-37,400*	-7,020*	0	-3,190*	-3,830*
May	-31,200*	-6,700*	-160*	-2,910*	-3,630*
Jun	-43,100*	8,130*	-3,020*	-2,310*	-2,810*
Jul	-74,300*	-11,220*	-6,410*	-4,110*	-700*
Aug	-75,400*	-3,290*	-1,780*	-1,430*	-80*
Sep	-88,100*	-560	-380	-190	N/A
Oct	-62,400*	-6,790*	-6,160*	-630*	-2
Nov	-55,700*	-6,660*	-1,940*	-4,660*	-60
Dec	-45,200*	-9,250*	-1,010*	-4,550*	-3,690*

Table 4: Monthly sea ice area loss for the NH and each subregion on a year-to-year basis (e.g., January 1980-January 1981). Red cells indicate months when maximum significant sea ice area loss occurred (vice-versa for blue cells). * signifies p-value < 0.05.

Month	*NH (km^2)*	*BB-DS-LS (km^2)*	*BB (km^2)*	*DS (km^2)*	*LS (km^2)*
Jan	14,555,661	1,214,618	504,339	460,732	249,547
Feb	15,484,635	1,369,568	506,424	510,017	353,127
Mar	15,651,441	1,394,565	506,875	537,760	349,929
Apr	14,807,170	1,306,199	506,875	509,531	289,793
May	13,259,722	1,116,244	504,566	422,899	188,779

Table 5: Monthly sea ice area coverages for the NH and each subregion averaged from 1980-2015. Red cells indicate month of maximum sea ice area (vice-versa for blue cells).

Month	*NH (km^2)*	*BB-DS-LS (km^2)*	*BB (km^2)*	*DS (km^2)*	*LS (km^2)*
Jun	11,646,684	820,408	430,069	310,764	79,574
Jul	9,314,201	420,920	238,872	173,281	8,767
Aug	6,802,118	94,878	61,615	32,396	868
Sep	6,065,712	58,889	50,972	7,917	0
Oct	8,468,108	215,191	202,240	12,934	17
Nov	10,633,646	617,188	443,368	172,934	885
Dec	12,895,304	905,834	489,411	356,339	60,084

Table 5 Continued

3.1.2.1: NH Sea Ice Variability

The NH's 430-month trend shows a loss of 5,000 km^2/month of sea ice (59,000 km^2/year or 2.1 million km^2 total; Figure 3 and Table 3). The NH's absolute maximum sea ice area occurred in March 1988 reaching 16.4 million km^2, whereas its overall minimum occurred in September 2012 at an area of 3.5 million km^2 (Table 6). The mean sea ice area was 11.6 million km^2. At the individual monthly scale, the NH lost the most sea ice area between each September (88,000 km^2), but lost the least between each May (31,000 km^2; Table 4). The NH's average sea ice area for the entire 430-month period occurred in March (15.7 million km^2) whereas September had the lowest (6 million km^2; Table 5).

The NH's annual sea ice area minimums show more variation than the maximums from 1980-2015. From 1980-1995, annual maximums surpassed 15.7 million km^2, but decreased in 1995. Beginning in 1996, the NH's annual maximum dropped below 15.5 million km^2 for the first time. From 2008-2011, annual maximums gradually decreased from 15.4 million km^2 to

14.5 million km^2, and repeats for 2012-2015. From 1980-1989 annual minimums were from 6.7 to 7.8 million km^2. In 1995, the annual minimum dropped below 6 million km^2 for the first time, followed by the overall highest minimum in 1996 (8 million km^2). From 2002 onwards, all

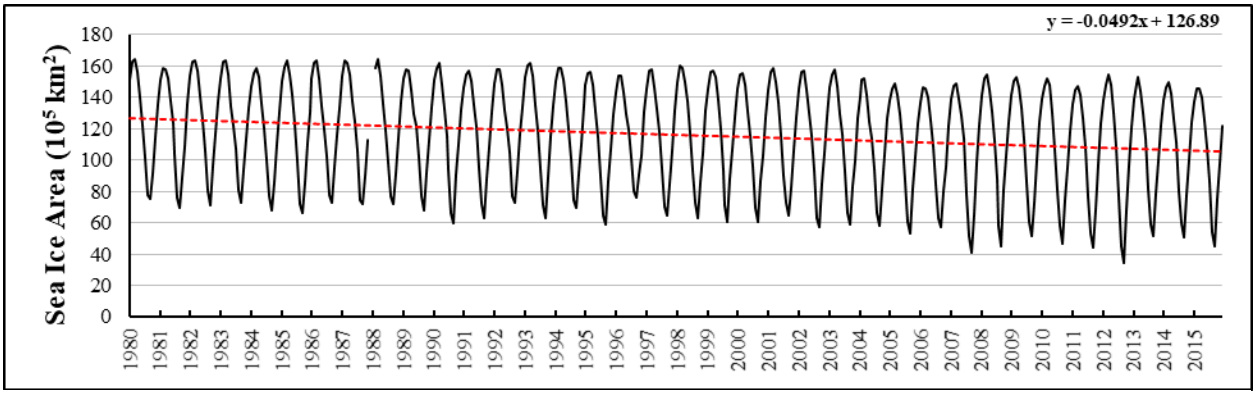

Figure 3: The NH's 430-month sea ice area time series with trend line in red. Slope equation in upper-right corner.

Region/Subregion	***Max (km^2)***	***Min (km^2)***	***Mean (km^2)***	***St. Dev. (km^2)***
NH	16,426,875 *(Mar '88)*	3,455,625 *(Sep '12)*	11,622,297	3,300,729
BB-DS-LS	1,776,758 *(Mar '83)*	25,625 *(Sep '14)*	793,306	504,195
BB	506,875 *(41.4% of time period)*	16,875 *(Aug '14)*	369,881	180,295
DS	759,375 *(Mar '93)*	3,750 *(Sep '86, '87, '88)*	291,751	208,531
LS	538,008 *(Feb '84)*	0 *(28.1% of time period)*	131,674	154,723

Table 6: 430-month maximum, minimum, mean, and standard deviation sea ice area statistics for the NH and each subregion.

annual minimums were below 6 million km^2. 2006-2007's minimums dropped by over 1.5 million km^2 from 6 million to 4 million km^2 (the largest annual change across the time period). 2008-2009's minimums increased to 5.2 million km^2, followed by the NH's lowest sea ice area minimum in 2012 (3.5 million km^2).

322-month seasonally standardized and detrended values for the NH show more extreme negative than positive monthly deviations across the time period. The strongest negative deviations occurred in the last decade where five minimums surpassed -1.00 standard deviations (SD) (Figure 4). Sea ice areas deviations remained small through most of the first decade. Then in early 1989, one of the largest monthly negative deviations occurred in the time period surpassing -1.50 SD. 1993-1994 saw moderate positive deviations (0.38 to 1.13 SD). From 1995 to early 1996, sea ice area experienced small-moderate negative monthly deviations (up to -0.83

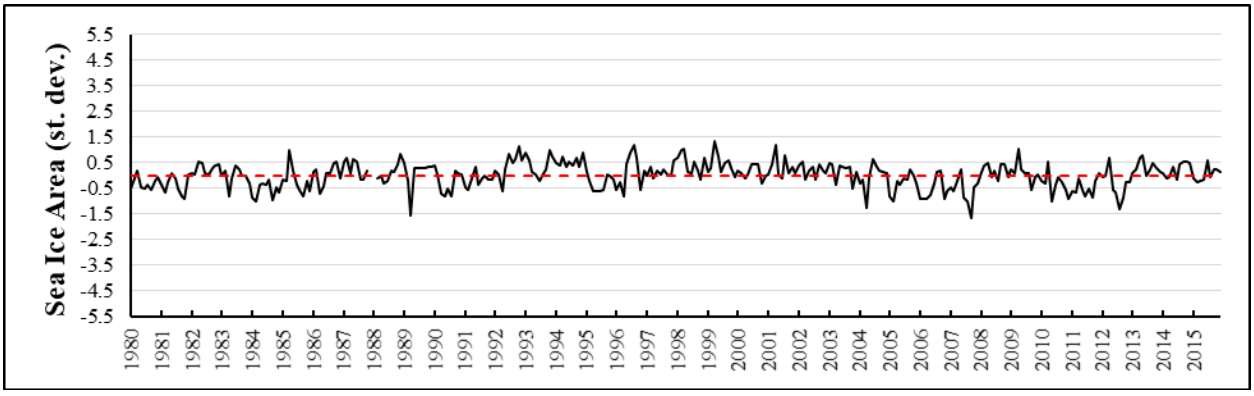

Figure 4: The NH's 322-month sea ice area variability (seasonally standardized and detrended).

SD), then rapidly shifted to one of the largest positive deviations of the time period (reaching 1.17 SD). The largest positive deviations of the entire time period occurred in early 1999 and

2001 surpassing 1.20 SD). Deviations became weaker until early 2004. From 2004-2008, monthly deviations were dominantly negative, in early 2004 to late 2006 several minimums greater than -0.90 SD occurred. The largest negative deviation of the time period occurred in late 2007 reaching -1.64 SD, while another large negative deviation surpassed -1.30 SD in mid-2012.

3.1.2.2: BB-DS-LS Sea Ice Variability

BB-DS-LS's 430-month sea ice area trend shows a more gradual decline than the NH, losing 650 km^2/month (8,000 km^2/year or 290,000 km^2 total; Figure 5 and Table 3). BB-DS-LS's largest sea ice maximum occurred in March 1983 reaching 1.78 million km^2 (81% of BB-DS-LS's total area) with the mean being 793,000 km^2 (36% of BB-DS-LS's total area) and minimum (September 2014) reaching 25,500 km^2 (1% of BB-DS-LS's total area). Between each July, BB-DS-LS experienced the most significant sea ice area loss (11,220 km^2), whereas the least was lost between every August (3,300 km^2; Table 4). Similar to the NH, March had the highest average sea ice area (1.4 million km^2) and September had the lowest (59,000 km^2).

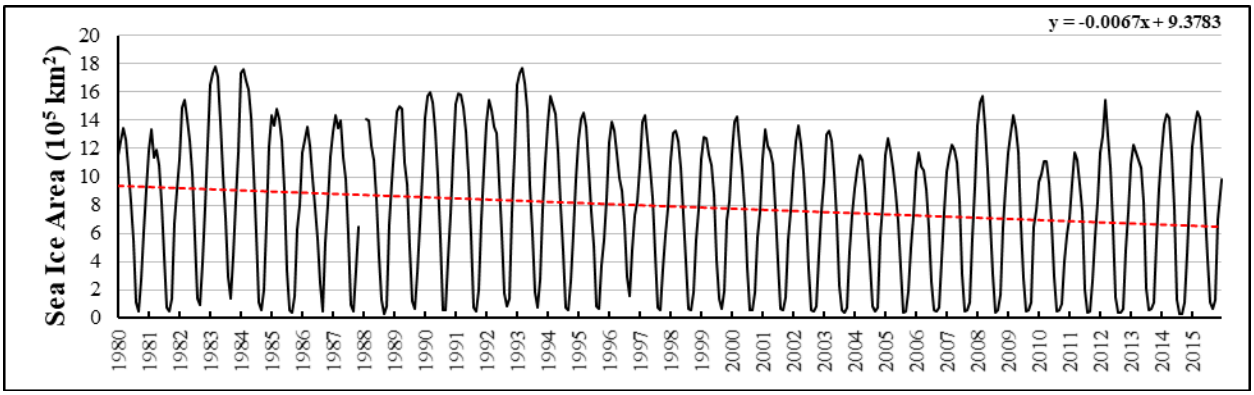

Figure 5: BB-DS-LS's 430-month sea ice area time series with trend line in red. Slope equation in upper-right corner.

BB-DS-LS's 430-month sea ice area time series shows more variation in the annual maximums than the minimums (opposite of the NH). Through most of the time period annual minimums were between 40,000-85,000 km^2. The largest shifts in the annual minimum occurred in 1983 and 1996, increasing to 141,000 km^2 and 158,000 km^2. Annual maximums at the beginning of the time period were 1.34 million km^2. Starting in 1982, maximums progressively increased until the absolute maximum was reached in early 1983 (1.78 million km^2). 1984's maximum was slightly below the absolute maximum, giving these two years the highest sea ice area maximums across the time period. After 1984, maximums decreased through 1986 reaching 1.36 million km^2. After 1986, annual maximums increased once more until the second highest maximum occurred in 1993 (1.74 million km^2). By 1999, annual maximums decreased to 1.28 million km^2. In 2008, annual maximums increased to 1.57 million km^2 (the largest after 1993). In 2009-2010, maximums decreased to 1.11 million km^2, which was the largest change between two consecutive annual maximums.

BB-DS-LS's 322-month (seasonally standardized and detrended) sea ice area time series (Figure 6) was similar to the NH's showing many similar large negative deviations in 1981, 1986, 1988, 2002, 2004, 2006, and 2011, reaching similar values around -1.5 SD. However, BB-DS-LS's deviations had larger variability, with larger positive deviations than the NH. 1981-1982 experienced small-large negative deviations before becoming positive at the end of 1982. 1983 through mid-1984 had progressively increasing positive deviations with a local maximum in mid-1983 at 2.00 SD. 1985-1986 experienced negative deviations with several between mid-1985 and 1986 approaching -1.25 to -1.53 SD (some of the highest negative deviations during the time period). The latter-half of 1986 experienced an abrupt change to positive deviations reaching 1.86 SD.

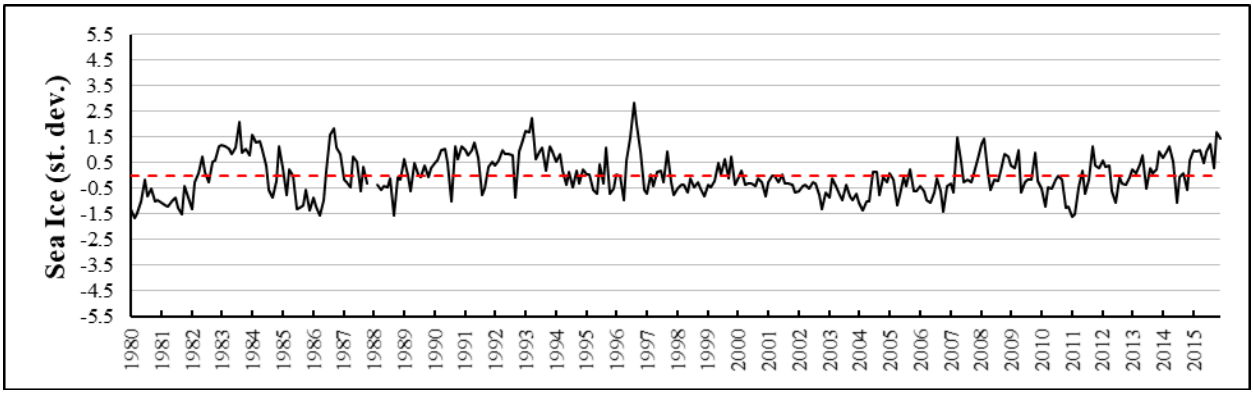

Figure 6: BB-DS-LS's 322-month sea ice area variability (seasonally standardized and detrended).

From 1990 to mid-1993, BB-DS-LS experienced abrupt shifts between moderate negative (-0.50 to -1.02 SD) and positive deviations (1.03 to 2.23 SD), with 1993's maximum being the second largest across the time period (2.23 SD). The largest positive deviation occurred in August 1996 reaching 2.84 SD. From 1997-2006 negative deviations were more common, with the latter-half of 1999 having the only positive deviations in this period. Negative deviations were progressively larger after 2000 surpassing -1.00 SD on five occasions. 2007-2008 had moderately-positive deviations return (1.42 and 1.49 SD). From 2009-2015, deviations fluctuated between moderately positive and weak; however more negative than positive deviations surpassed 1.00 SD during this period. 2011's minimum (-1.61 SD) was the second largest negative deviation in the time period. 2015's maximum (1.70 SD) was the largest positive deviation since 1996.

3.1.2.3: BB Sea Ice Variability

BB's 430-month time series (Figure 7) shows the weakest negative trend in sea ice area over the period. Each month BB lost 150 km^2 (2,000 km^2/year or 69,500 km^2 total; Table 3).

Unlike the NH and other subregions, BB's maximum sea ice area reached its entire area (507,000 km^2) being completely ice-covered for 41.4% of the time period (178 months; Table 6). Due to this unique characteristic, BB's sea ice area time series shows more variation with the annual minimums. The mean sea ice area for BB was 370,000 km^2 (73% of BB's total area) with the absolute minimum area being 17,000 km^2 (3% of BB's total area), which occurred in August 2014. At the individual monthly scale, the most sea ice area was lost between each July (same as BB-DS-LS), losing 6,400 km^2 (Table 4). BB was the only subregion to have lost no sea ice in any month (March and April) across the entire time period. Similar to BB-DS-LS and the NH, BB's lowest average sea ice coverage was in September (51,000 km^2; Table 5).

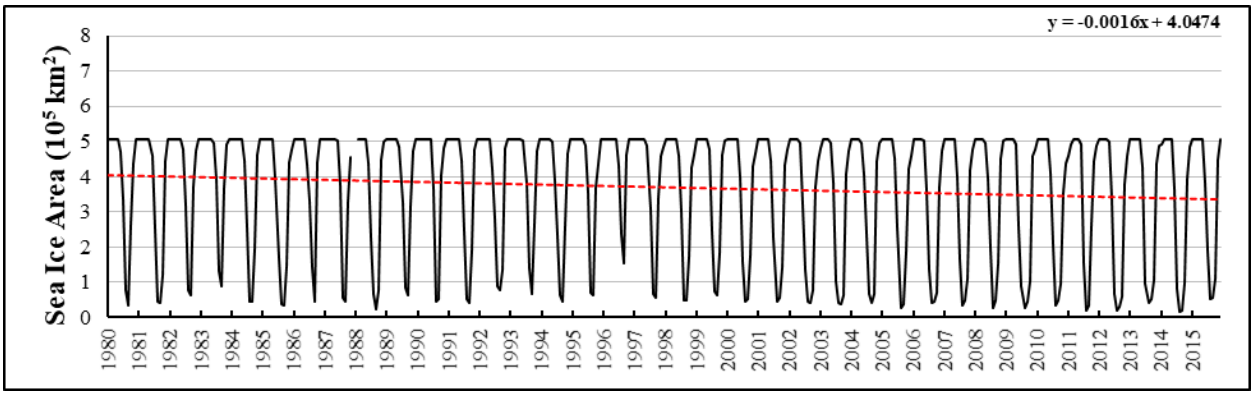

Figure 7: BB's 430-month sea ice area time series with trend line in red. Slope equation in upper-right corner.

For most the of the 430-month time period, annual minimums were between 40,000-85,000 km^2 (the same as BB-DS-LS due to DS and LS minimums being essentially zero each year; Figure 7). Also similar to BB-DS-LS, the largest shifts in sea ice area minimums for BB occurred in 1983 and 1996, drastically increasing to 89,400 km^2 and 153,800 km^2. 1984-1987's

minimums remained around 43,000 km^2 then in 1988 dropped to 23,000 km^2. The following year the minimum rose to 63,800 km^2, then returned to 42,500-43,850 km^2 in 1990-1991. 1992's annual minimum rose to 78,100 km^2, then gradually decreased back to 44,400 km^2 by 1994. The largest sea ice area minimum occurred in 1996, increasing to 54,400 km^2. The minimum fluctuated between 35,600km^2 and 63,100 km^2 until 2005 when it dropped to 28,000 km^2. The minimum then increased in 2006-2007 between 34,400 km^2 to 41,300 km^2. However, it decreased to 25,000 km^2 in 2008, remaining below 30,000 km^2 in 2009. In 2010 the minimum increased up to 33,800 km^2, but dropped down to 18,800 km^2 the next two years. The minimum then increased up to 40,600 km^2 in 2013, but was followed by the absolute minimum (just under 17,000 km^2) of the time period in 2014.

Like BB-DS-LS, BB's 322-month sea ice area time series shows general similarity with the NH's (Figure 8). However, more frequent (but larger) negative deviations are seen across the last decade of the time period. Compared to BB-DS-LS, there are similar maximums in 1983, 1986, 1996, 2007, 2008, and 2014 and minimums in 1981, 1985, 1988, 2002-2006, 2011-2012, and 2014. Most variation is within 2.5 SD. However, there are two distinct deviations that have larger magnitudes than BB-DS-LS and the NH. The latter part of 1986 saw the first abrupt change to a moderate positive deviation (1.50 SD). 1987 saw weaker positive deviations which transitioned to moderately negative in 1988 (-1.45 SD). In 1990, deviations shifted back to positive again in 1990 (-0.74 to 1.37 SD). 1993-1994 saw the highest positive deviation maximum since 1986 (1.62 SD), but deviations decreased to moderately negative (-1.18 SD) by the end of 1994. The absolute maximum positive deviation occurred in mid-1996, surpassing 4.00 SD. Deviations returned back within 1.50 SD by 1997. Deviations became moderately negative in 1998 reaching -1.39 SD. The beginning of 2001 saw weak positive deviations

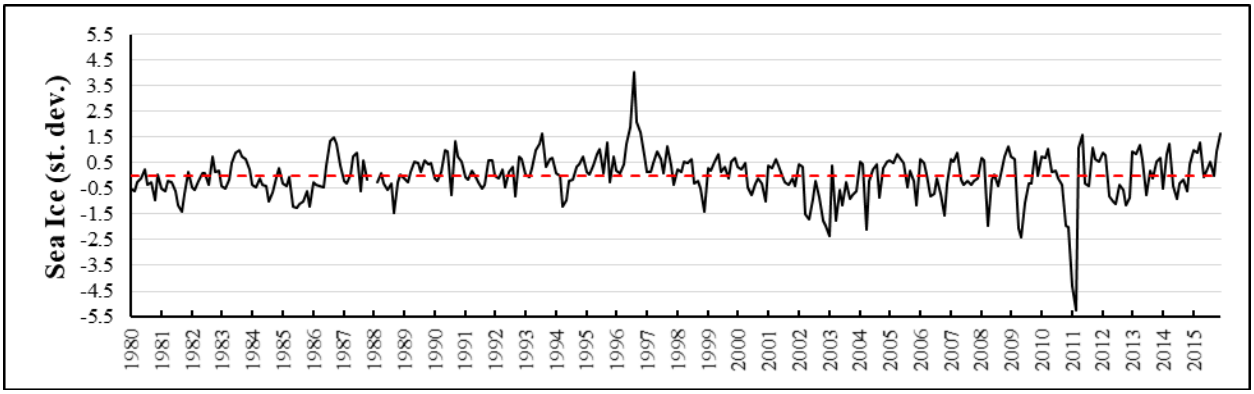

Figure 8: BB's 322-month sea ice area variability (seasonally standardized and detrended).

progressively growing to a large negative deviation by the beginning of 2003 (-2.35 SD). Through 2003, deviations remained negative, but progressively became smaller. The early part of 2004 saw a sudden moderate negative deviation reaching -2.12 SD. Each local negative deviation became larger over time (-1.55 SD in 2006, -1.95 SD in 2008, and -2.50 SD in 2009) until the largest negative deviation of the time period occurred in early 2011 (-5.26 SD). By mid-2011, deviations became moderately positive, gradually became smaller through 2012. The last three years of the time period saw rapid change between weak positive and negative deviations.

3.1.2.4: DS Sea Ice Variability

For most of the period, DS's annual minimums were below 15,000 km^2 (25,000-70,000 km^2 lower than BB; Figure 9). DS's largest shifts in annual sea ice maximums occurred between 2011-2013 where sea ice area increased 180,000 km^2 then decreased 205,000 km^2 respectively. DS's sea ice variability shows three unique maximums (1983, 1984, and 1993), each achieving over 90% coverage of DS's total area. DS's sea ice area time series shows the highest rate of decline among BB, DS, and LS over the 430-month period. In each month, DS lost 275 km^2

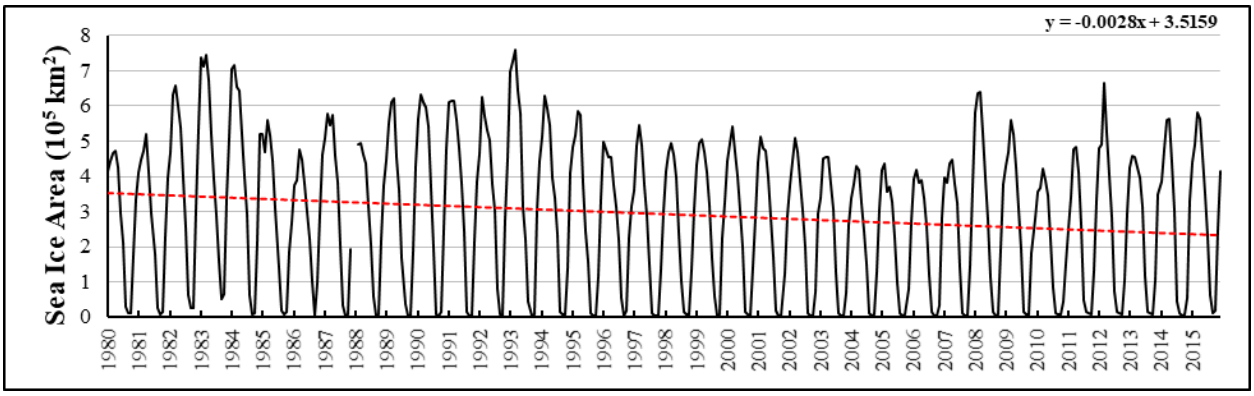

Figure 9: DS's 430-month sea ice area time series with trend line in red. Slope equation in upper-right corner

(3,300 km^2/year or 119,200 km^2 total; Table 3). The absolute sea ice maximum for DS occurred in March 1993 (759,400 km^2; Table 6) and was the only subregion where the absolute maximum occurred after 1990. Unlike the NH and other subregions, DS's sea ice area minimum occurred during September in three consecutive years within the first decade (1986-1988). The least significant amount of sea ice area was lost between each October (630 km^2) (six months after BB, two months after BB-DS-LS, and five months after the NH). On the other hand, DS lost the most significant amount of sea ice area (4,700 km^2) between each January (six months before BB and BB-DS-LS, and eight months before the NH; Table 4). Similar to the NH, BB-DS-LS, and BB, DS had its largest average sea ice cover in March (538,000 km^2), which is also the largest average monthly coverage across all the subregions (Table 5).

DS's 430-month time series shares similar annual minimums with BB-DS-LS where each one approaches close to ice-free. The one shared trait with BB-DS-LS and BB's time series is the larger minimum in 1983. DS's time series also shows variation mainly with the annual maximums, with five distinct events in 1983, 1984, 1993, 2008, and 2012 (similar to BB-DS-LS). Annual sea ice area maximums at increased until 1983, reaching 745,000 km^2. From 1984-

1986, maximums decreased around to 475,000 km^2. In 1989, maximums began surpassing 600,000 km^2 until the largest sea ice area maximum of the time period occurred in 1993 (759,400 km^2). From 1994-2007, maximums decreased to 420,000 km^2; this fourteen-year period had the lowest consecutive maximums of the entire time period. 2008's maximum increased to 638,100 km^2, the first time since 1994 where a maximum was above 600,000 km^2. 2009-2010's maximums decreased down to 422,500 km^2 then increased to 664,400 km^2 in 2012; which was the largest maximum since 1993. The highest sea ice area minimum of the time period occurred in 1983 (51,900 km^2). Annual minimums after 1983 decreased, remaining below 15,000 km^2 until the lowest occurred from 1986-1988 (3,750 km^2). Minimums remained below 25,000 km^2 for the rest of the time period.

DS's 322-month time series shares similar patterns with the NH, BB-DS-LS, and BB's (Figure 10). However, there are more frequent negative deviations across the last decade of the time period, and the sea ice area deviations throughout the entire time period are larger than the NH. DS had the largest positive deviation out of all of the regions, including the NH. Additionally, DS had its largest negative deviation near the end of the time period. However it

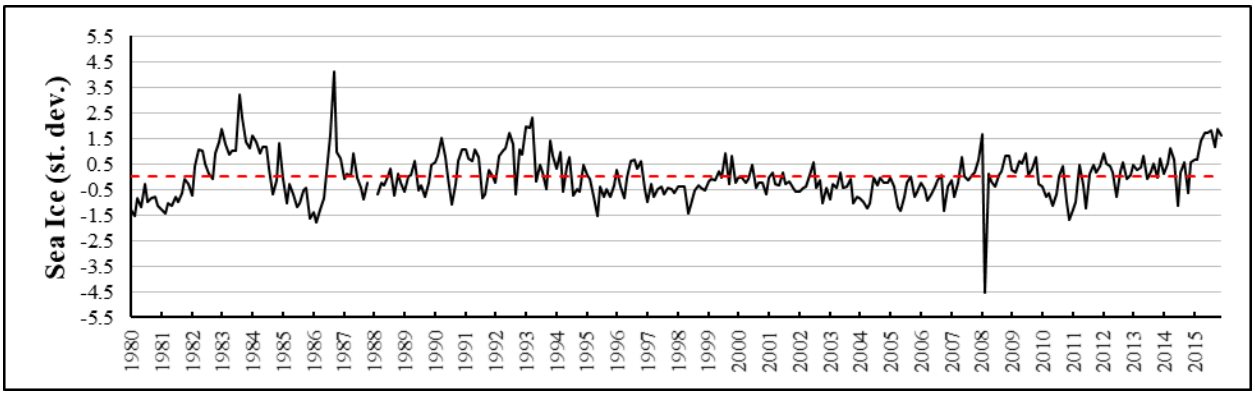

Figure 10: DS's 322-month sea ice area variability (seasonally standardized and detrended).

occurred in 2008 instead of 2011, like BB. It is worth noting the NH experienced one of its largest negative deviations (-1.50 standard deviations) in 2008 as well. Between mid-1982 and early 1985, positive deviations ranged from 0.90 to 3.22 SD. Through 1985, deviations became negative until early 1986 when the second largest negative deviation occurred (-1.78 SD). The largest positive deviation of the entire time period occurred at the end of 1986 (4.14 SD). In 1987, deviations became smaller with the latter-half of the year having the weakest deviations until early 1990. Through 1993, deviations became larger ranging from -1.03 to 2.30 SD. Up to early 2007, deviations were mostly negative reaching -1.51 SD. 2007 saw a gradual transition towards small-moderately positive deviations up to 1.65 SD. In early 2008, the largest negative of the time period occurred (-4.50 SD); which had smaller magnitude than the 2011 minimum in BB). In 2015, positive deviations increased, reaching 1.87 SD, the largest positive deviations observed since 1993.

3.1.2.5: LS Sea Ice Variability

LS had the lowest annual minimums due to being ice-free every September (only subregion to be ice-free in any month; Figure 11); furthermore, LS was ice-free for 28.1% (121 months) of the time period. LS experienced the second largest decline in sea ice, when compared to the other subregions (Table 3). In each month LS lost 230 km^2 (2,750 km^2/year or 99,400 km^2 total). The largest sea ice maximum occurred in February 1984 (538,008 km^2) (59.3% of LS's total area; Table 6). LS lost the most significant sea ice area between each January (6,000), eight months before the NH (Table 4). Average maximum sea ice coverage occurred in February (353,000 km^2), one month before the NH and the other subregions (Table 5).

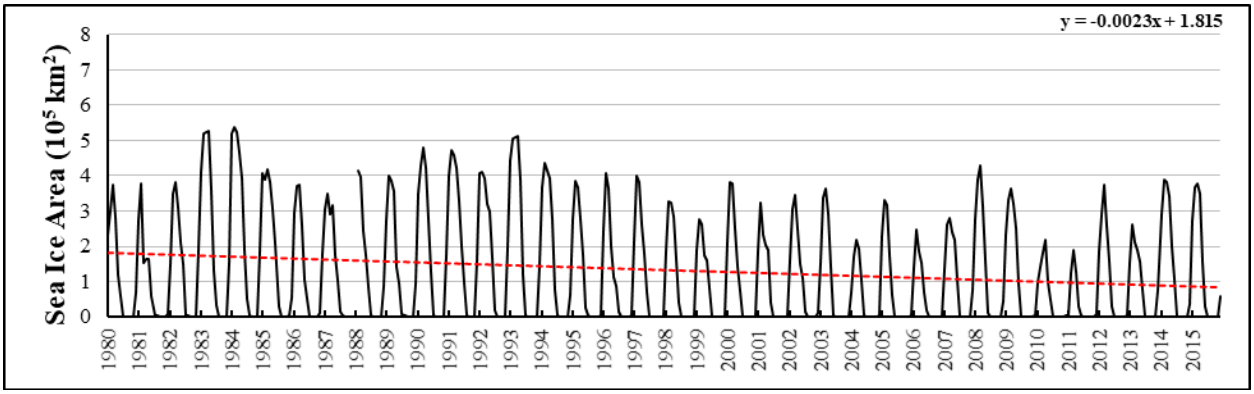

Figure 11: LS's 430-month sea ice area time series with trend line in red. Slope equation in upper-right corner.

LS's 430-month time series shows large variation in the annual maximums with four distinct events in 1983, 1984, 1993, and 2008. The largest shifts in annual maximums occurred from 2011-2012 when maximum coverage increased by over 180,000 km^2. Annual maximums started were between 375,500-382,500 km^2 until 1982. The two highest maximums of the time period occurred in 1984, reaching 519,250 km^2 and 538,000 km^2 (absolute maximum). By 1987 annual maximums decreased to 349,300 km^2. By the end of the decade maximums increased to 479,900 km^2, which was followed by another decrease in 1991-1992 to 405,500 km^2. 1993 had the highest maximum since 1984, surpassing 500,000 km^2. 2008 had the largest maximum since 1994, and the last maximum to surpass 400,000 km^2. 2009-2011's maximums rapidly decreased with 2011 being the only year the maximum fell below 190,000 km^2.

LS's 322-month time series (Figure 12) shows more frequent, and higher, negative deviations across the last decade (2004-2015) of the time period like the NH. LS's sea ice variability also has the largest positive deviations. The largest sea ice area maximum across the entire time period occurred in late 1983 reaching 5.19 SD (the largest deviation in the NH and any subregion). By the start of 1984, deviations became moderately positive (1.35 and 1.85 SD).

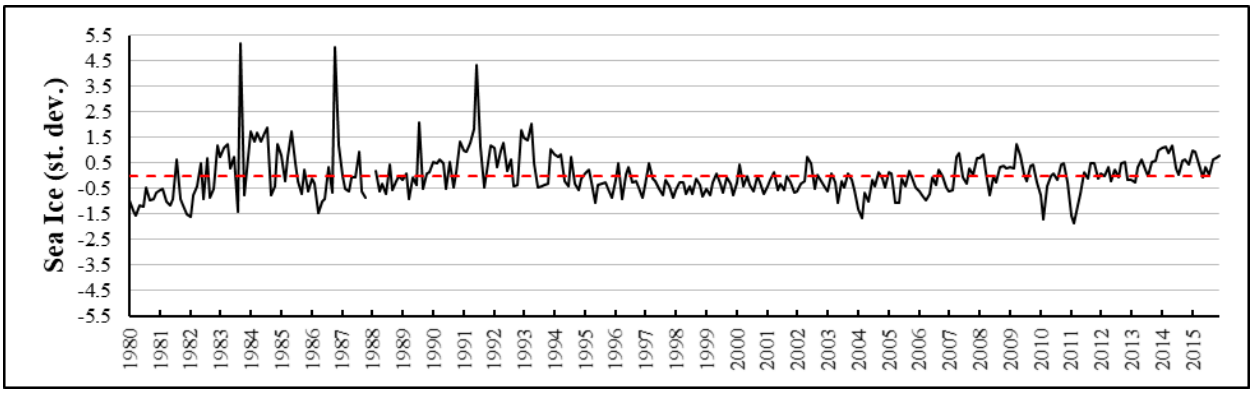

Figure 12: LS's 322-month sea ice area (seasonally standardized and detrended).

Deviations decreased over the next two years reaching -1.45 SD by mid-1986. Deviations became positive and reached the second highest maximum across the time period at 5.03 SD by 1987. In summer 1991, the third largest maximum of the time period occurred (4.34 SD). Through 1991-1992, positive deviations decreased to 1.16 to 1.28 SD. The first-half of 1993 saw small increases in positive deviations reaching 1.75 to 2.03 SD. The end of 1993 saw the last positive deviation above 1.00 SD for fifteen-years (1.05 SD). From 1994-2006, most monthly deviations were small to moderately negative remaining below -1.50 SD. The third largest negative deviation occurred in early 2004 reaching -1.66 SD. The winter and spring months of 2008 had small negative deviations which became moderately positive by the beginning of 2009 (1.21 SD). The second-half of 2009-2011 experienced the two largest negative deviations of the entire time period, reaching -1.71 and 1.85 SD.

3.1.3: Objective 1 Results Overview

Objective 1 aimed to establish what the sea ice area variability was in each subregion and how it compared to the NH from 1980-2015. Comparing the raw 430-month data, significant

correlations were inflated due to seasonality and long-term trends. After seasonally standardizing and detrending the values, correlations remained significant but dropped by over half. For the raw monthly-based datasets (e.g., January 1980-2015), long-term trends also biased correlations, but at a lesser magnitude. Each subregion's time series depicted significant negative trends with DS losing the most sea ice area out of all the subregions, followed by LS, then BB. Although the subregions are geographically connected, their sea ice area variabilities are unique from each other and the NH's. All regions (excluding BB) experienced their maximum coverages across the first-half of the period during spring. However, the NH, BB-DS-LS, and BB experienced their minimum coverages after 2010, and every subregion and the NH experienced their overall minimum coverages during late summer/early autumn. The regions were more closely aligned with their maximum/minimum mean coverages. The months that experienced the most/least amount of sea ice loss were more distributed throughout the 12-month range, depicting large shifts in coverage occurring in different months. Sea ice deviations further revealed the unique sea ice variability between each subregion and the NH. Each subregion experienced larger deviations in sea ice than the NH, with larger positive deviations occurring more frequently before 1996 and weaker, more consistent negative deviations occurring after 2000. These Objective 1 results show that each subregion lost sea ice over the time period, like the NH, but at different magnitudes. Also, the results show that even though BB, DS, and LS are contiguous, sea ice variability is unique in each subregion and each greatly differ from the NH's variability at both the individual monthly and long-term scales. With the local variability described, the next step is to determine cyclone variability in BB-DS-LS and its subregions.

3.2 Objective 2: What is the Cyclone Variability in BB, DS, and LS from 1980-2015?

Objective 2's goal was to identify the individual monthly and long-term cyclone variability for BB-DS-LS and its three subregions from 1980-2015. The results present an overview of the significant observations in the 430 and 322-month, as well as the individual monthly, cyclone variable datasets.

3.2.1: Total Number of Cyclones Long-Term and Monthly Variability

Across the 430-month time period, 7,548 cyclones with at least one time step in BB-DS-LS were recorded, 3,052 were in BB; 2,706 in DS; and 3,322 in LS. The sum of the cyclones within the three subregions exceeded BB-DS-LS's total, resulting from certain cyclones persisting across multiple months and/or traveling into multiple subregions. Every subregions' total number of cyclones time series shows little to no trend (Figures 13a-d). BB-DS-LS's trend experienced the most variation with a range (or difference in minimum and maximum) of 26 cyclones, BB's was 16, and DS and LS's was 13. BB-DS-LS's total number of cyclones typically remained between 10-25 events per month. During April and June-September, there were seven occasions (at least once a decade) when fewer than 10 cyclones occurred. Across January-March, September, and November-December, over 25 cyclones occurred on fourteen occasions, primarily during and after the 1990s. BB, DS, and LS's total monthly number of cyclones rarely exceeded 14. However, monthly minimums frequently dropped below 5 cyclones. No cyclones occurred in BB in July 2002 (the only subregion having zero cyclone activity in any month). BB was also the only subregion having a month with more than 15 cyclones occurring (January 2015).

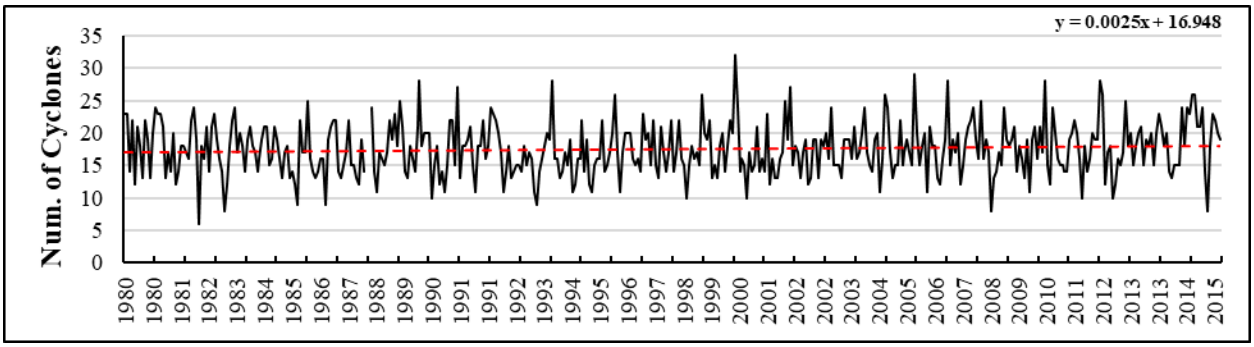

Figure 13a: BB-DS-LS's total number of cyclones time series with trend line in red. Slope equation in upper-right corner.

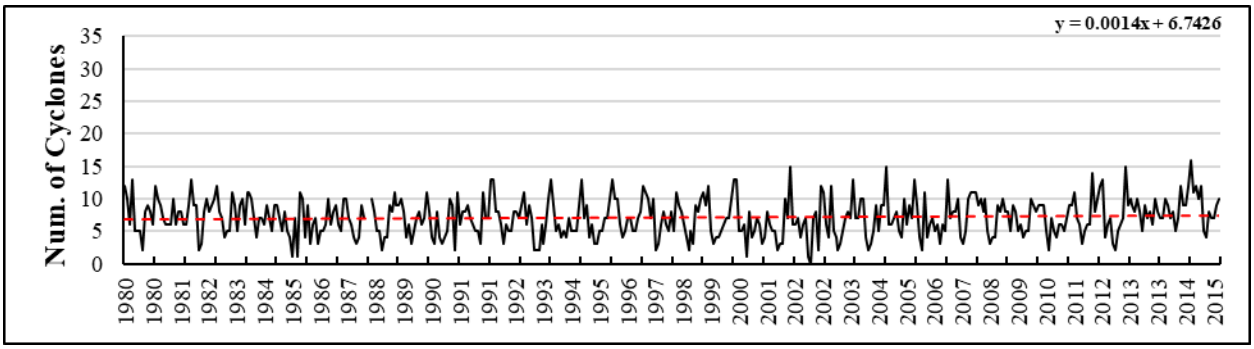

Figure 13b: BB's total number of cyclones time series with trend line in red. Slope equation in upper-right corner.

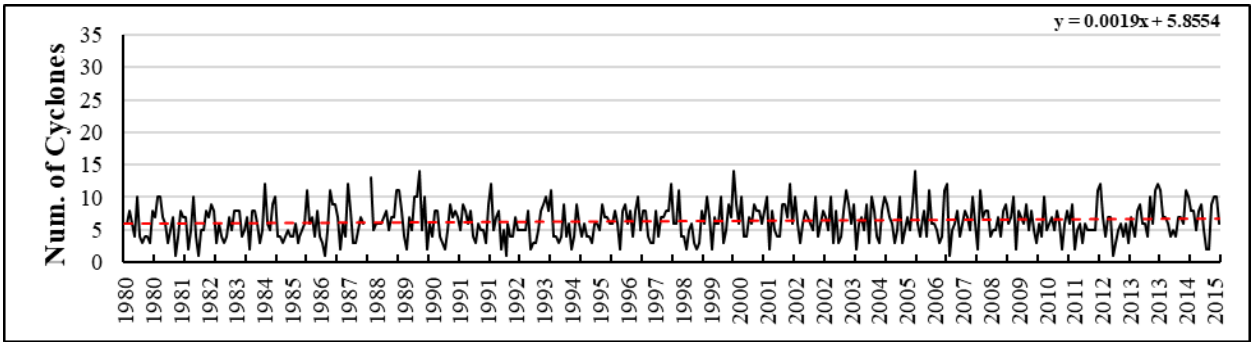

Figure 13c: DS's total number of cyclones time series with trend line in red. Slope equation in upper-right corner.

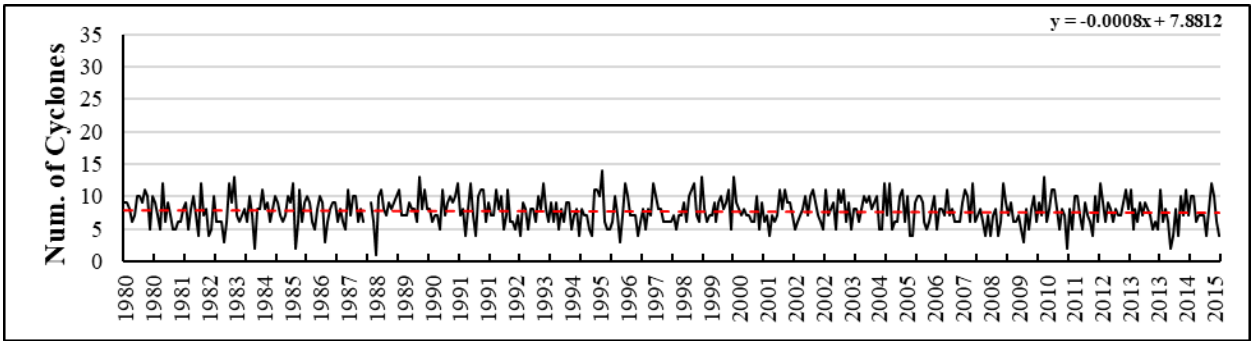

Figure 13d: LS's total number of cyclones time series with trend line in red. Slope equation in upper-right corner.

For BB-DS-LS and BB, January had the highest monthly average (21 and 10) and maximum monthly number of cyclones (32 and 16). June had their lowest monthly average number of cyclones (15 and 4) and their lowest monthly minimum number of cyclones (6 and 1). DS's highest monthly average was in December (8), whereas its lowest monthly average was in July (5). DS's highest maximum monthly total number of cyclones occurred in January, September, and December (14). DS's lowest minimum monthly total number of cyclones occurring in February, June-September (1). LS's highest monthly average occurred in July (9); whereas LS's lowest occurred in April (6). LS's highest monthly maximum occurred in September (14); LS's lowest monthly minimum occurred in April (1). At the annual scale, 2015 had the highest number of cyclones for BB-DS-LS and BB (242 and 111), while 1987 had BB-DS-LS's lowest (180) while 2006 had BB's (68). DS's highest annual number of cyclones occurred in 1988 and 2000 (91); while LS's lowest was in 1985 (52). LS's highest annual number of cyclones occurred in 1980 (104); while LS's lowest was in 2009 (80). Each year, 210 cyclones were within BB-DS-LS, 85 in BB, 75 in DS, and 93 in LS.

All subregions experienced fewer total numbers of cyclones per individual month (e.g. January 1980-2015), moving from January-April (Figure 14). BB had the highest totals during January-April (1980-2015), LS had the second highest. However BB's totals decreased during summer (starting in May). LS's totals increased and were the highest during summer, DS had the second highest, while BB had the lowest. From summer to winter, BB and DS's totals began to gradually increase, while LS's decreased. LS gradually declined and plateaued through December. Besides June, DS had the lowest variation and totals across every month for the subregions. BB-DS-LS's individual monthly variability reflects BB and DS's patterns: higher

totals starting in January which decrease through June and then increase again through December.

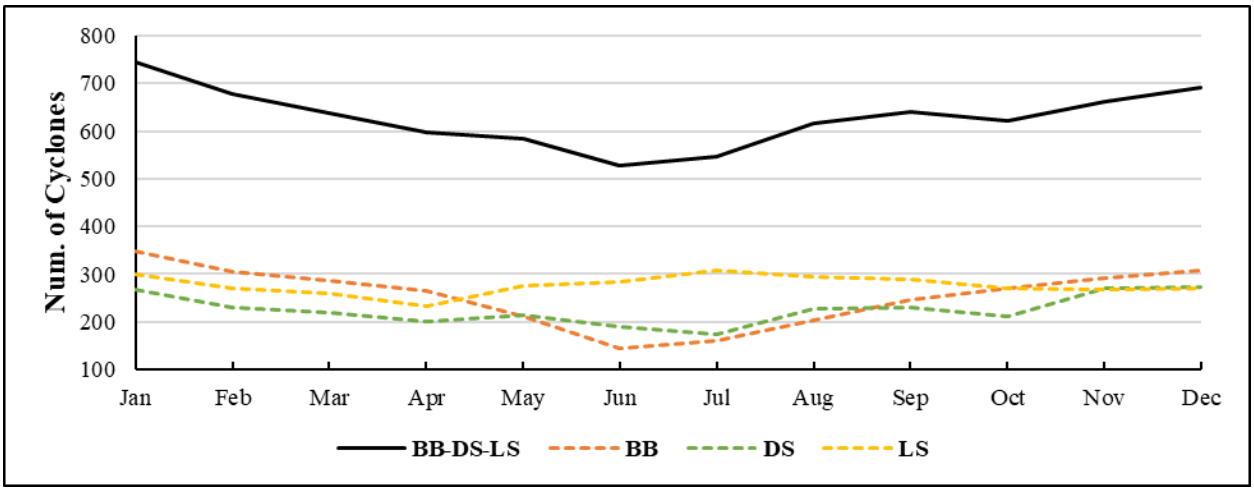

Figure 14: Total number of cyclones in each subregion from 1980-2015 per monthly basis.

Since no significant trends were seen in the 430-month datasets, seasonally standardizing and detrending did not affect correlations for this variable. Therefore, only the 322-month and detrended monthly comparisons will be mentioned. BB-DS-LS was significantly correlated with each subregion: BB (0.62), DS (0.56), and LS (0.58). Correlations among the subregions were only significant for DS/LS (0.14) and DS/BB (0.22). For the individual monthly detrended datasets, January had the highest significant correlation (0.74) while August had the lowest (0.40) for BB-DS-LS/BB. June had the highest (0.73) while July had the lowest (0.36) for BB-DS-LS/DS. November had the highest (0.67) while June had the lowest (0.34) for BB-DS-LS/LS. Comparing only BB, DS, and LS, DS/LS were only significantly correlated in January (0.48) and September (0.38); whereas BB/DS were only significantly correlated in April (0.37).

3.2.2: Minimum Central Pressure Long-Term and Monthly Variability

BB-DS-LS's average minimum central pressures for each individual month (e.g., January's 1980-2015 minimum central pressures averaged), values ranged between 989 hPa (January) to 1003 hPa (May); the overall mean was 997 hPa. BB's had the highest values of all the subregions, ranging between 997 hPa (January) to 1008 hPa (April); the overall mean was 1002 hPa. DS's values ranged from 987 hPa (January) to 1002 hPa (May and June); the overall mean was 996 hPa. LS's had the lowest values, ranging from 981 hPa (January and December) to 1000 hPa (May); with the mean being 992 hPa. December 1991 had the lowest recorded monthly minimum central pressure for BB-DS-LS (982 hPa), January 1991 for BB (983 hPa), December 1983 for DS (976 hPa), and January 2009 for LS (972 hPa). Similar to total number of cyclones, all subregions' minimum central pressure time series (Figures 15a-d) show little to no trend across the 430-month time period. BB, DS, and LS's show more apparent shifts and more extreme maximums/minimum events than BB-DS-LS's.

All subregions (except LS), had their lowest individual monthly average minimum central pressures in January: BB-DS-LS (989 hPa), BB (997 hPa), and DS (987 hPa). For LS, December had the lowest average (981 hPa). At the annual scale, 1990 had the lowest average minimum central pressures for BB-DS-LS (993 hPa), BB (998 hPa), and DS (991 hPa), and 2002 for LS (989 hPa).

Across each individual month (e.g., January 1980-2015), winter months typically had the lowest while summer had the highest average minimum central pressures. LS's average minimum central pressures are the lowest in January-February before increasing closer with DS from March-May. DS and LS's pressures increased more rapidly than BB's, and surpassed BB's pressures in July-August. BB's minimum central pressure for January-April and September-

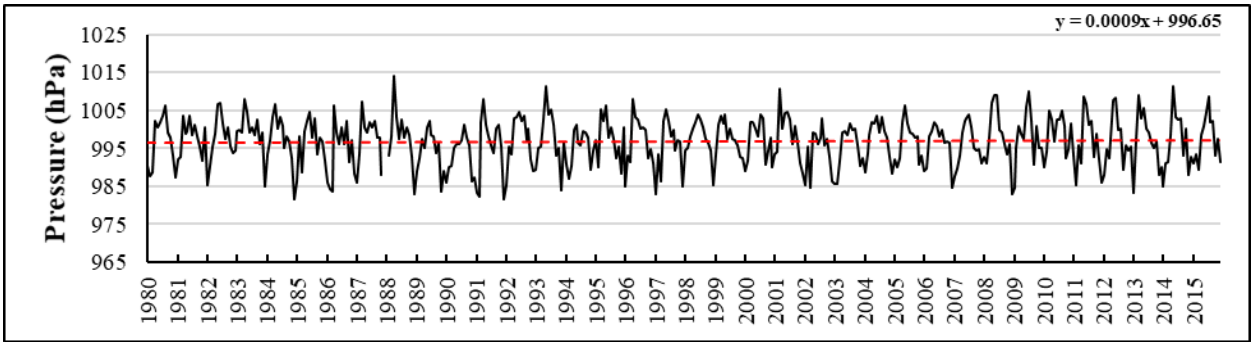

Figure 15a: BB-DS-LS's minimum central pressure time series with trend line in red. Slope equation in upper-right corner.

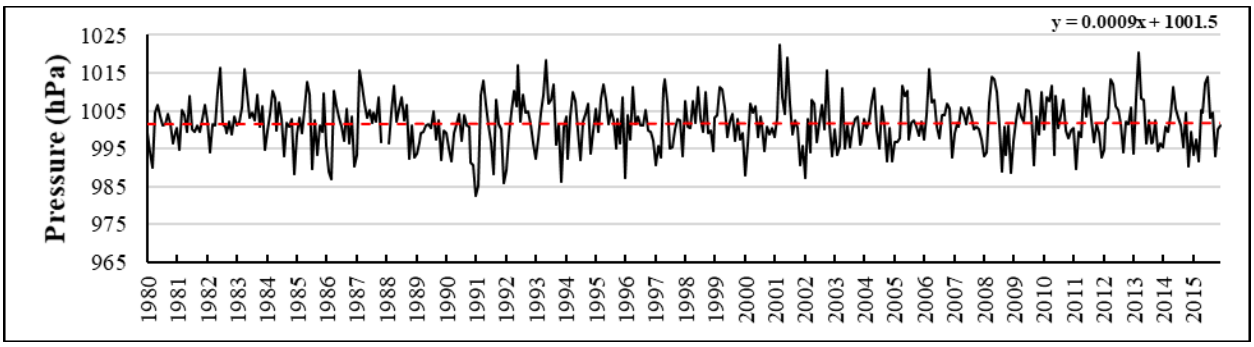

Figure 15b: BB's minimum central pressure time series with trend line in red. Slope equation in upper-right corner.

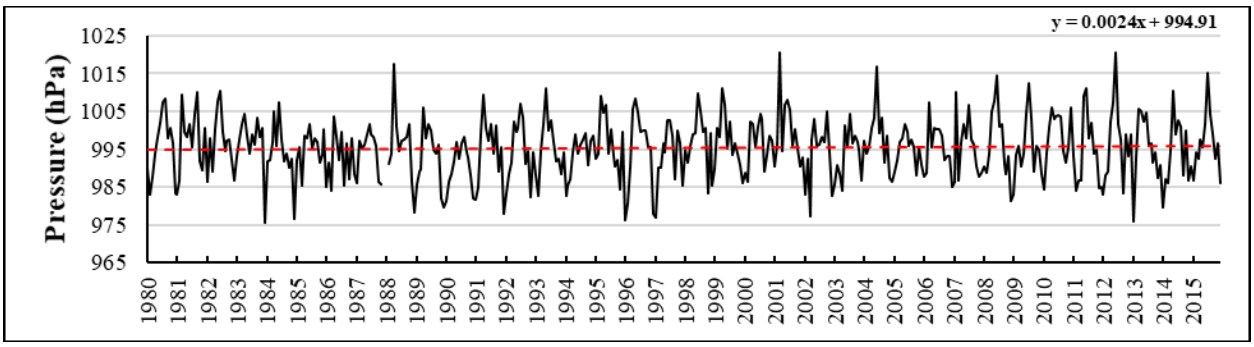

Figure 15c: DS's minimum central pressure time series with trend line in red. Slope equation in upper-right corner.

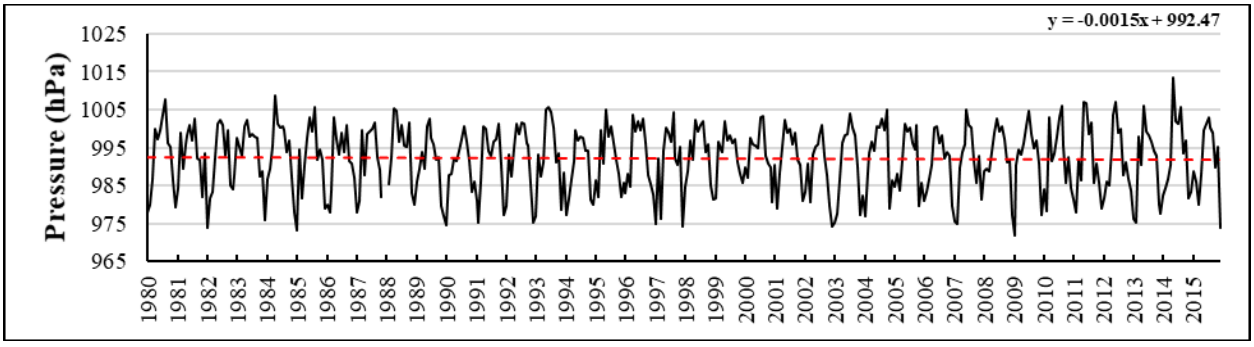

Figure 15d: LS's minimum central pressure time series with trend line in red. Slope equation in upper-right corner.

December was the highest out of all the subregions. BB's pressures aligned most closely with BB-DS-LS's, however all subregions' pressures had greater increases from January-May than during summer and autumn, where pressures plateaued, then decreased through December (Figure 16).

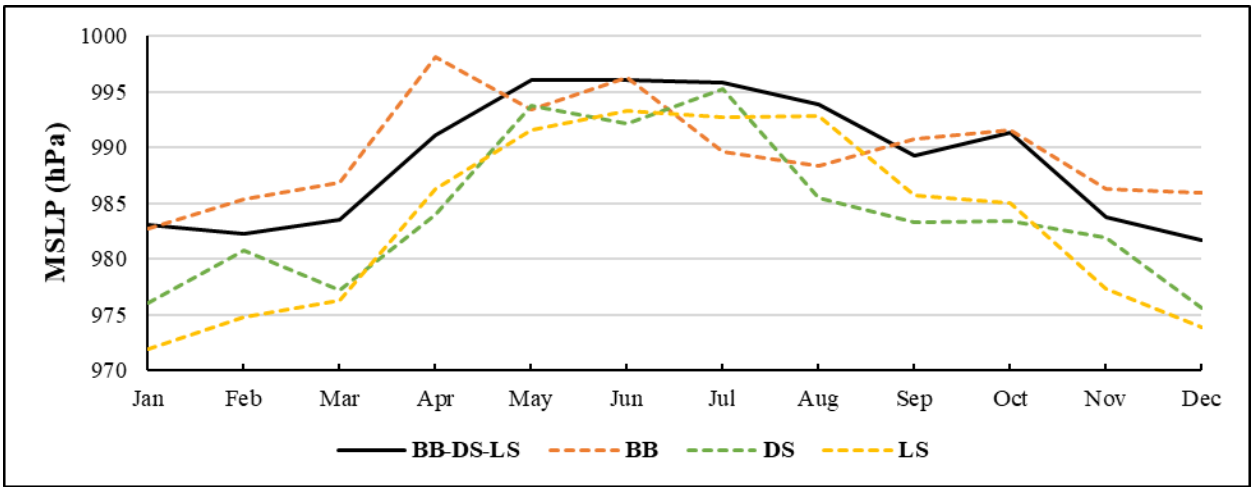

Figure 16: Monthly average minimum central pressure of subsetted cyclone time steps within each subregion from 1980-2015.

Although there were no significant trends in the 430-month datasets, seasonally standardizing and detrending the minimum central pressure datasets did change the correlations more than with total number of cyclones. For consistency, only the 322-month and detrended monthly significant correlations will be mentioned. BB-DS-LS is positively correlated with each subregion: BB (0.66), DS (0.65), and LS (0.73). Between BB, DS, and LS correlations are weaker: BB/DS (0.41), BB/LS (0.19), and DS/LS (0.38).

Similar to total number of cyclones, detrended monthly correlations did not change as much as seasonally standardizing and detrending the 430-month datasets. In March-May, July, and November all detrended subregions were significantly correlated. All correlations between BB-DS-LS and the subregions' (and BB, DS, LS comparisons) average minimum central pressures were moderate-strong, with higher correlations associated with the BB-DS-LS/subregion comparisons. For BB-DS-LS/BB, March had the highest significant correlation (0.88), whereas October had the lowest (0.34). For BB-DS-LS/DS, March had the highest (0.83), whereas February had the lowest (0.36). For BB-DS-LS/LS, July had the highest (0.83), whereas October had the lowest (0.66).

3.2.3: Total Cyclogenesis/Cyclolysis Events Long-Term and Monthly Variability

Within BB-DS-LS, 3,983 cyclogenesis and 5,103 cyclolysis events were observed from 1980-2015; 1,918 and 2,313 events within BB; 1,158 and 1,538 events within DS; finally, 903 and 1,241 events in LS; therefore, all subregions had more cyclolysis than cyclogenesis events. The sums of each subregion's cyclogenesis and cyclolysis events were less than BB-DS-LS's total due to certain cyclones having multiple time steps marked as either event and/or crossed between subregions (leading to a slight underrepresentation in the annual total number of cyclogenesis and cyclolysis events).

BB-DS-LS's cyclogenesis events show the only significant positive trend for across the entire time period; the subregions show no trend for either event (Figures 17a-d; 18a-d). BB-DS-LS's monthly cyclogenesis and cyclolysis events had the highest ranges (or difference in minimum and maximum) with 20 cyclogenesis and 22 cyclolysis events. The cyclogenesis ranges for each subregion were: 12 (BB), 10 (DS), and 9 (LS). The cyclolysis ranges for each

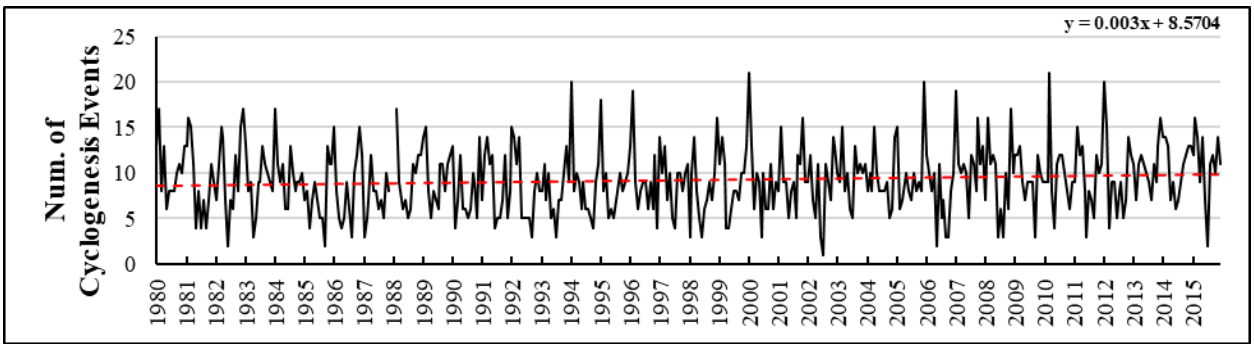

Figure 17a: BB-DS-LS's total cyclogenesis events time series with trend line in red. Slope equation in upper-right corner.

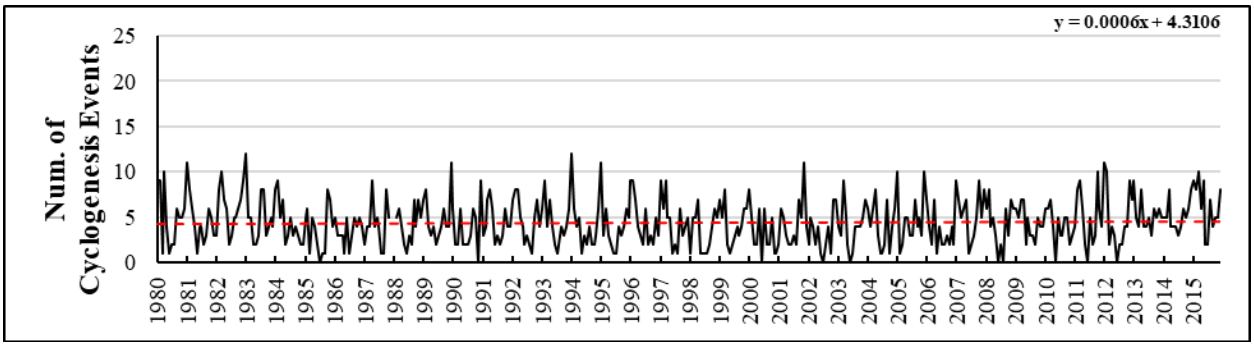

Figure 17b: BB's total cyclogenesis events time series with trend line in red. Slope equation in upper-right corner.

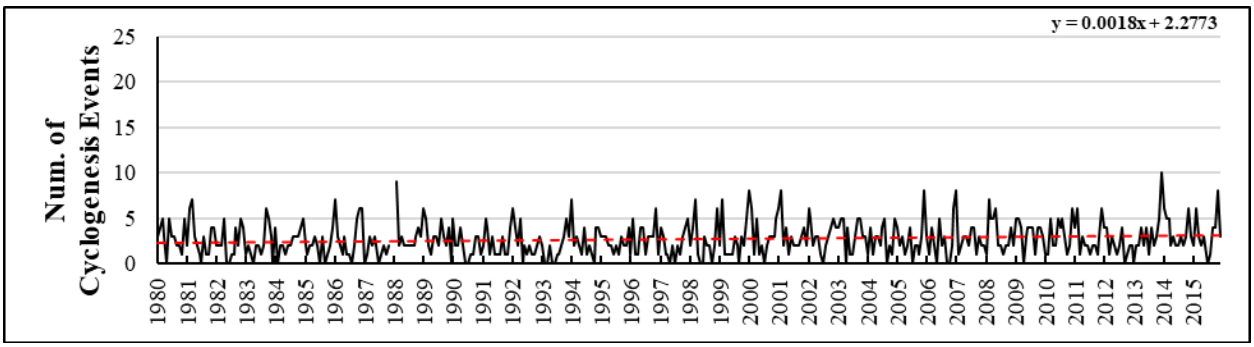

Figure 17c: DS's total cyclogenesis events time series with trend line in red. Slope equation in upper-right corner.

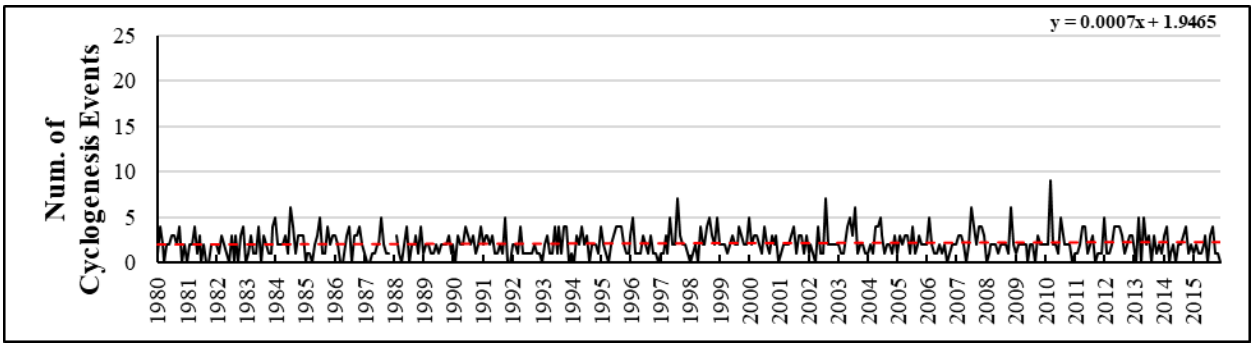

Figure 17d: LS's total cyclogenesis events time series with trend line in red. Slope equation in upper-right corner.

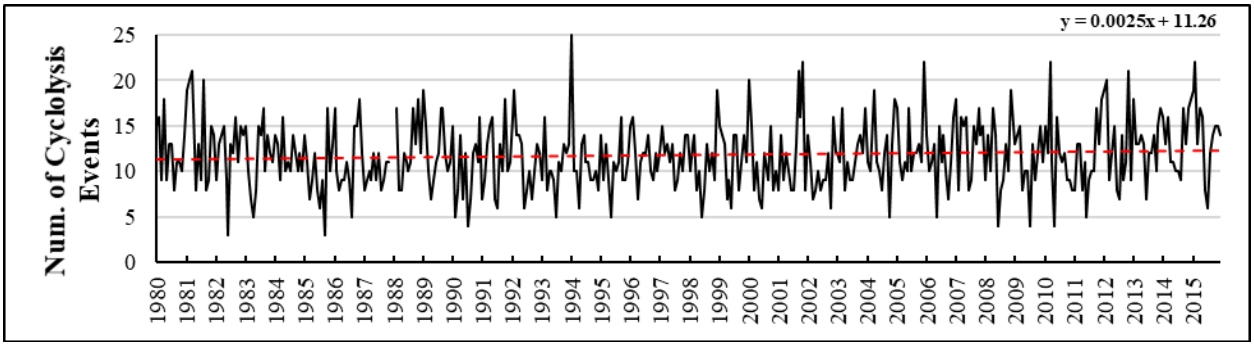

Figure 18a: BB-DS-LS's total cyclolysis events time series with trend line in red. Slope equation in upper-right corner.

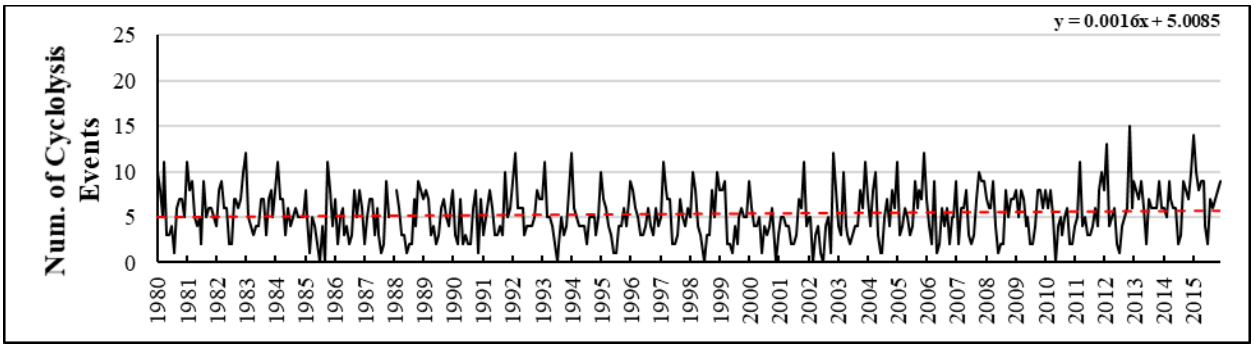

Figure 18b: BB's total cyclolysis events time series with trend line in red. Slope equation in upper-right corner.

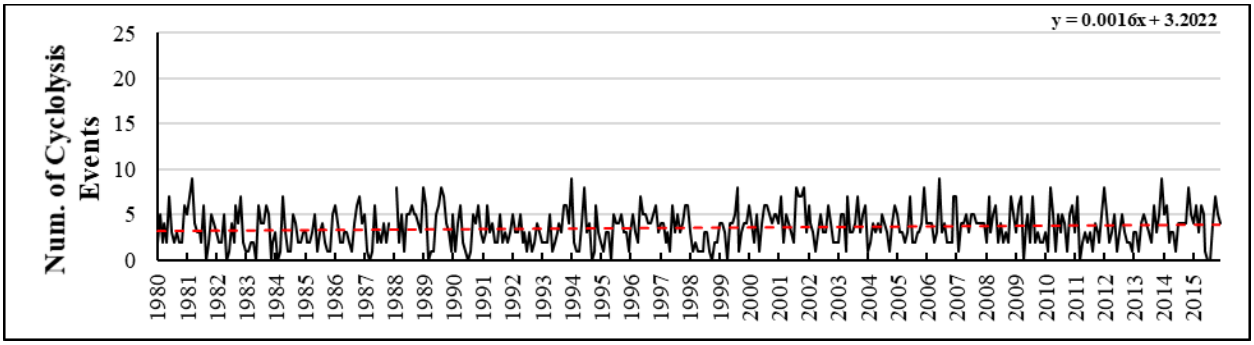

Figure 18c: DS's total cyclolysis events time series with trend line in red. Slope equation in upper-right corner.

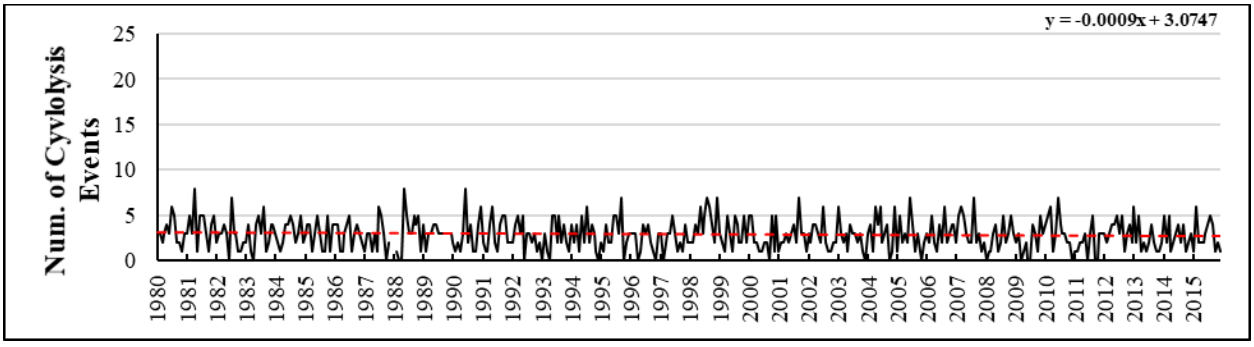

Figure 18d: LS's total cyclolysis events time series with trend line in red. Slope equation in upper-right corner.

subregion was: 15 (BB), 9 (DS), and 7 (LS). BB-DS-LS's number of cyclogenesis events typically remained between 3-18 while its cyclolysis events remained between 5-20 each month. However, May-July and September had fewer than 3 cyclogenesis events observed on four different occasions (1985, 2002, 2006, and 2015). May, June, July and September had fewer than 5 cyclolysis events observed on six different occasions (1982, 1985, 1990, 2008, 2009, and 2010). January-March and December had over 18 cyclogenesis events observed on six occasions (1994, 1996, 2000, 2005, 2010, and 2012). January-March, August-September, and November-December had more than 20 cyclolysis events observed on eight different occasions (1981, 1994, 2001, 2005, 2010, 2012, and 2015).

The highest maximum number of monthly cyclogenesis events in BB-DS-LS occurred in January and March (21), while maximum number of cyclolysis events occurred in January (25). January also had the highest overall total number of cyclogenesis and cyclolysis events (433 and 514). BB-DS-LS's lowest monthly maximum (14) and overall total number (338) of cyclolysis events occurred in July. BB had the highest monthly maximum (12) and overall total number (243) cyclogenesis events in January. Additionally, BB had the highest monthly maximum (15 in November) and total number of cyclolysis events (269 in January) of any subregion. For BB-DS-LS and BB, June had the lowest monthly maximum (11 and 5) and overall total number (235 and 78) of cyclogenesis events. For BB, November (June) had the highest monthly maximum number of cyclolysis events (15) while June had the lowest maximum (6). Also for BB, January had the highest overall total number (269) of cyclolysis events while July had the lowest (97). DS and LS never experienced more than 10 cyclogenesis or cyclolysis events each month. DS's highest monthly maximum (10) and total number (140) of cyclogenesis events occurred in December, while the lowest for both occurred in July (4 and 54). December and July also had the

highest and lowest overall total number of cyclogenesis events (804 and 428). DS's highest monthly maximum cyclolysis events occurred in January, March, June, and December (9), while DS's lowest monthly maximum cyclolysis events occurred in July (6). The highest overall total number of cyclolysis events DS occurred in November (150) while the overall lowest total was in March (104). For LS, March had the highest monthly maximum number of cyclogenesis events (9) while April had the lowest (4). However, August and April had the highest and lowest overall totals (92 and 57). LS's highest monthly maximum for cyclolysis events occurred in April-May, and June (8), while LS's lowest was in October and November (5), however August and October had the highest and lowest overall totals (132 and 81). In every subregion, monthly cyclogenesis and cyclolysis minimums reached zero, but at different frequencies (May-August, and November for BB; every month but November for DS; every month for LS).

At the annual timescale, 2007 had the highest number of cyclogenesis events (137); whereas 1987 had the lowest (86). 1981 had the highest number of cyclolysis events (173) while 1987 had the lowest (118) for BB-DS-LS. BB's highest number of cyclogenesis events occurred in 2015 (75), while BB's lowest occurred in 1998 and 2002 (39). 2015 had BB's highest number of cyclolysis events (93) whereas 2002 had it lowest number (48). DS experienced its highest annual number of cyclogenesis events in 2014 (42); whereas DS's lowest occurred in 1987 and 1993 (19). 2001 had the highest number of cyclolysis events (60), while 1998 had the lowest for DS (20). LS's highest number of cyclogenesis events occurred in 1984 and 2007 (35); whereas 1987 had the lowest number for LS (17). The highest annual number of cyclolysis events occurred in 1998 (51) while the lowest occurred in 2011 (23). On average, 111 cyclogenesis and 142 cyclolysis events occurred annually within BB-DS-LS; 53 and 64 events in BB; 32 and 43 events in DS; finally, 25 and 34 events in LS.

Comparing the total number of cyclogenesis and cyclolysis events summed across every individual month (Figures 19a-b), BB had the most distinctive variation out of all the subregions for both events. It also had the highest number of both events during winter which decreased (as did DS at a lower magnitude) through spring and summer. DS and LS's variabilities for both events were less and overlapped between 75-150 events mainly during the spring and autumn months.

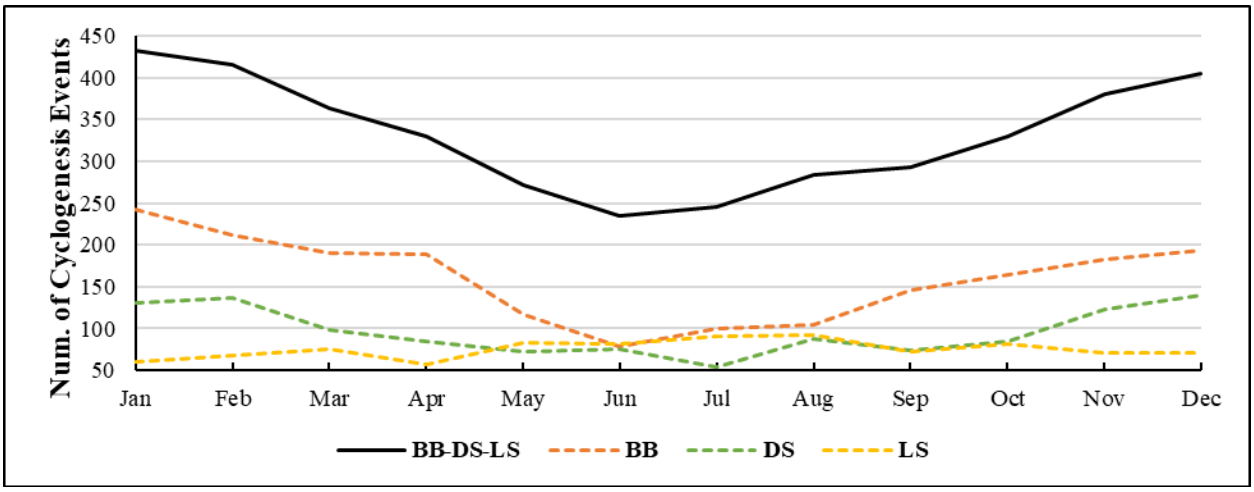

Figure 19a: Total number of cyclogenesis events in each subregion from 1980 to 2015 per monthly basis.

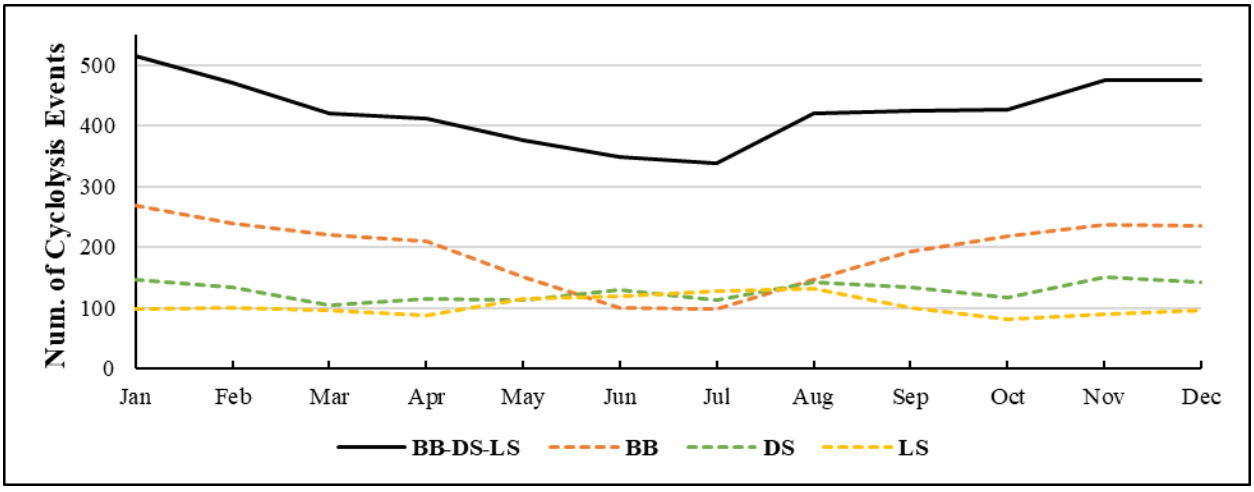

Figure 19b: Total number of cyclolysis events in each subregion from 1980-2015 per monthly basis.

Similar to previous variables, detrending the cyclogenesis and cyclolysis monthly datasets did not drop correlations as much as seasonally standardizing and detrending the 430-month datasets. Therefore, only the 322-month and detrended monthly significant correlations will be mentioned. Across the cyclogenesis datasets, BB-DS-LS had significant correlations with each subregion: BB (0.67), DS (0.55), and LS (0.48). Across the cyclolysis datasets, BB-DS-LS's significant correlations with each subregion were slightly lower: BB (0.64), DS (0.54), and LS (0.44). Correlations between subregions were mostly insignificant. BB-DS-LS/BB detrended monthly cyclogenesis datasets had the highest significant correlation in January (0.75) while the lowest occurred in July (0.53). BB-DS-LS/DS's highest significant cyclogenesis correlation occurred in February (0.70), while the lowest was in October (0.42). BB-DS-LS/LS's highest significant cyclogenesis correlation occurred in September (0.67), while the lowest was in December (0.47). For cyclolysis, BB-DS-LS/BB had the highest significant correlation in April (0.78) while the lowest was in June (0.34). The highest significant correlation for BB-DS-LS/DS occurred in June and September (0.66), while the lowest occurred in November (0.36). BB-DS-LS/LS's highest significant correlation occurred in June (0.68), while the lowest occurred in May (0.44). BB, DS, and LS were not significantly correlated with each other in any month for both variables.

3.2.4: Maximum Local Laplacian Long-Term and Monthly Variability

Within BB-DS-LS across the 430-month time period, the highest monthly maximum laplacian scores ranged between 16 to 26 mPa/km^{-2}. BB's ranged between 14 to 21 mPa/km^{-2}. DS experienced higher monthly maximum scores than BB and BB-DS-LS, ranging from 15 to

29 mPa/km^{-2}. LS had the highest monthly maximum scores (strongest pressure gradients and cyclone intensities) out of all of the subregions ranging from 19 to 36 mPa/km^{-2}.

Similar to previous variables, the monthly maximum laplacian scores for BB and DS show little to no trend, however LS and BB-DS-LS show small, but insignificant positive trends (Figures 20a-d). For BB-DS-LS, maximum laplacian scores typically were 22 mPa/km^{-2} each year. December 1984 had the highest maximum score for BB-DS-LS (26 mPa/km^{-2}), while July 2009 had the lowest score (8 mPa/km^{-2}). For BB, maximum laplacian scores were typically 16.5 mPa/km^{-2} each year. November 1990 had the overall highest maximum score (21 mPa/km^{-2}), while June 1992 had the lowest score (5.5 mPa/km^{-2}) for BB. For DS, maximum laplacian scores were typically 23 mPa/km^{-2} each year. DS experienced its highest maximum score in December 1984 (29 mPa/km^{-2}); whereas DS's lowest occurred in August 1980 (7 mPa/km^{-2}). LS's maximum laplacian scores were typically 29 mPa/km^{-2} each year. The highest maximum score for LS occurred in December 1994 (36 mPa/km^{-2}) while the lowest was in July 2010 (9 mPa/km^{-2}). At the annual scale, BB-DS-LS's highest average annual maximum score occurred in 1984 (27 mPa/km^{-2}), while 2010 had the lowest (19 mPa/km^{-2}). BB's highest score occurred in 1990 (21 mPa/km^{-2}), whereas the lowest occurred in 1987 (13 mPa/km^{-2}). 1984 had DS's highest score (29 mPa/km^{-2}), while 1985 had DS's lowest (18 mPa/km^{-2}) score. Finally, LS's highest score was in 1994 (36 mPa/km^{-2}), while LS's lowest was in 1990 (24 mPa/km^{-2}).

Maximum laplacian scores averaged across each individual month (e.g., January 1980-2015) show a shared pattern across the subregions where winter months typically had the highest scores and ranges (vice-versa for summer months). BB had the lowest averaged scores in every month. DS and LS's scores were both higher than BB-DS-LS's, however DS's scores

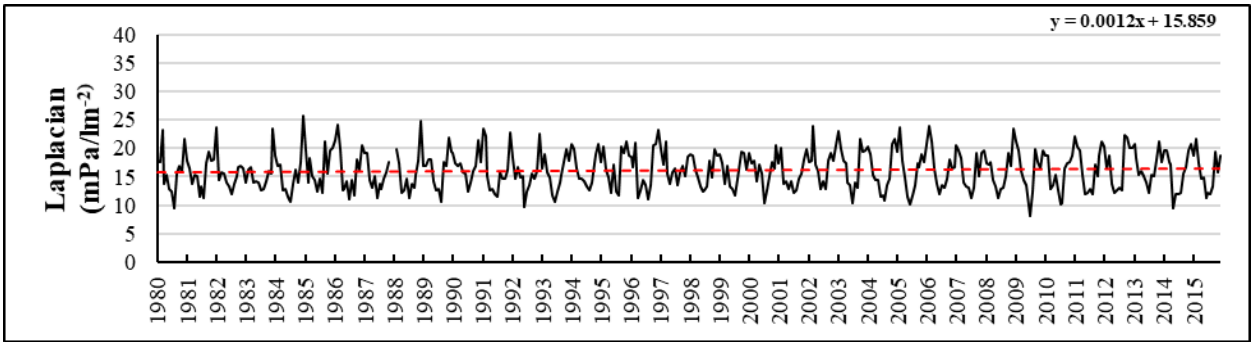

Figure 20a: BB-DS-LS's maximum laplacian time series with trend line in red. Slope equation in upper-right corner.

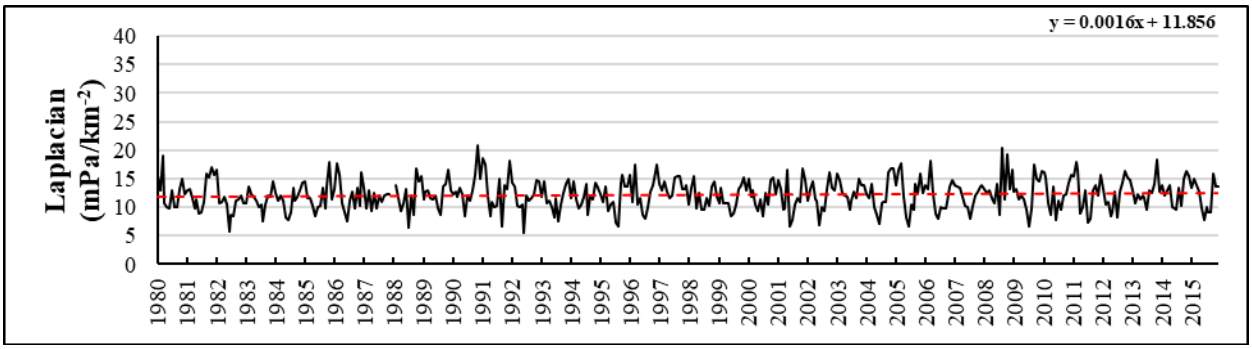

Figure 20b: BB's maximum laplacian time series with trend line in red. Slope equation in upper-right corner.

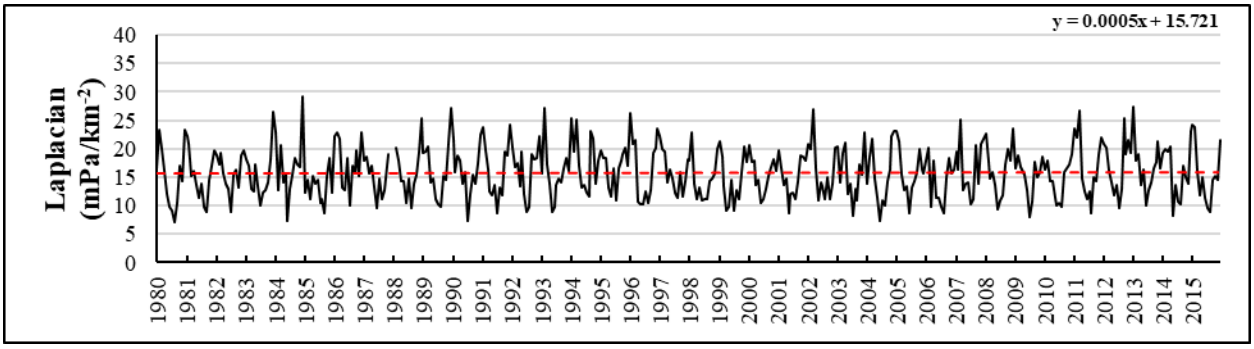

Figure 20c: DS's maximum laplacian time series with trend line in red. Slope equation in upper-right corner.

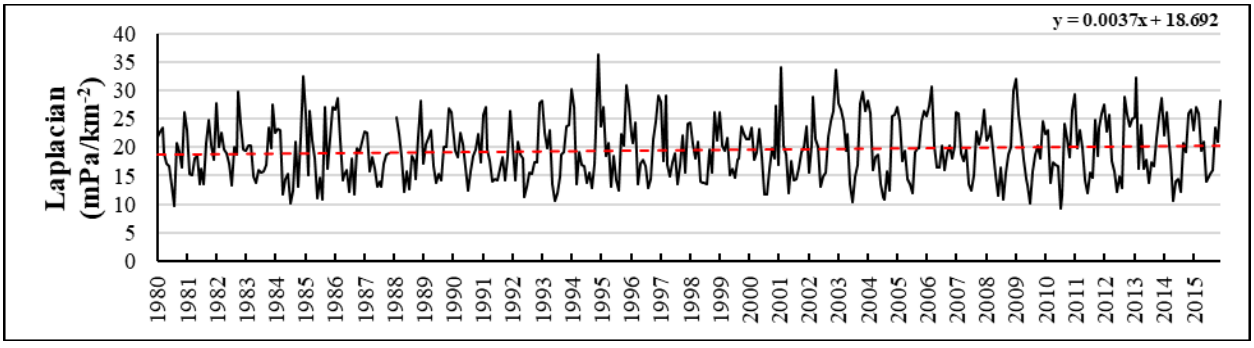

Figure 20d: LS's maximum laplacian time series with trend line in red. Slope equation in upper-right corner.

declined beneath BB-DS-LS's from May-November, then followed BB-DS-LS's pattern through December. LS's scores were the highest across all months, coming closest with BB-DS-LS's during summer (Figure 21).

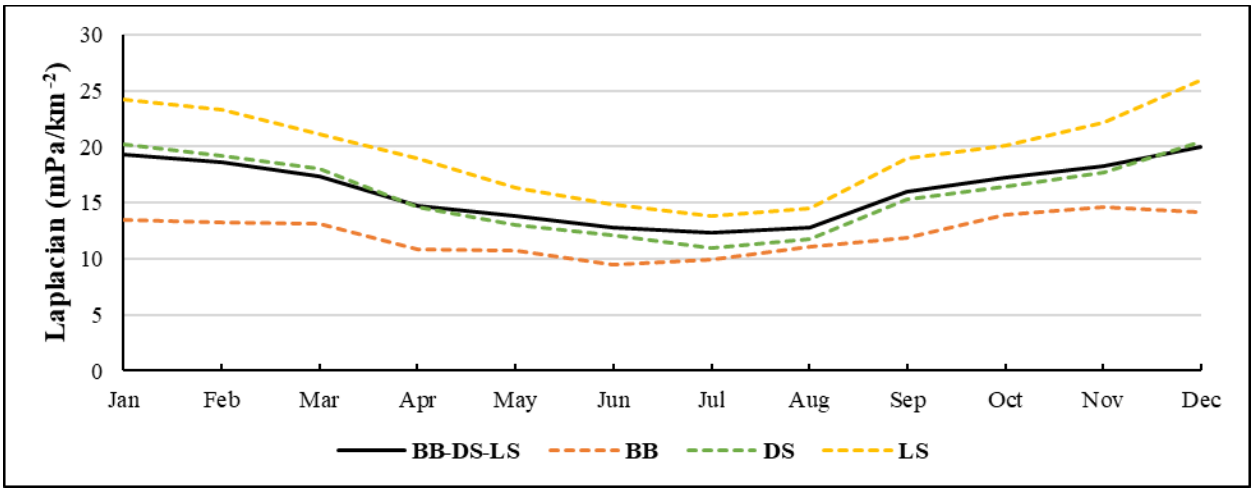

Figure 21: Monthly average maximum laplacian within each subregion from 1980-2015 per monthly basis.

Unlike previous variables, after seasonally standardizing and detrending the 430-month datasets, correlations dropped by about half for most comparisons. To maintain consistency, only the 322-month and detrended monthly correlations will be mentioned. Correlations were positive and moderate-strong and significant between BB-DS-LS and each subregion: BB (0.42), DS (0.42), and LS (0.71). No subregions were significantly correlation with each other in the 322-month datasets for this variable.

In the detrended monthly datasets, significant correlations between BB-DS-LS and the subregions widely varied (more than previous variables) between months. For most months, the

highest significant correlations were associated with BB-DS-LS/LS, with DS's second, and BB's being the lowest. From February-April, July-August, and November-December all subregions were significantly correlated with BB-DS-LS. For BB-DS-LS/BB's correlations, March had the highest significant correlation (0.70), while August had the lowest (0.34) significant correlation.

For BB-DS-LS/DS, December had the highest (0.65), while July had the lowest significant correlation (0.33). BB-DS-LS/LS's highest significant correlation occurred in September (0.82), while the lowest occurred in December (0.64). As for subregional comparisons, DS/BB were significantly correlated in February (0.37) and December (0.45); DS/LS were significantly correlated only in August (0.33).

3.2.5: Mean Latitude Long-Term and Monthly Variability

Within BB-DS-LS across the 430-month period, the average monthly mean latitude of all cyclones ranged mainly from 58° N to 70° N (within LS and DS's boundaries; Figure 22). Due to BB being the most northerly region, average monthly mean latitude values were the highest (70° N to 77° N). DS's values ranged between 62° N to 66° N. Finally, LS's values ranged between 53° N to 57° N. Looking at the monthly averaged mean latitude values, BB, DS, and LS's mean latitudes show less extreme shifts between maximums/minimums than BB-DS-LS's. Furthermore, each subregion's highest maximums and lowest minimums did not occur in the same months or years.

At the annual timescale, 2014 had the highest annual average latitude (66° N), while 2002 had the lowest (63° N) for BB-DS-LS. BB's highest occurred in 1999 (78° N), while BB's lowest occurred in 1983 (73° N). DS's highest occurred in 1998 (65° N) while DS's lowest occurred in 1990 (64° N). LS's highest occurred in 2003 (56° N), while DS's lowest occurred in

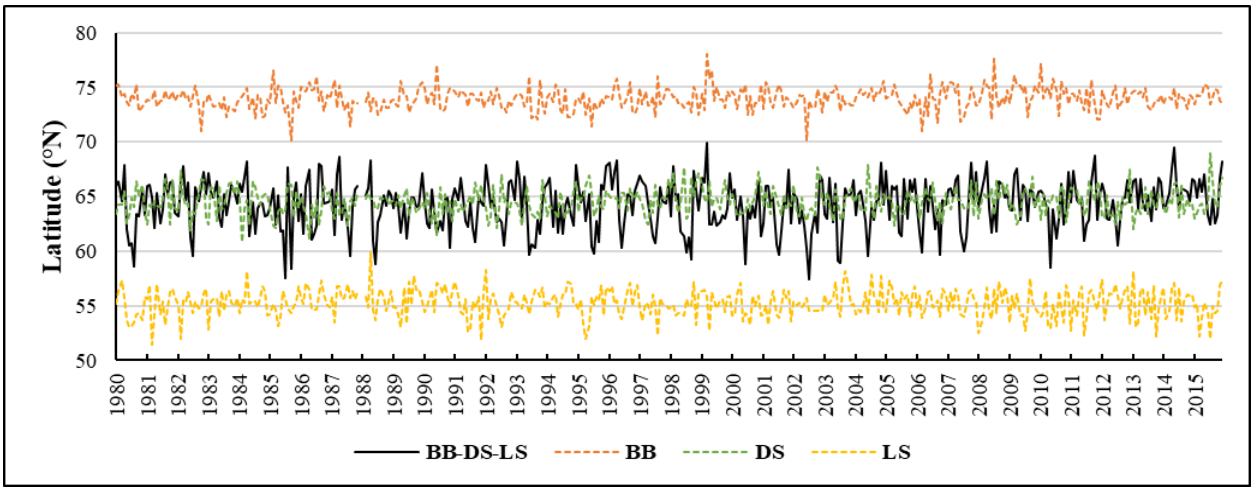

Figure 22: Mean latitude of cyclone time steps in each subregion from 1980-2015.

1980 and 2015 (54.5° N). The monthly mean latitude values averaged across each individual month (e.g., January 1980-2015; Figure 23), show each subregion's mean latitudes remained static across all months, with only BB-DS-LS's latitude values showing variation, decreasing

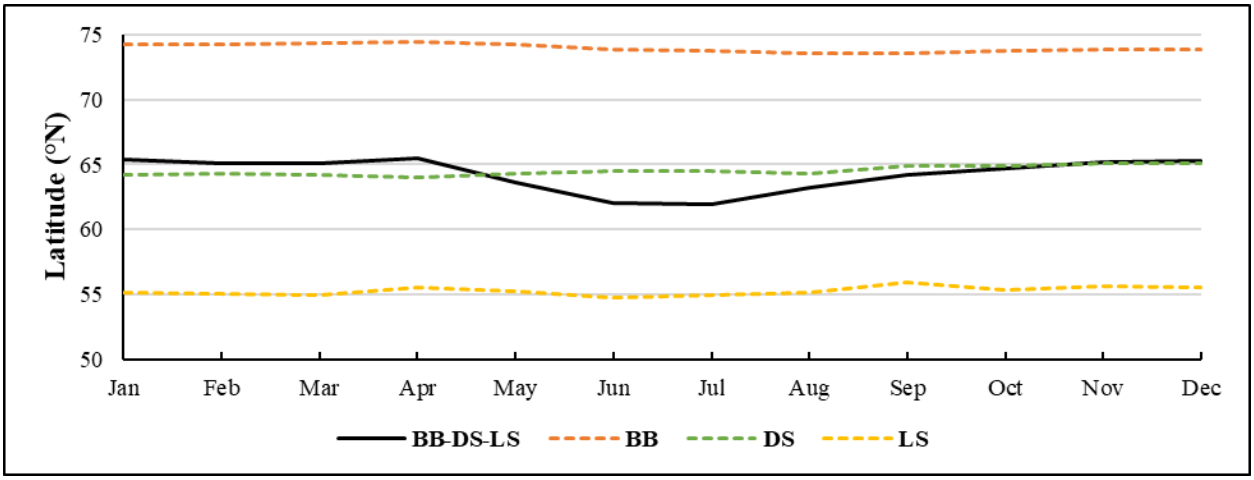

Figure 23: Mean latitude of cyclone time steps in each subregion from 1980-2015 per monthly basis.

from April (at 66° N) to June (at 63° N). From July-December, monthly latitudes gradually increase again.

After seasonally standardizing and detrending the 430-month datasets, correlations had less variation compared to previous variables. Therefore, to maintain consistency only the 322-month and detrended monthly correlations will be mentioned. The only significant comparisons were BB-DS-LS/DS (0.15) and BB-DS-LS/LS (0.71). For the subregion comparisons, only DS/BB (0.18) and DS/LS (0.21) were significantly correlated. Similar to laplacian, significant correlations between BB-DS-LS and the subregions detrended monthly datasets widely differed from month to month. September was the only month when all subregions were significantly correlated with BB-DS-LS. For most months, the highest significant correlations were associated with BB-DS-LS/LS (except for March), then BB-DS-LS/DS (except for September), with BB-DS-LS/BB having the lowest.

Similar to previous variables, significant correlations show less change after detrending the monthly datasets than seasonally standardized and detrending the 430-month datasets. For BB-DS-LS/BB, March had the highest) significant correlation for mean latitude (0.75), while September had lowest (0.50). BB-DS-LS/DS's highest occurred in May (0.40), while March had the lowest (0.34). BB-DS-LS/LS's highest significant correlation occurred in May (0.66), while the lowest occurred in December (0.40). For the subregion comparisons, DS/LS had the highest significant correlation in July (0.54); DS/BB in November (0.40); and BB/LS in August (0.44).

3.2.6: Mean Longitude Long-Term and Monthly Variability

For BB-DS-LS, average monthly mean longitude values typically remained between 56° W and 64° W (Figures 24a-d). Across July-August and November, longitudes were east of 56°

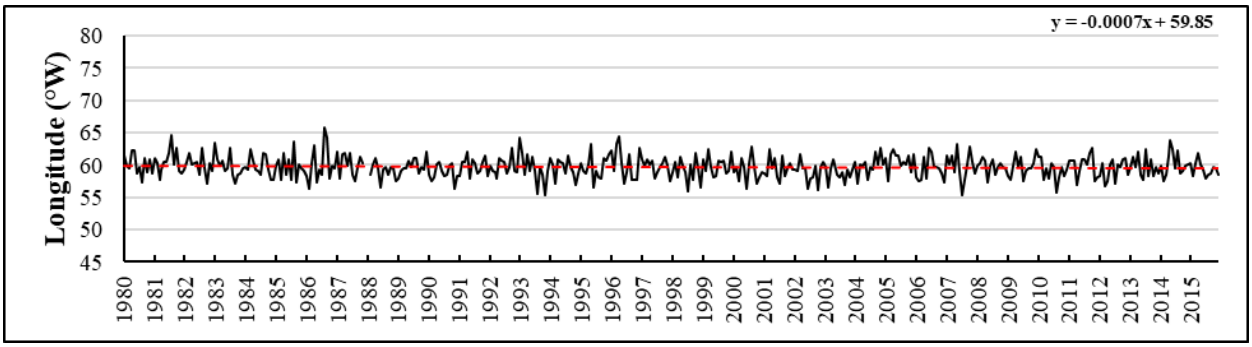

Figure 24a: BB-DS-LS's cyclones mean longitude time series with trend line in red. Slope equation in upper-right corner.

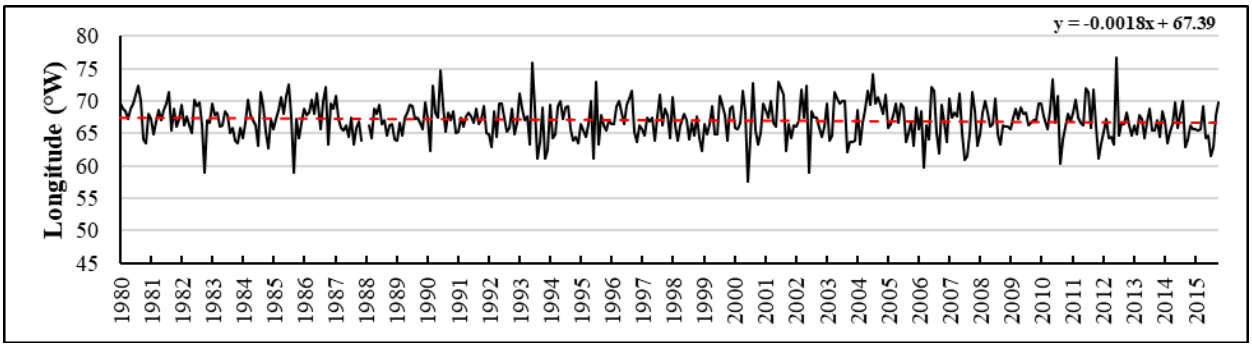

Figure 24b: BB's cyclones mean longitude time series with trend line in red. Slope equation in upper-right corner.

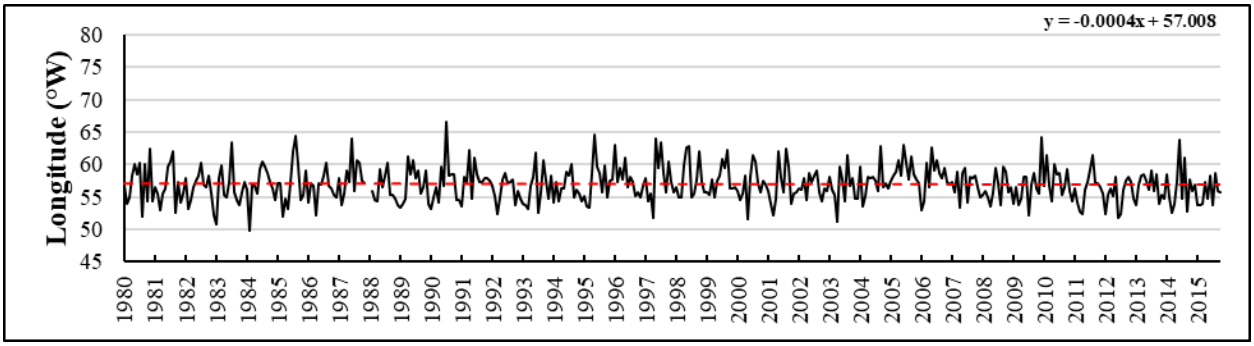

Figure 24c: DS's cyclones mean longitude time series with trend line in red. Slope equation in upper-right corner.

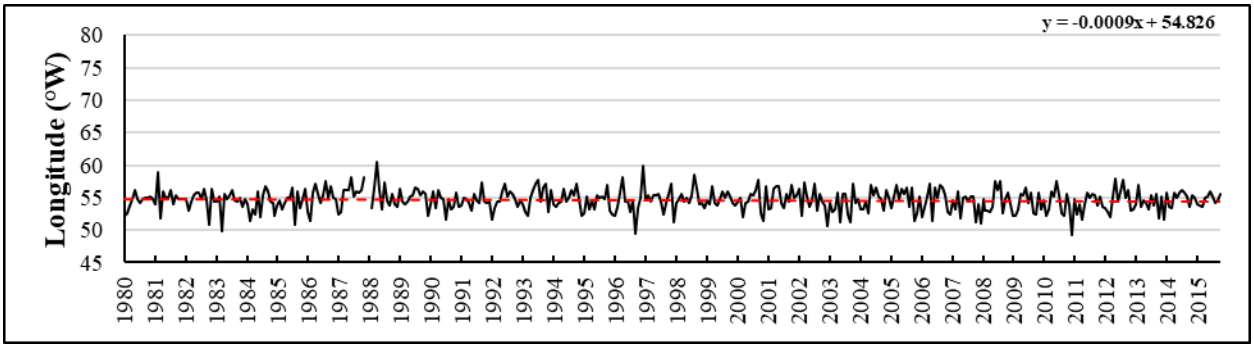

Figure 24d: LS's cyclones mean longitude time series with trend line in red. Slope equation in upper-right corner.

W on four occasions (1995, 2007, and 2010). On the other hand, January, March-May, and August-September had longitudes west of 64° W on four occasions (1981, 1986, 1993, and 1996). July 2007 had the east-most averaged mean longitudes (55° W), while August 1986 had the west-most (66° W) for BB-DS-LS. BB, DS, and LS's averaged mean longitudes show more extreme shifts (and larger ranges) between maximums/minimums than BB-DS-LS's. Furthermore, each subregion's western-most and eastern-most longitudes did not occur in the same months or years. BB's eastern-most mean longitudes were in June 2000 (57.5° W) while June 2012 had the western-most mean (77° W). DS's eastern-most mean longitude was in February 1984 (50° W), while July 1990 had the western-most mean (66.5° W). LS's eastern-most mean longitude was in December 2015 (50° W), while the western-most mean was in April 1988 (60.5° W).

At the annual scale, 1990 had the eastern-most averaged mean longitudes (59° W), while 2005 had the western-most (61° W) mean longitudes for BB-DS-LS. BB's eastern-most mean occurred in 2015 (65.5° W), while the western-most mean occurred in 2004 (69° W). DS's eastern-most mean occurred in 2012 (55.5° W), while the western-most mean occurred in 2005 (59° W). LS's east-most mean occurred in 2007 (54° W), while the west-most mean occurred in 1987 (55.5° W). The averaged mean latitude values for each individual month (e.g., January 1980-2015), show BB, DS, and LS's longitudes migrating westward in summer and eastward in winter, likely due to the sea ice edge retreating/advancing (Figure 25). DS's mean longitudes show the most variation out of the three subregions especially between April and May. LS's longitudes remained mostly static across every month with only small, gradual shifts. Interestingly, BB-DS-LS's mean latitudes show a different pattern, likely due to BB having more cyclones in winter and LS having more in summer.

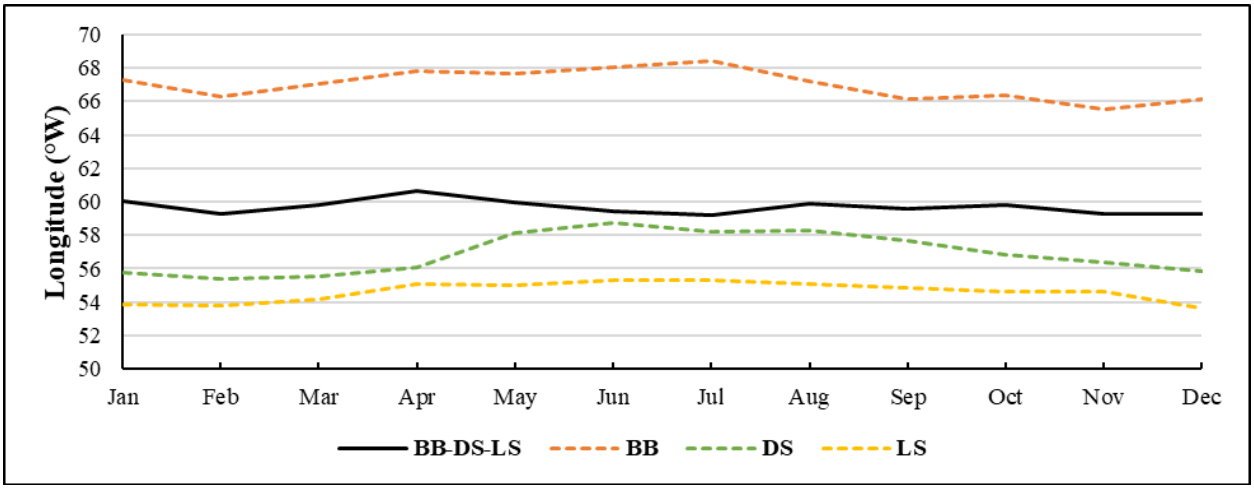

Figure 25: Mean longitude of cyclone time steps in each subregion from 1980-2015 per monthly basis.

Similar to previous variables, seasonally standardizing and detrending the 430-month datasets did not drastically change the correlations, therefore only the 322-month and detrended monthly significant correlations will be mentioned. BB-DS-LS's significant correlations were weak-moderately positive with its subregions: BB (0.48), DS (0.37), and LS (0.21). For the subregion comparisons, DS/BB were significantly correlated (0.11); however, DS/LS and BB/LS were not. Similar to previous variables, significant correlations show less change after detrending the individual monthly datasets than after seasonally standardizing and detrending the 430-month datasets. Significant correlations between BB-DS-LS and the subregions widely differed from month to month. For most months, the highest significant correlations were associated with BB-DS-LS/BB (except February-March and June-July). BB-DS-LS/DS's significant correlations were often the second highest. However, BB-DS-LS/LS's significant correlations shifted the most out of all the subregions, alternating between having the highest or second highest significant correlations. For BB-DS-LS/BB, August and December had the highest (0.62) significant correlation, while May had the lowest (0.30). For BB-DS-LS/DS, August had the

highest significant correlation (0.59), while October had the lowest (0.35). BB-DS-LS/LS's highest significant correlation occurred in March (0.56); whereas the lowest occurred in April (0.36). April and June were the only months where all subregions were significantly correlated with BB-DS-LS. For the subregion comparisons, BB/LS were only significantly correlated in February (0.40) and DS/LS in June (0.42). BB/DS had no significant correlations in any month. Overall, no subregions were significantly correlated with each other during January, March-May, and July-December.

3.2.7: Objective 2 Results Overview

Objective 2 aimed to establish what the cyclone variability was in/between each subregion from 1980-2015. For most variables (except laplacian), significant correlations did not drastically decrease after seasonally standardizing and detrending the 430-month datasets (unlike the sea ice datasets). Furthermore, across most variables' individual monthly datasets, significant correlations dropped less after detrending their values (compared to seasonally standardizing and detrending the 430-month datasets). The only positive significant trend was associated with BB-DS-LS's cyclogenesis events across the 430-month period. BB had the highest range of cyclone events out of the subregions, but LS had the highest overall total across the entire time period. BB and DS experienced the most cyclones during winter whereas LS experienced the most during spring and summer. Furthermore, the annual maximums/minimums of each subregion occurred in different years compared to the other subregions. Across each individual month, significant correlations between subregions were generally higher than with the 322-month datasets, however BB was not significantly correlated with LS in any total number of cyclone datasets. BB had the highest monthly average minimum central pressures across the time period,

whereas LS had the lowest. Every subregion experienced their highest minimum monthly central pressures during summer (vice-versa in winter); however each subregion's overall lowest monthly values occurred in different years. LS had the highest significant correlation with BB-DS-LS across the 322-month period with the central pressure datasets, however BB-DS-LS/BB had the highest in the individual monthly datasets. Across all subregions for minimum central pressure, the lowest significant correlations with BB-DS-LS occurred during winter months. BB had highest total number of cyclogenesis and cyclolysis events; whereas LS had the lowest. Although every subregion experienced more cyclolysis than cyclogenesis events, DS and LS had more variability in their total number of cyclogenesis events, whereas BB and BB-DS-LS experienced the opposite. BB and DS were most similar, with their highest number of both events occurring in winter (vice-versa in summer), whereas LS was more unique, where both its highest and lowest numbers were during late spring through summer. BB and DS's annual maximums of both events occurred closer together, however DS and LS's annual minimums of both events were closer together. BB and DS had the highest significant correlations with BB-DS-LS's cyclogenesis events during winter; whereas LS's highest were in summer. No subregions' cyclogenesis and cyclolysis events were significantly correlated in any month. LS had the highest variability and maximum monthly laplacian scores out of all of the subregions. Every subregion's overall maximum laplacian scores occurred during winter in different years across the first-half of the period. In general, the highest maximum scores occurred during winter (vice-versa in summer). LS had the highest significant correlation with BB-DS-LS across the 322-month period and across most individual months; however, no subregions were significantly correlated with each other. Furthermore, BB's laplacian significant correlations with BB-DS-LS had the most variability between months; whereas LS's has the least. Most cyclones had mean

latitudes within LS and DS's boundaries. The highest annual mean latitudes for each subregion occurred from 1999-2003, whereas their lowest were more spread out across different decades. For longitude, DS and BB's values had the most variability, shifting westward during early summer (vice-versa in autumn and winter) as a result of variation in the sea ice edge; LS's values show much less variability.

Objective 2's identified each subregion's general cyclone variability based upon several common cyclone characteristics. Similar to Objective 1, these results show that even though BB, DS, and LS are geographically connected, cyclone variability within each subregion is unique at multiple timescales.

3.3 Objective 3: What are the Influences of Local Sea Ice Area vs. Teleconnections on Cyclone Variability in Baffin Bay, Davis Strait, and Labrador Sea?

Objective 3's goal (and the overall research question) was to identify the monthly and long-term influences of local (sea ice) and remote (teleconnections) drivers with each cyclone variable from 1980-2015 in BB-DS-LS and every subregion (BB, DS, and LS). Understanding the influence both drivers have on cyclone variability in BB, DS, and LS can help illustrate how unique BB-DS-LS is compared to the North Atlantic. Objective 3's results present an overview of the significant relationships between both drivers and each cyclone variable for every subregion. Due to large number and magnitude of significant correlations, only the key observations will be mentioned.

3.3.1: Sea Ice and Cyclone Variability

Between all 322-month sea ice and cyclone variables comparisons (Figure 26), 15% were significantly correlated; all remaining below 0.25. BB-DS-LS's sea ice dataset had the most significant correlations (14), then DS's (13), then LS's (7), and finally BB's (2). The longitude datasets had the highest number of significant correlations (17), whereas the central pressure and laplacian datasets had the lowest (0-1). No cyclone variable had consistent significant correlations across every subregion.

BB-DS-LS's sea ice area had the strongest significant correlation with BB's cyclogenesis (0.19) and cyclolysis (0.21) events, while the weakest was with BB and DS's maximum laplacian scores, and DS's minimum longitudes (all 0.12). BB-DS-LS's sea ice dataset was also significantly correlated with BB-DS-LS's and BB's latitude datasets, BB's total number of cyclones, and DS's maximum and mean longitudes datasets. BB's sea ice area was only significantly with BB's mean and minimum longitude datasets (both 0.12). DS's sea ice area had its strongest significant correlation with BB's cyclogenesis and cyclolysis events and DS's maximum (0.21) and mean (0.22) longitude datasets, while the weakest was with LS's minimum longitude (0.11). DS's sea ice area was also significantly correlated with BB-DS-LS's latitude datasets, BB's total number of cyclones, and BB and DS's longitude datasets (0.17 to 0.19). LS's sea ice area (like DS's) had its strongest significant correlation with BB's cyclolysis events (0.20) while the weakest was with BB-DS-LS's minimum latitude dataset (0.11). LS's sea ice area was also significantly correlated with BB-DS-LS's maximum and mean latitudes, BB's total number of cyclones, and DS's maximum and mean longitude datasets (0.12 to 0.16).

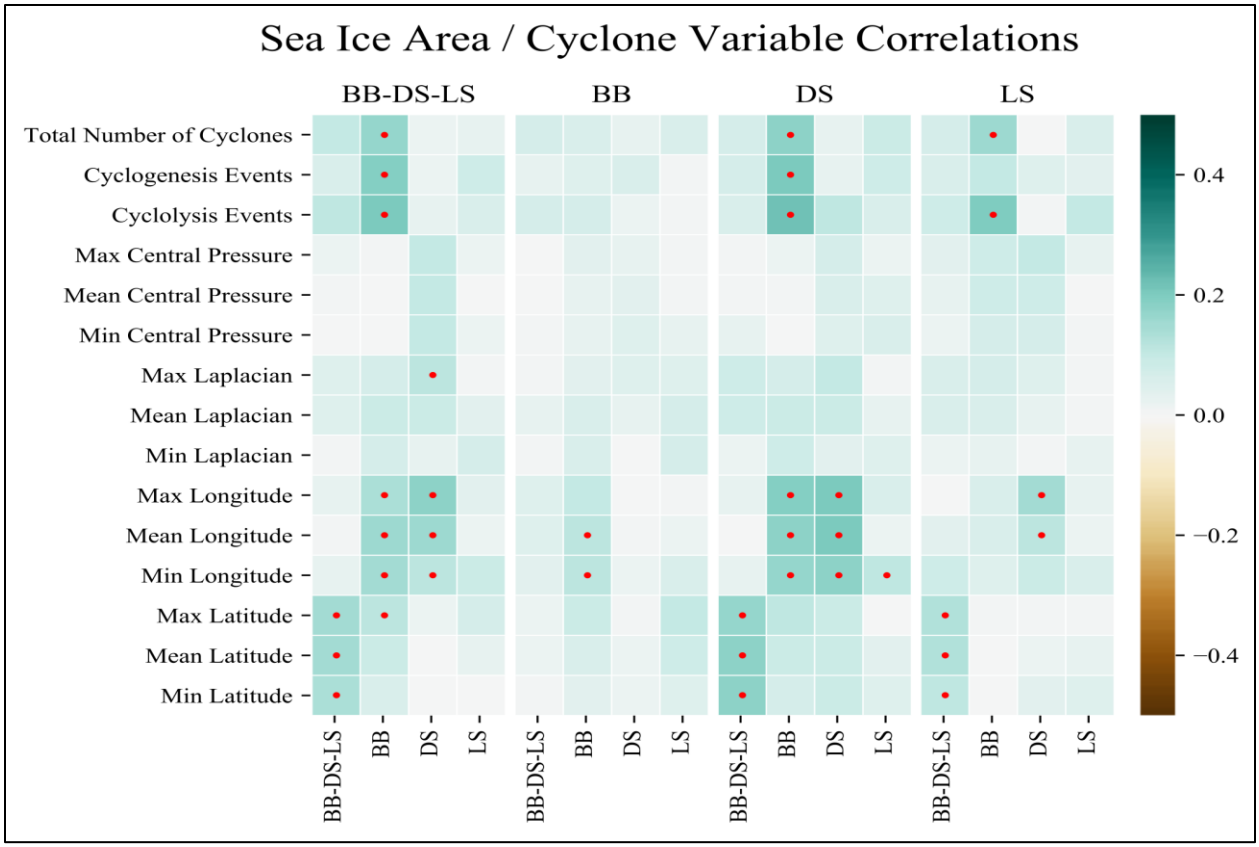

Figure 26: 322-month correlations between each cyclone variable and each subregion's sea ice area. Red dot indicates p-value < 0.05.

3.3.2: Teleconnections and Cyclone Variability

Between all 322-month teleconnection and cyclone variables comparisons (Figure 27), 25% were significantly correlated. The NAO and AO had the most significant correlations (33 and 30), followed by the EAWR (11), then the PNA and PEP (both 6), and finally the PDO (5). Of all cyclone variables, the central pressure datasets had the most significant correlations (41) while central pressure and laplacian datasets had the lowest (0-1). The NAO's significant correlations ranged from 0.12 to 0.42, with the weakest being attributed mainly with every subregions' longitude and laplacian; while the strongest were with BB-DS- LS's total number of

cyclones, and every subregion's central pressure. Furthermore, all subregions' total number of cyclones were significantly correlated with the NAO. The AO's significant correlations ranged from 0.11 to 0.42 with the weakest correlations being attributed with every subregions' laplacian, latitude, and longitude; while the strongest were with every subregion's central pressure. Furthermore, every subregions' maximum, mean and minimum central pressure datasets were significantly correlated with the AO (0.24 to 0.42; 0.19 to 0.41; 0.14 to 0.39). The PDO, PNA, and PEP had the smallest ranges (and total numbers) of significant correlations (all being < 0.20). The PDO and PNA typically had significant correlations with BB-DS-LS and BB's

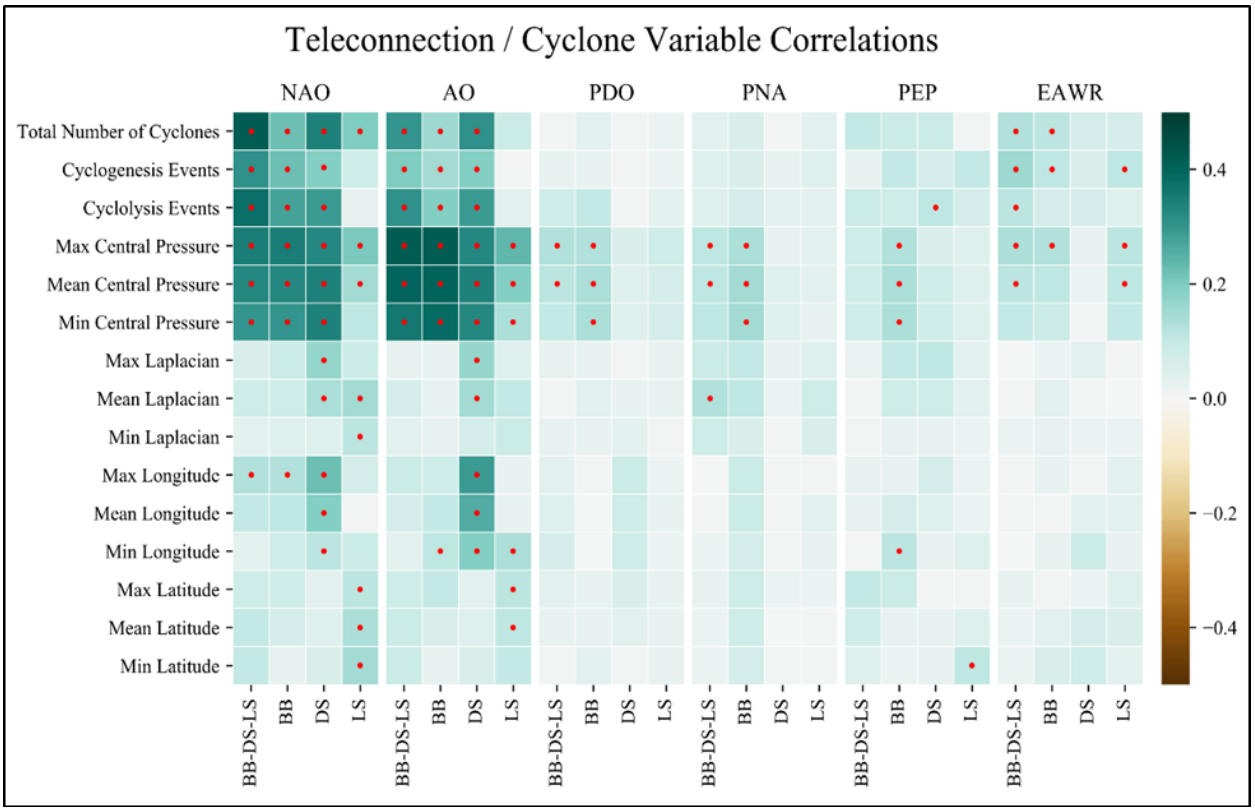

Figure 27: 322-month correlations between each cyclone variable and each teleconnection pattern. Red dot indicates p-value < 0.05.

central pressure datasets, while the PEP was mainly significantly correlated with BB's central pressure. All had their highest significant correlations with BB's minimum central pressure (0.13 to 0.15). The EAWR's significant correlations were also < 0.20, yet had a higher total number than the PDO, PNA, and PEP. The EAWR was mainly significantly correlated with BB-DS-LS's total number of cyclones, central pressure, cyclogenesis, and cyclolysis events; however there were also significant correlations with BB and LS's maximum central pressure and total cyclogenesis events.

3.3.3: Individual Monthly Sea Ice and Cyclone Variability

Out of all the individual monthly sea ice and cyclone variables comparisons (Figure 28), 7.5% were significantly correlated, January had the highest totals (29), while April had the lowest (4). Unlike the 322-month comparisons, DS's sea ice area had the highest number of significant correlations (77), followed by BB-DS-LS (52), then LS (37), and finally BB (34). The cyclolysis events datasets had the most significant correlations (19), however mean longitude had the second highest total (18). Latitude datasets had the lowest totals (8-11). Overall, sea ice's individual monthly significant correlations were stronger than the 322-month's. Comparing the subregions, it appears the strength and frequency of each's significant correlations do not consistently occur in the same seasons or months.

BB-DS-LS's individual monthly significant sea ice area correlations ranged from 0.33 to 0.56, with the weakest correlations being attributed mainly with BB's minimum laplacian, DS's mean longitude, and LS's cyclolysis events; whereas the strongest were with LS's maximum longitude. BB-DS-LS's sea ice area was also significantly correlated with BB-DS-LS and DS's

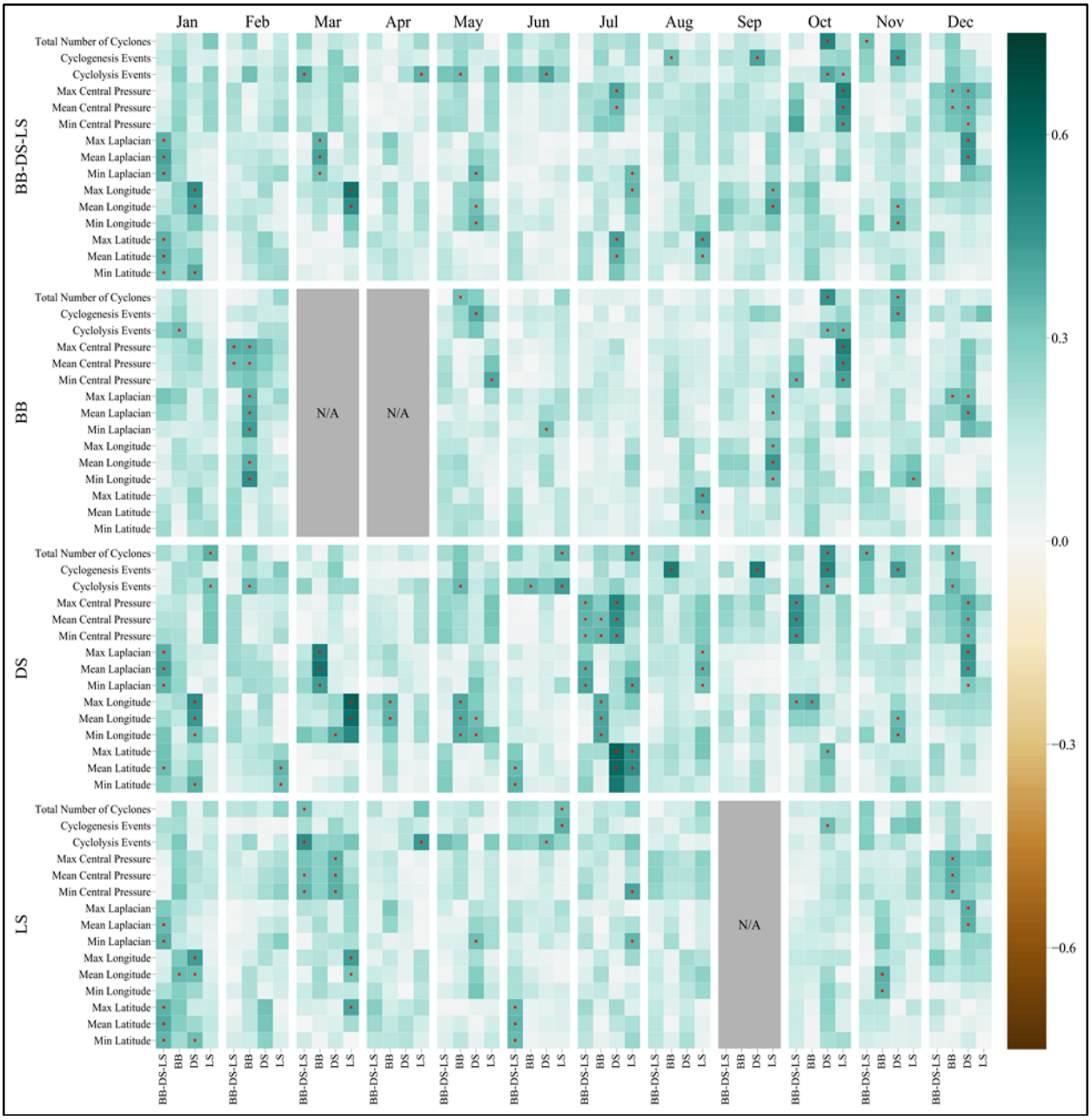

Figure 28: Individual monthly correlations between each cyclone variable and each subregion's sea ice area. Red dot indicates p-value < 0.05. Grey boxes indicate comparisons that could not be done.

total number of cyclones in early winter (0.34 and 0.50). Furthermore, every subregion's mean central pressures were significantly correlated with BB-DS-LS's sea ice area during early-mid

winter (0.34 to 0.48). Only a few significant correlations were with the cyclogenesis datasets, however every subregion's cyclolysis events were significantly correlated in spring-early summer (0.35 to 0.40). BB-DS-LS and BB's laplacian datasets were significantly correlated with BB-DS-LS's sea ice in winter-early spring (0.33 to 0.42). There were also several significant correlations with the latitude and longitude datasets across different months, however no distinct patterns were seen.

BB's significant sea ice area correlations ranged from 0.33 to 0.51, with the weakest correlations being attributed mainly with BB's total number of cyclones and LS's mean laplacian; whereas the strongest were with LS's maximum central pressure. BB's sea ice area was significantly correlated with BB and DS's total number of cyclones only in a few months. BB-DS-LS and BB's maximum and mean central pressures were significantly correlated with BB's sea ice in February while LS's same central pressures were in October (0.34 to 0.51). BB, DS, and LS's cyclolysis events were significantly correlated with BB's sea ice area across different months during early-mid winter (0.34 to 0.36). BB, DS, and LS's maximum and mean laplacian datasets were significantly correlated with BB's sea ice in different months from late autumn-late winter (0.33 to 0.41). There were also several significant correlations with the latitude and longitude datasets in different months, however no distinct patterns were seen.

DS's significant sea ice area correlations ranged from 0.33 to 0.61 (larger than BB's), with the weakest correlations being attributed mainly with LS's maximum and minimum laplacian; whereas the strongest were with DS's maximum latitude and LS's maximum longitude. Every subregion's total number of cyclones was significantly correlated with DS's sea ice area during early to mid-winter (0.35 to 0.46). All but LS's mean and minimum central pressure datasets were significantly correlated with DS's sea ice area in July (0.34 to 0.48). The

laplacian datasets had several significant correlations in different months; however no distinct patterns were seen. BB-DS-LS, DS, and LS's mean latitudes were significantly correlated with DS's sea ice area in summer (0.35 to 0.59). BB's longitude datasets were significantly correlated with DS's sea ice area in May and July (0.37 to 0.41); additional significant correlations with every subregion's longitude datasets occurred across different months.

LS's significant sea ice area correlations ranged from 0.32 to 0.48 (weakest of all subregions), with the weakest correlations being attributed mainly with LS's mean longitude; whereas the strongest were with BB-DS-LS's cyclolysis events. BB-DS-LS and LS's total number of cyclones were significantly correlated with LS's sea ice area in a few months, but no distinct patterns were seen. Similarly, every subregions' central pressure datasets were significantly correlated in different months mainly in winter (0.34 to 0.38). DS and LS's cyclogenesis datasets were significantly correlated across different months (all < 0.40), but no distinct patterns were seen. However, these same subregions' cyclolysis events were significantly correlated with LS's sea ice area in spring-summer (0.35 to 0.48). The laplacian and latitude datasets also had several significant correlations across different months (all < 0.40). BB, DS and LS's mean longitude datasets were significantly correlated with LS's sea ice area in different months across winter (0.32 to 0.38).

3.3.4: Individual Monthly Teleconnection and Cyclone Variability

Out of all individual monthly teleconnection and cyclone variables comparisons (Figure 29), 12.5% were significantly correlated, with April having the highest total (71), while September had the lowest (17). Similar to the 322-month comparisons, the NAO and AO had the most significant correlations (197 and 165), however the PNA (57) and PEP (50) were higher

than the EAWR (47), but the PDO (32) was still the lowest. Out of all cyclone variables, central pressure had the most significant correlations (72-82) while latitude had the lowest (15-16). Overall, the individual monthly significant correlations were stronger than the 322-month's. The strongest typically occurred during spring-summer (vice-versa for winter).

The NAO's significant correlations ranged from 0.33 to 0.71, with the weakest being attributed mainly with BB-DS-LS's total number of cyclones, DS and LS's cyclogenesis events and laplacian; whereas the strongest were with BB-DS-LS's central pressure. Overall, central pressure datasets were significantly correlated with the NAO in the most months out of any variable (7 months for BB-DS-LS, BB, and DS; 5 months for LS). All subregions' total number of cyclones were significantly correlated with the NAO in August. Central pressure in every subregion had significant correlations with the NAO generally occurring in two to three-month increments (e.g., February-April, June-July, and September-October). BB-DS-LS, BB, and DS's cyclogenesis and cyclolysis events had the most significant correlations with the NAO in January-February, June, and August-November (0.33 to 0.62). Laplacian scores in every subregion were significantly correlated with the NAO mainly in March-June and August (0.33 to 0.58). BB's latitude datasets were mainly significantly correlated with the NAO in winter (0.39 to 0.45) whereas LS's were in summer (0.40 to 0.43). DS's longitude datasets were also significantly correlated with the NAO in winter and summer (0.36 to 0.62).

The AO's significant correlations ranged from 0.33 to 0.71 (same as the NAO). The weakest were with BB-DS-LS's cyclogenesis events, DS's cyclolysis events and mean latitude, and BB-DS-LS's maximum longitude; whereas the strongest were with BB's central pressure. Overall, central pressure datasets were significantly correlated with the AO in the most months out of any variable. Every subregion's (excluding BB) total number of cyclones were

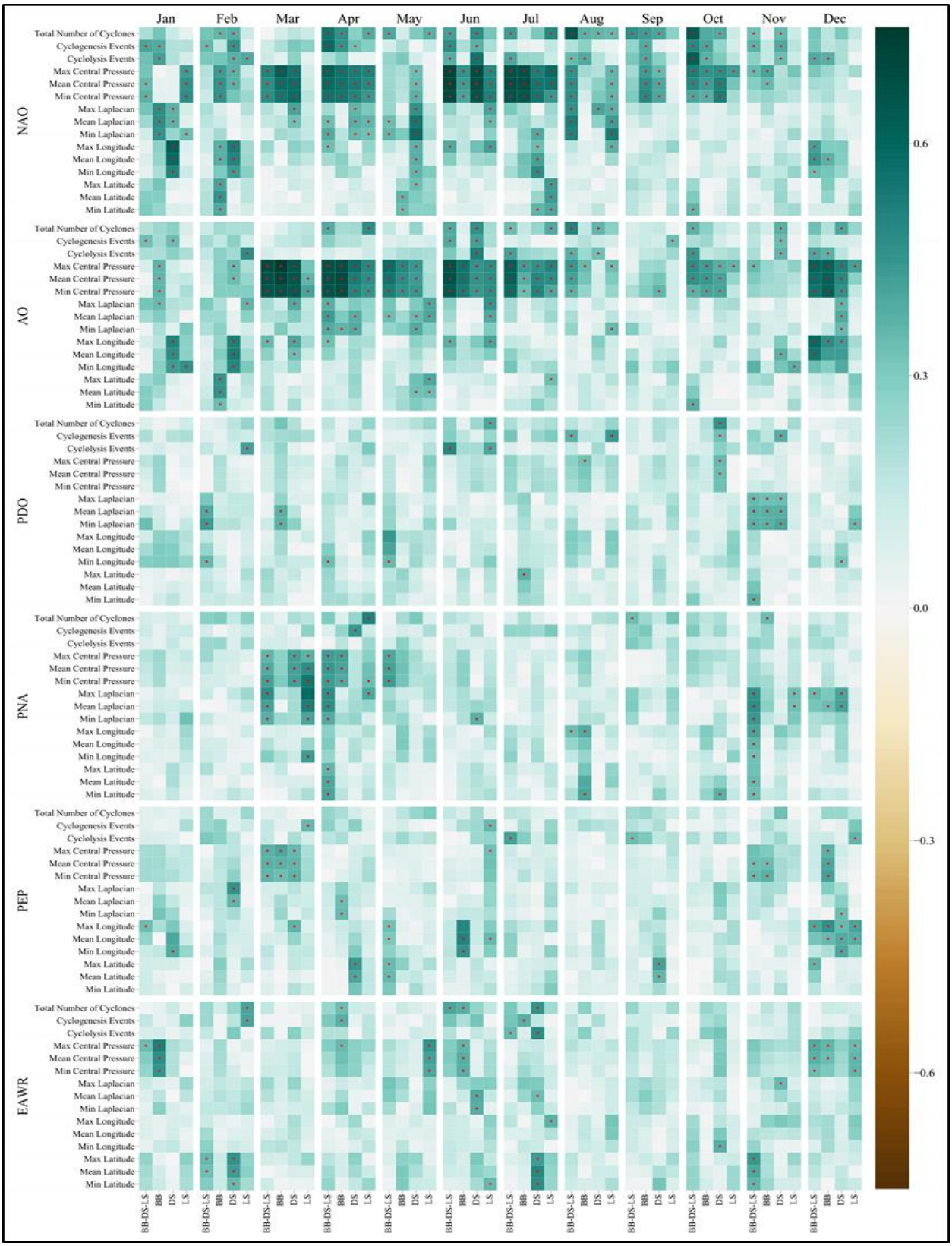

Figure 29: Individual monthly correlations between each cyclone variable and each teleconnection pattern. Red dot indicates p-value < 0.05.

significantly correlated with the AO in early-late summer (0.34 to 0.50). Similarly, every subregion's central pressure datasets were significantly correlated with the AO in March-June, October, and December (0.34 to 0.75), with the strongest correlations occurring in late-spring. Generally, every subregion's cyclogenesis or cyclolysis events were significantly correlated with the AO in January and July-August (0.33 to 0.51). Each subregion's maximum laplacian datasets were significantly correlated in mid-late winter (0.35 to 0.39), however the mean and minimum scores had slightly higher significant correlations (< 0.05 difference) during summer. BB's latitude datasets were only significantly correlated in February (0.34 to 0.45). Most of each subregions' longitude datasets were significantly correlated mainly in January-March and November-December (0.33 to 0.55).

The PDO's significant correlations ranged from 0.32 to 0.49 (lower than the NAO and AO). The weakest were with DS's minimum latitude, while the strongest were with BB-DS-LS's cyclolysis events. DS's total number of cyclones were significantly correlated with the PDO only in June (0.45), while LS's were significantly correlated with the PDO in October (0.40). BB and DS's maximum central pressure datasets were significantly correlated with the PDO in late summer and early autumn (0.33 and 0.35). BB-DS-LS, DS, and LS's cyclogenesis events were significantly correlated in different months in late summer and early winter, however BB-DS-LS and LS's cyclolysis events (0.49 and 0.42) were significantly correlated earlier in June. Every subregion's laplacian datasets typically had significant correlation in February-March and November-December (0.33 to 0.43). The latitude and longitude datasets only had a few significant correlations (all > 0.40) across different months, but no distinct patterns were seen.

The PNA's significant correlations ranged from 0.33 to 0.54 (lower than the NAO and AO, but higher than the PDO). The weakest were with BB-DS-LS's maximum longitude and

LS's minimum laplacian, while the strongest were with LS's minimum central pressure. LS's total number of cyclones only had a few significant correlations with the highest (0.51) in April. Every subregion's central pressure datasets were significantly correlated with the PNA in March (0.34) and April (0.54). No subregion's cyclolysis events were significantly correlated with the PNA. DS's April cyclogenesis events had the only significant correlation for this variable with the PNA. BB-DS-LS laplacian datasets were significantly correlated with the PNA in March-April and November (0.38 to 0.48). BB-DS-LS, DS, and LS's max laplacian scores were significantly correlated with the PNA in winter (0.35 to 0.40), however LS's mean and minimum scores were also significantly correlated in March. BB-DS-LS's latitude datasets were significantly correlated with the PNA only in April (0.36 to 0.41). There longitude datasets only had a few significant correlations (most < 0.40) across different months.

The PEP's significant correlations ranged from 0.31 to 0.46 (lower than the NAO, AO, PDO, and PNA). The weakest were with BB-DS-LS's mean longitude, while the strongest were with BB's maximum and minimum longitude. The total number of cyclones datasets did not have any significant correlations with the PEP. BB-DS-LS, BB, and DS's central pressure datasets were significantly correlated with the PEP in March (0.36 to 0.42) and November (0.34 to 0.40). The cyclogenesis, cyclolysis, laplacian, and latitude datasets only had a few significant correlations (most < 0.40). Every subregions' maximum (west-most) longitude datasets were significantly correlated in December (0.35 to 0.46).

The EAWR's significant correlations ranged from 0.33 to 0.51 (higher than the PDO and PEP). The weakest were with BB-DS-LS's mean latitude, while the strongest were with BB's maximum central pressure. BB-DS-LS and DS's total number of cyclones were significantly correlated with the EAWR in summer (0.38 and 0.45). BB-DS-LS, BB, and LS central pressure

datasets were significantly correlated with the EAWR during winter (0.35 to 0.51). BB's cyclogenesis and BB-DS-LS and DS's cyclolysis events were significantly correlated in July (0.35 to 0.38). Laplacian datasets had few significant correlations with the EAWR (all < 0.40) across different months. BB-DS-LS and DS's maximum and mean latitude datasets were significantly correlated with the EAWR in February (0.35 and 0.45; 0.43 and 0.44). None of the longitude datasets had significant correlations with the EAWR.

3.3.5: Objective 3 Results Overview

Objective 3 aimed to answer the overall research question by determining how local and remote drivers influence cyclone variability in and between each subregion from 1980-2015. Across the individual and 322-month comparisons for both potential drivers, all significant correlations were positive. For the 322-month comparisons, 15% of the local driver and 25% of the remote driver's correlations were significant. For the local driver, BB-DS-LS's sea ice area had the most significant correlations followed by DS, then LS, and finally BB having the lowest.

The NAO and AO had the highest numbers for the remote driver, followed by the EAWR, PNA/PEP, and the PDO. All local driver's significant correlations remained below 0.25, whereas the remote driver's remained below 0.50. The longitude datasets has the highest number of significant correlations with the local driver, while the central pressure datasets had the most with the remote driver. However, when only looking at the NAO and AO, the central pressure datasets had the strongest significant correlations. For the individual monthly comparisons with the cyclone variables, similar to the 322-month comparisons, fewer local than remote driver comparisons were significantly correlated (7.5 vs. 12.5%). January had the highest total significant correlations, while April had the lowest for the local driver. However, April had the

highest number of significant correlations for the remote driver, while September has the least. Unlike the 322-month local driver comparisons, DS had the most significant correlations, while BB still had the least. However, the NAO and AO still had the highest for the remote driver, while the PDO had the lowest. Cyclolysis and longitude had the highest number of significant correlations for the local drivers, while central pressure had the highest for the remote drivers. For both drivers, latitude datasets had the lowest number of significant correlations. The individual monthly comparisons for both drivers had higher ranges and overall values than the 322-month comparisons (0.32 to 0.71). DS had the highest range and overall highest magnitude significant correlations of the local drivers, while the NAO and AO had the highest for the remote driver comparisons. These results successfully identified several possible relationships between sea ice and teleconnections variability with cyclone variability in BB, DS, and LS. Furthermore, these results show that across multidecadal timescales, the NAO and AO have the strongest correlations with central pressure of cyclones in every subregion; this relationship is also evident for the PDO, PNA, and EAWR, but at much weaker correlations. At a lower magnitude, BB-DS-LS's sea ice area has a likely relationship with the longitudinal position of cyclones in DS, while also potentially affecting the number of cyclogenesis and cyclolysis events within BB-DS-LS.

4. DISCUSSION AND CONCLUSION

4.1: Objective 1

Objective 1's goal was to establish what the sea ice area variability was in each subregion and how it compared to the NH's from 1980-2015. Objective 1's results additionally intended to create sea ice variability datasets to determine the influence of sea ice in BB-DS-LS as a local driver of cyclone variability (later discussed in Objective 3). However, it was also intended to identify how sea ice varies in each subregion of BB-DS-LS and how this compares to the NH to better understand how distinct these subregions are relative to the larger region of which they are a part. The results illustrate:

1. Across different timescales, the NH, BB-DS-LS, and its subregions all have significant negative trends in sea ice area, but at different magnitudes.
2. Although BB-DS-LS and each subregion's sea ice variabilities are significantly correlated with the NH's (even after accounting for seasonality and long-term trends), less than one-third of the variance of each subregion's sea ice variability is explained by the NH's variability.
3. Significant relationships between BB-DS-LS and each subregion with the NH greatly vary across each month and are influenced by long-term trends.
4. DS and LS lost the most sea ice area during winter months, while the NH, BB-DS-LS, and BB lost the most during summer months.
5. The highest and lowest average sea ice coverage occurred in the same months for the NH and all subregions.
6. In general, the lowest overall sea ice minimums occurred after 2005, while the maximums occurred before 1996.

Understanding long-term sea ice variability between BB-DS-LS and its subregions to the NH requires the use of consistent datasets spanning several decades. A number of studies have focused on sea ice in BB-DS-LS over the past several decades (Wang et al. 1994; Parkinson, 1995; Mysak et al. 1996; Stern and Heide-Jørgensen, 2003; Heide-Jørgensen et al. 2007a; Bi et al. 2019). However, only Cavalieri and Parkinson (2012) provide a consistent long-term dataset (using only satellite-derived data) for BB-DS-LS, but not for each subregion. Additionally, few studies have even compared BB-DS-LS with the NH at any timescale (Parkinson et al. 1999; Onarheim et al. 2018). It is hard to compare these studies because not only do the boundaries of BB-DS-LS differ, but each subregion also tends to be labeled differently. Additionally, the 15% coverage threshold used by NSIDC potentially exaggerates the actual coverage and variability occurring in these subregions. Even so, this study provides one of the most detailed sea ice comparisons between the NH and BB-DS-LS, as well as between BB, DS, and LS, creating a holistic overview of local sea ice variability.

The NH's 430-month anomalies align with published values from NSIDC. The NH and BB-DS-LS's 430-month sea ice area datasets show good agreement with the results of Cavalieri and Parkinson (2012) over 1980-2010, despite the somewhat different domain. Sea ice area maximums occurring in the first-half of the time period also align with the NH's and BB-DS-LS's observations. Even though the 1980-2015 trends are more negative than their 1980-2010 trends, the same conclusion was reached: BB-DS-LS's (and each of its subregions') sea ice variability depicts a negative trend at a weaker magnitudes than the NH's. After removing seasonality and long-term trends, comparisons still show weak significant correlations between every subregion's and the NH's sea ice area variabilities. These results agree with the findings of Onarheim et al. (2018), who discuss the large interannual variability in sea ice cover in

polar/subpolar seas (including BB-DS-LS) is mostly due to abrupt shifts in seasonality between months, thus influencing the rate of sea ice export and expansion within and between each subregion. The NH, BB-DS-LS, and BB's lowest monthly sea ice area variabilities also agree with the results of Onarheim et al. (2018), who found the largest variabilities in the NH's sea ice extent from 1979-2016 occurred in late summer. BB and the NH's similar sea ice variability could be linked to how they are both connected to the Arctic Ocean and being the farthest north, are subjected to a similar atmospheric forcing regime, which aligns with Wang et al. (1994) and Stern and Heide-Jørgensen (2003) findings of positive correlations existing between winter sea ice concentration in BB and a one-year lagged response to shifts in the NAO. DS and LS's sea ice variability in winter supports the study of Heide-Jørgensen et al. (2007a-b) who identified winter sea ice coverage in DS to be positively correlated and statistically significant with the AO, but not with the NAO, from 1979-2002; additionally they also found sea ice anomalies between DS and LS during winter were positively correlated and statistically significant across the same time period. However, Partington et al. (2003) found that only LS has positive sea ice anomalies with the NAO (likely associated with different boundaries used). The NH's months of maximum and minimum monthly sea ice area loss align with the results of Onarheim et al. (2018), however BB-DS-LS's maximum month occurs in January in their study, which could be related to the type of boundaries used. Their results also confirm that September has the lowest average monthly coverage for BB-DS-LS and the NH. DS's lowest minimums occurring abruptly after some its highest maximums in the mid-eighties is likely due to increases in salinity levels and/or shifts in atmospheric forcing from the NAO which is supported by Mysak et al. (1996), Belkin et al. (1998), and Alexander et al. (2004). According to Belkin et al. (1998), a similar salinity anomaly was likely responsible for DS's large minimum in 1993 and subsequent decline. DS's

highest variability of sea ice area out of the subregions was earlier identified by Environmental Working Group (2000) and Stern and Hedie-Jørgensen (2003), who claimed DS and LS were the most variable subpolar regions in the NH from 1972-1994. DS experiencing the highest variability of sea ice area out of all three subregions is likely a result of its location. Its southeastern portion is close to the warmer, saltier North Atlantic while its northwestern side is close to the colder, fresher waters of BB. This, in turn, could potentially lead to the west side of the DS being predominately sea ice covered while the east side remains ice-free (Hedie-Jørgensen et al. 2007a-b). Furthermore, these authors propose if certain years see more sea ice exported from BB and a weaker (colder and fresher) West Greenland Current in LS, then the sea ice edge could shift more eastward than normal (or vice-versa). Further research is needed comparing each subregions' sea ice variabilities with teleconnections to investigate whether sea ice variability in BB-DS-LS could be a proxy for certain teleconnection shifts.

4.2: Objective 2

Objective 2's goal was to establish what the cyclone variability was within/between each subregion from 1980-2015 based upon several cyclone variables. Objective 2's results also intended to develop cyclone variability datasets to compare the influence of sea ice and teleconnections (later discussed in Objective 3). It was also intended to serve as an overview of cyclone activity in BB-DS-LS to better understand how distinct these subregions are against each other. The results illustrate:

1. The highest number of cyclones, lowest minimum central pressures, and highest laplacian scores occur in LS.
2. The highest number of cyclogenesis and cyclolysis events occur in BB.
3. Every subregion experiences more cyclolysis then cyclogenesis events.

4. BB-DS-LS's cyclogenesis was the only cyclone variable with a significant trend (positive) across the 430-month period.
5. More cyclones occur during winter in BB and DS (vice-versa for LS).
6. Comparing the same cyclone variable between subregions, significant correlations are higher in individual months than across the overall 430-month time period.
7. Storm tracks in DS and BB shift westward during summer (vice-versa in winter).

Understanding long-term cyclone variability within BB-DS-LS's subregions (like with sea-ice variability) requires the use of consistent datasets spanning several decades. Currently, few publications even discuss cyclones in BB-DS-LS (Serreze, 1995; Chen et al. 1997; Serreze et al. 1997; Hanson et al. 2004; Wang et al. 2006; Tsukernik et al. 2007; Simmonds et al. 2008; Serreze and Barry, 2014; Koyama et al. 2017, Wei et al. 2017). However, even with these studies, there are no long-term assessments or definitive conclusions on cyclone variability for BB, DS, and LS as separate subregions. This study provides detailed cyclone variability estimates based upon several common variables used in the literature to provide a solid understanding of general cyclone variability in BB-DS-LS.

Although the results of this study show BB-DS-LS's cyclogenesis events having a significant positive trend, no existing literature discusses this trend. Murray and Simmonds (1995) found no distinct change in overall cyclone and cyclogenesis events, laplacian, and central pressure during the month of January from 1983-1989. Similarly, Koyama et al. (2017) found cyclogenesis and laplacian scores of cyclones have only increased in certain areas that are outside of BB-DS-LS, however they found cyclone deepening rates in BB-DS-LS are half of the rates in the North Atlantic. The results of Brümmer et al. (2000) agree with the observations that more cyclolysis than cyclogenesis events occur in the Arctic overall. LS experiencing the highest

number and strongest cyclones is likely due to its close proximity to the North Atlantic storm track. This observation aligns with Chen at al. (1997) and Tsukernik et al. (2007) who mentioned cyclones entering LS are primarily mature systems continuing south of Greenland or one system continuing north in DS and BB after bifurcation. Furthermore, Romero and Emanuel (2017) conclude that the North Atlantic cyclone track is predicated to shift northward, with LS experiencing more (but not necessarily stronger) cyclones over the next century, which will likely lead to increased bifurcation events. However none of the literature mention DS experiencing the least number of cyclones out of all the subregions, which may be due to DS being grouped with BB or LS in other studies. DS having weaker central pressures (cyclones were likely in the early stages of deepening or filling) than in LS aligns with Serreze (1995) and Chen et al. (1997) observations of how central pressures of cyclones in DS gradually weaken. BB having the highest number of cyclogenesis and cyclolysis events in winter also supports the results of these studies as well as Serreze and Barry (2014) who mention BB's notoriety for being a hotspot of cyclone rejuvenation and decay during the winter seasons. Although the literature mentions cyclone bifurcation events at Greenland's southern tip is fairly common (Chen et al. 1997; Kurz, 2004; Tsukernik et al. 2007), the results of this study show less than 2% of all cyclones in LS entered BB, suggesting most cyclones that travel northward from LS only make it to DS before experiencing cyclolysis or moving over Greenland. Most cyclones in BB either form in that subregion (Brümmer et al. 2000; Chen et al. 1997) or migrate from eastern Canada. Further research is needed to determine the percentage of cyclones that experienced bifurcation and the extent of their northward progression through BB-DS-LS. Regardless of origin, most cyclones that enter DS and BB remain within these subregions, however there are several instances of systems continuing through Nares Strait into the Arctic Ocean during late

summer which supports the observations of Chen et al. (1997). With cyclogenesis events occurring more frequently in DS and BB during autumn and spring, it is likely the area of open water along West Greenland as well as the North Water act as moisture sources, but the presence of strong, persistent northerly winds as well as the steep topography likely hinder northward migration, as seen with the lack of movement in several time steps for cyclones within DS and BB. Murray and Simmonds (1995) support this theory by identifying that most cyclones in their model north of 55° N (regardless of their longitude position) experienced significant decreases in speed and intensity and topographical barriers constrained areas of baroclinicity and the displacement of storm tracks in subregions across the NH. With only minimum laplacian and central pressure correlations remaining statistically significant after seasonally standardizing and detrending, it appears the magnitude of pressure gradients and the number cyclogenesis and cyclolysis events between subregions have a likely connection with seasonality, which is also supported by the fact that the highest laplacian scores occurred during winter, when the strongest temperature gradients exist along the North Atlantic storm track. Due to the lack of long-term significant trends as well as abrupt shifts in correlations between months, it is apparent that cyclone variability is greater between months than across the overall long-term timescale. For example, DS and LS were significantly correlated during summer (likely due to LS's maximum number of cyclones occurring at this time), whereas during autumn and winter, BB and DS were (likely due to DS and BB's maximum number of cyclones occurring at this time). While general comparisons can be made between the results from this study to the limited existing literature, more research is needed to better understand cyclone variability between these subregions, from where they migrate, and how local features (e.g., topography, the North Water, and local wind patterns) affect them.

4.3: Objective 3

Objective 3's goal was to answer the overall research question of what are the influences of local and remote drivers on cyclone variability in BB-DS-LS and each subregion from 1980-2015. Objective 3 was intended to compare the local and remote driver datasets at the 322-month and individual monthly timescales. The results illustrate:

1. Overall, remote drivers have more and stronger significant correlations with the cyclone variables than the local drivers across the 322-month and individual monthly timescales.
2. Significant correlations for both drivers with cyclone variables are stronger at the individual monthly scale than at the overall 322-month scale.
3. For the remote drivers, the NAO and AO had the strongest significant correlations with the cyclone variables across both timescales, while the PDO and PNA had the weakest.
4. For the local drivers, BB-DS-LS's sea ice area had the most significant correlations with the cyclone variables at the 322-month while DS's sea ice area had the most across the individual monthly timescale.
5. Different cyclone variables tend to be more significantly correlated with certain drivers across the timescales.
6. January had the highest number of significant correlations with the local sea ice, while April had the highest for teleconnections.

While some publications discuss general teleconnection influence and sea ice variability in BB-DS-LS as a whole (Mysak et al. 1996; Serreze et al. 1997; Belkin et al. 1998, Alexander, 2004), none view all three subregions separately as unique environments which fluctuate

differently. Additionally, no studies compare cyclone variability between each subregion and between prominent features like teleconnections and sea ice. The results of Objective 3 provide the first detailed comparisons of cyclone variability with sea ice and teleconnections in BB-DS-LS.

Results from this study show that for the total number of cyclones, cyclogenesis events, and laplacian scores, the most significant correlations appeared in months leading up to when sea ice maximums occurred, or before large shifts in sea ice area took place (usually October-January and June-July for BB, DS, and LS). However, as each subregions's sea ice area approached their maximum and minimum, few to no significant correlations were seen in these months. The conclusions of Johnson (1980), Overland and Pease (1982), and Murray and Simmonds (1995) align with this observation, mentioning that when looking at cyclone tracks (and similar atmospheric data), local atmospheric conditions are significantly related to sea ice during periods of extreme sea ice shifts (i.e., large increases/decreases in area).

The cyclolysis events and longitude variables had the most frequent significant correlations with sea ice comparisons at the long-term timescale, likely due to eastward/westward shifts of sea ice impacting eastward/westward shifts in cyclone tracks and the deepening rate of cyclones (loss of moisture source over sea ice). DS and LS's sea ice areas mainly had weak significant positive correlations with BB's cyclolysis events, which make sense because DS and LS are south of BB. Therefore, if sea ice area increases in these subregions it will have increased in BB. Furthermore, cyclones traveling through DS and LS would have less moisture due to the presence of sea ice, hence, cyclolysis would more likely to take place in BB. Additionally, BB's mean and minimum (eastern-most) longitude values, being significantly correlated with BB and DS's sea ice areas make sense because when sea ice area increases in BB

and DS the sea ice edge advances eastward, likely adjusting the cyclone's track more eastward as well. Based on the monthly comparisons, June and October had the most significant positive correlations. This is likely because these months also had the largest fluctuations in sea ice area. Due to the lack of literature pertaining to sea ice and cyclone comparisons in these subregions, further research is needed to better understand and determine these relationships.

For the remote driver comparisons, the NAO and AO having overwhelmingly the most significant correlations at both timescales makes sense due to BB-DS-LS being near the Icelandic Low on the Atlantic-side of the Arctic, where these patterns have the most influence on low and mid-level atmospheric flow (Wang et al. 1994; Hurrell and van Loon, 1997; and Cook et al. 1998). Additionally, the central pressure datasets having the most significant correlations supports the observation of these patterns varying in-phase with each other, affecting the pressure structure of the atmosphere in BB-DS-LS. Due to BB-DS-LS's location between the North Atlantic and Arctic Oceans, it makes sense that the NAO and AO impact this region the most because they have the most influence on the atmospheric structure between the Atlantic-side of the Arctic and midlatitudes than the other patterns (e.g., Thompson and Wallace, 1998 and 2000a-b; Dickson et al. 2000).

The AO having the highest significant correlations with the central pressure datasets is likely due to the AO's broad vertical profile extending into the stratosphere, thus influencing the general atmospheric flow and having more effect on a cyclone's core structure; whereas the NAO's influence is seen mainly at lower levels. Dickson et al. (2000) mention several variables that have been found to influence the strength of these patterns over the North Atlantic, including: changes in wind speed, distribution and intensity of cyclones, sea surface temperature, and sea ice extent and export in DS and LS. Due to the lack of literature pertaining to the NAO

and AO's effects on cyclones in BB-DS-LS, and the fact that not all cyclones that enter this region originate from the North Atlantic, future research should confirm the dominant impact of the NAO and AO patterns on the entire cyclone record for each subregion. Dickson et al. (2000) do conclude that local reductions in sea ice in the North Atlantic can influence the NAO and result in increased local cyclone activity, however this is only mentioned for areas outside of BB-DS-DS. Within BB-DS-LS, Mysak et al. (1996) proposed that during positive NAO phases, positive sea ice area and negative salinity anomalies are seen in DS and LS, which strengthen northerly winds to persist longer, reducing the temperature gradient across BB-DS-LS and increasing the sea level pressure. Even though the sea ice comparisons with central pressure from this study show no strong nor significant correlations with sea ice at the 322-month time scale, sea ice still has the potential to be an indirect driver towards low-level atmospheric conditions in BB-DS-LS in certain months. LS's lowest cyclone count being in early spring is likely responsible due to the Icelandic Low's increased strength during winter and spring inhibiting many cyclones from migrating north of LS. This observation agrees with Dickson et al. (1996) who remarked that during positive NAO phases, storm tracks in the North Atlantic usually shift north and east of Greenland. To be more certain of these relationships, further research needs to be conducted on how sea ice area influences the central pressure of cyclones, and additionally, how sea ice in BB-DS-LS is related to the NAO and AO's variability. The laplacian datasets show fewer significant correlations with the NAO and AO across the entire period and at the monthly-scale, suggesting that overall, the NAO and AO potentially have no significant influence on the laplacian score of cyclones, or pressure gradient of cyclones in BB-DS-LS. Koyama et al. (2017) support this observation and explain that short-term changes in cyclone intensity are diminished looking across long periods of time, and that sub-decadal or smaller

timeframes are needed. For the longitude datasets, the NAO and AO show the most and strongest significant correlations with each subregion. This likely enforces the sea ice relationship in DS and LS with the NAO in Dickson et al. (2000), and the previously mentioned shifting sea ice edge in DS affecting the longitude positions of cyclones.

At both timescales, the PDO and PNA show sparse significant correlations, which indicate these patterns are not consistently and/or strongly related to cyclone variability in BB-DS-LS. However, the PNA's cluster of weak significant correlations in March and April with central pressure could support the theory of Baxter and Nigam (2013) who claim a weak relationship between the PNA and NAO in the North Atlantic. For the PDO, due to it being an extension of ENSO, it was expected to have more apparent correlations with sea ice, especially in LS since previous studies have found it to have impacts on sea ice in the North Atlantic (Gloersen, 1995; Mysak et al. 1996; Alexander, 2004). However, Mantua and Hare (2002) identified most of the PDO's influence to be mainly in the North Pacific and western United States. The PEP's weak significant correlations with BB's central pressure and DS's cyclolysis datasets in the winter months may be related to the PEP's positive phase of strengthening the circumpolar vortex further south in the North Atlantic (Wang and Zhang, 2015), thus making the pressure gradient across BB-DS-LS more uniform. The EAWR's weak, sporadic significant correlations with total number of cyclones, cyclogenesis events, and central pressure datasets between BB, DS, and LS is likely due to the EAWR's positive phases in winter result in positive temperature anomalies over eastern Canada (Lim, 2015) promoting cyclone development (but not stronger cyclones necessarily). Further research needs to be done on how the PEP and EAWR affect atmospheric flow upstream near Greenland and how they're interconnected with the NAO and AO.

Based upon the results of this study, across the overall 322-month and individual monthly time scales, it appears local sea ice area have the overall strongest relationship with the longitudinal position of cyclones, while remote teleconnections have the strongest relationship with the central pressure of cyclones. Out of every local and remote driver, the NAO and AO had the strongest influence on cyclone variability in BB-DS-LS. While these remote drivers had the strongest significant relationships with the majority of cyclone variables, many of the local drivers still have significant relationships with certain cyclone variables, and to be noted, these relationships are different between time scales. Although BB, DS, and LS are geographically connected, they are very unique subregions and require more research on the atmospheric and cryospheric processes that characterize their distinctiveness.

4.4: Conclusions

This study investigated the influence of local sea ice and remote teleconnection patterns on cyclone variability within BB-DS-LS from 1980-2015. This study also provided, for the first time, individual sea ice and cyclone variability estimates for BB, DS, and LS.

Sea ice variability in every subregion experienced significant sea ice area loss across the overall 430-month period, but at lower magnitudes than the NH. All subregions experienced their highest maximum coverages and positive deviations during the first half of the time period during late winter and early spring, which could be attributed to salinity anomalies and are coupled with shifts in the NAO. All but DS had their lowest coverages in the last decade, but the lowest minimums occurred during late summer.

Cyclone variability shows no distinct trends across the time period, except for BB-DS-LS's cyclogenesis events. LS had the strongest and highest amount of cyclones while BB had the

weakest cyclones, but the highest number of both cyclogenesis and cyclolysis events. Although all three subregions are connected, very few cyclones actually migrated through all three subregions. Most cyclones that entered LS originated from the North Atlantic, and either continued south of Greenland or moved northward, but then experienced cyclolysis in DS. Even though cyclogenesis occurs in DS and BB, the majority are existing systems which migrate from eastern Canada. Several cases of cyclones continuing over Greenland or through Nares Strait were also seen during summer.

Both the local and remote drivers had the most significant correlations with the longitude variables across the overall 322-month period. However at the individual monthly scale, central pressure was most significantly correlated with teleconnections, cyclolysis and longitude with the local sea ice. Overall, remote driver comparisons had the highest frequency of significant correlations with each subregion. The NAO and AO had the strongest and highest number of significant correlations with the subregions.

To conclude, when considering sea ice as a local driver and teleconnections as a remote driver in terms of affecting cyclone variability in BB-DS-LS, the remote driver tends to have the most influence. While BB, DS, and LS have been routinely considered part of the North Atlantic, the results of this study prove these subregions are unique. Given the lack of literature pertaining to these subregions, many questions remain about BB-DS-LS that have yet to catch the attention of the greater multidisciplinary scientific community.

REFERENCES

Aagaard, K., & Carmack, E. C. (1989). The role of sea ice and other fresh water in the Arctic circulation. *Journal of Geophysical Research: Oceans*, 94(C10), 14485-14498.

Agnew, T. A. (1998). Drainage of multiyear sea ice from the Lincoln Sea. *CMOS Bulletin*, 26(4), 101-103.

Alexander, M. A., Bhatt, U. S., Walsh, J. E., Timlin, M. S., Miller, J. S., & Scott, J. D. (2004). The atmospheric response to realistic Arctic sea ice anomalies in an AGCM during winter. *Journal of Climate*, 17(5), 890-905.

Allen, J. T., Pezza, A. B., & Black, M. T. (2010). Explosive cyclogenesis: A global climatology comparing multiple reanalyses. *Journal of Climate*, 23(24), 6468-6484.

Ambaum, M. H., Hoskins, B. J., & Stephenson, D. B. (2001). Arctic oscillation or North Atlantic oscillation?. *Journal of Climate*, 14(16), 3495-3507.

American Meteorological Society. (2012). Conditional instability of the second kind. In *AMS Glossary of Meteorology*.

American Meteorological Society. (2012). Cyclogenesis. In *AMS Glossary of Meteorology*.

American Meteorological Society. (2012). Cyclolysis. In *AMS Glossary of Meteorology*.

American Meteorological Society. (2012). Deepening. In *AMS Glossary of Meteorology*.

American Meteorological Society. (2012). Teleconnection. In *AMS Glossary of Meteorology*.

American Meteorological Society. (2012). Wind-induced surface heat exchange. In *AMS Glossary of Meteorology*.

Anthes, R. A., Kuo, Y. H., & Gyakum, J. R. (1983). Numerical simulations of a case of explosive marine cyclogenesis. *Monthly Weather Review*, 111(6), 1174-1188.

Atallah, E. H., & Bosart, L. F. (2003). The extratropical transition and precipitation distribution of Hurricane Floyd (1999). *Monthly Weather Review*, 131(6), 1063-1081.

Atlas, R. (1987). The role of oceanic fluxes and initial data in the numerical prediction of an intense coastal storm. *Dynamics of Atmospheres and Oceans*, 10(4), 359-388.

Azad, R., & Sorteberg, A. (2014). The vorticity budgets of North Atlantic winter extratropical cyclone life cycles in MERRA reanalysis. Part II: Decaying phase. *Journal of the Atmospheric Sciences*, 71(9), 3129-3143.

Azetsu-Scott, K., Petrie, B., Yeats, P., & Lee, C. (2012). Composition and fluxes of freshwater through Davis Strait using multiple chemical tracers. *Journal of Geophysical Research: Oceans*, 117(C12).

Barber, D. G., Hanesiak, J. M., Chan, W., & Piwowar, J. (2001). Sea-ice and meteorological conditions in Northern Baffin Bay and the North Water polynya between 1979 and 1996. *Atmosphere-Ocean*, 39(3), 343-359.

Barnston, A. G., & Livezey, R. E. (1987). Classification, seasonality and persistence of low-frequency atmospheric circulation patterns. *Monthly Weather Review*, 115(6), 1083-1126.

Baxter, S., & Nigam, S. (2013). A subseasonal teleconnection analysis: PNA development and its relationship to the NAO. *Journal of Climate*, 26(18), 6733-6741.

Belkin, I. M., Levitus, S., Antonov, J., & Malmberg, S. A. (1998). "Great salinity anomalies" in the North Atlantic. *Progress in Oceanography*, 41(1), 1-68.

Bi, H., Zhang, Z., Wang, Y., Xu, X., Liang, Y., Huang, J., ... & Fu, M. (2019). Baffin Bay sea ice inflow and outflow: 1978–1979 to 2016–2017. *The Cryosphere*, 13(3), 1025-1042.

Bjerknes, J. (1919). On the structure of moving cyclones. *Monthly Weather Review*, 47(2), 95-99.

Bjerknes, J. (1922). Life cycle of cyclones and the polar front theory of atmospheric circulation. *Geophysisks Publikationer*, 3(1), 1-18.

Bjerknes, J., & Godske, C. L. (1936). On the Theory of Cyclone Formation at Extra Tropical Fronts. With 18 Figures in the Text. *Astrophysica Norvegica*, 1, 199.

Bjerknes, J., & Holmboe, J. (1944). On the theory of cyclones. *Journal of Meteorology*, 1(1), 1-22.

Black, R. X., & Dole, R. M. (1993). The dynamics of large-scale cyclogenesis over the North Pacific Ocean. *Journal of the Atmospheric Sciences*, 50(3), 421-442.

Blackmon, M. L. (1976). A climatological spectral study of the 500 mb geopotential height of the Northern Hemisphere. *Journal of the Atmospheric Sciences*, 33(8), 1607-1623.

Blackmon, M. L., Lee, Y. H., & Wallace, J. M. (1984). Horizontal structure of 500 mb height fluctuations with long, intermediate and short time scales. *Journal of the Atmospheric Sciences*, 41(6), 961-980.

Bladé, I. (1996). On the relationship of barotropic singular modes to the low-frequency variability of a general circulation model. *Journal of the Atmospheric Sciences*, 53(16), 2393-2399.

Blake, E. S., Kimberlain, T. B., Berg, R. J., Cangialosi, J. P., & Beven Ii, J. L. (2013). Tropical cyclone report: Hurricane sandy. National Hurricane Center, 12, 1-10.

Borges, M. D., & Sardeshmukh, P. D. (1995). Barotropic Rossby wave dynamics of zonally varying upper-level flows during northern winter. *Journal of the Atmospheric Sciences*, 52(21), 3779-3796.

Born, E. W. (1987). Aspects of present-day maritime subsistence hunting in the Thule area, Northwest Greenland. Between Greenland and America: Cross-cultural contacts and the environment in the Baffin Bay area. *Works of the Arctic Centre*, (10), 109-132.

Bosart, L. F. (1981). The Presidents' Day snowstorm of 18–19 February 1979: A subsynoptic-scale event. *Monthly Weather Review*, 109(7), 1542-1566.

Bosart, L. F., & Lin, S. C. (1984). A diagnostic analysis of the Presidents' Day storm of February 1979. *Monthly Weather Review*, 112(11), 2148-2177.

Bourke, R. H., Addison, V. G., & Paquette, R. G. (1989). Oceanography of Nares Strait and northern Baffin Bay in 1986 with emphasis on deep and bottom water formation. Journal of *Geophysical Research: Oceans*, 94(C6), 8289-8302.

Bracegirdle, T. J., & Gray, S. L. (2009). The dynamics of a polar low assessed using potential vorticity inversion. Quarterly Journal of the Royal Meteorological Society: *A Journal of the Atmospheric Sciences, Applied Meteorology and Physical Oceanography*, 135(641), 880-893.

Branstator, G. (1984). The relationship between zonal mean flow and quasi-stationary waves in the midtroposphere. *Journal of the Atmospheric Sciences*, 41(14), 2163-2178.

Branstator, G. (1990). Low-frequency patterns induced by stationary waves. *Journal of the Atmospheric Sciences*, 47(5), 629-649.

Branstator, G. (1992). The maintenance of low-frequency atmospheric anomalies. *Journal of the Atmospheric Sciences*, 49(20), 1924-1946.

Brayshaw, D. J., Hoskins, B., & Blackburn, M. (2009). The basic ingredients of the North Atlantic storm track. Part I: Land–sea contrast and orography. *Journal of the Atmospheric Sciences*, 66(9), 2539-2558.

Bresch, J. F., Reed, R. J., & Albright, M. D. (1997). A polar-low development over the Bering Sea: Analysis, numerical simulation, and sensitivity experiments. *Monthly Weather Review*, 125(12), 3109-3130.

Bretagna, G., Pedgley, D. E., & Pick, W. H. (1962). A course in elementary meteorology. Her Majesty stationery Office.

Brümmer, B., Thiemann, S., & Kirchgäßner, A. (2000). A cyclone statistics for the Arctic based on European Centrere-analysis data. *Meteorology and Atmospheric Physics*, 75(3-4), 233-250.

Brümmer, B., Müller, G., & Noer, G. (2009). A polar low pair over the Norwegian Sea. *Monthly Weather Review*, 137(8), 2559-2575.

Buckley, W. H. (1983). A Study of Extreme Waves and Their Effects on Ship Structure (No. SSC-320). Ship Structure Committee Washington DC.

Bushuk, M., Giannakis, D., & Majda, A. J. (2015). Arctic sea ice reemergence: The role of large-scale oceanic and atmospheric variability. *Journal of Climate*, 28(14), 5477-5509.

Businger, S., & Reed, R. J. (1989). Cyclogenesis in cold air masses. *Weather and Forecasting*, 4(2), 133-156.

Cai, M., & van den Dool, H. M. (1991). Low-frequency waves and traveling storm tracks. Part I: Barotropic component. *Journal of the Atmospheric Sciences*, 48(11), 1420-1436.

Campins, J., Genovés, A., Jansa, A., Guijarro, J. A., & Ramis, C. (2000). A catalogue and a classification of surface cyclones for the western Mediterranean. *International Journal of Climatology: A Journal of the Royal Meteorological Society*, 20(9), 969-984.

Carleton, A. M. (1996). Satellite climatological aspects of cold air mesocyclones in the Arctic and Antarctic. *Global Atmosphere and Ocean System*, 5(1), 1-42.

Carlson, T. N. (1991). Mid-latitude weather systems.

Carsey, F. D. (1982). Arctic sea ice distribution at end of summer 1973–1976 from satellite microwave data. *Journal of Geophysical Research: Oceans*, 87(C8), 5809-5835.

Carsey, F. D. (1992). Microwave remote sensing of sea ice. *American Geophysical Union*.

Casado, M. J., Pastor, M. A., & Doblas-Reyes, F. J. (2009). Euro-Atlantic circulation types and modes of variability in winter. *Theoretical and Applied Climatology*, 96(1-2), 17-29.

Cash, B. A., & Lee, S. (2000). Dynamical processes of block evolution. *Journal of the Atmospheric Sciences*, 57(19), 3202-3218.

Catto, J. L. (2016). Extratropical cyclone classification and its use in climate studies. *Reviews of Geophysics*, 54(2), 486-520.

Cavalieri, D. J., & Parkinson, C. L. (2012). Arctic sea ice variability and trends, 1979-2010. *The Cryosphere*, 6(4), 881.

Kar-Man Chang, E. (2018). CMIP5 projected change in Northern Hemisphere winter cyclones with associated extreme winds. *Journal of Climate*, 31(16), 6527-6542.

Charney, J. G. (1947). The dynamics of long waves in a baroclinic westerly current. *Journal of Meteorology*, 4(5), 136-162.

Chen, S. J., Kuo, Y. H., Zhang, P. Z., & Bai, Q. F. (1992). Climatology of explosive cyclones off the East Asian coast. *Monthly Weather Review*, 120(12), 3029-3035.

Chen, Q. S., Bromwich, D. H., & Bai, L. (1997). Precipitation over Greenland retrieved by a dynamic method and its relation to cyclonic activity. *Journal of Climate*, 10(5), 839-870.

Claud, C., Heinemann, G., Raustein, E., & Mcmurdie, L. (2004). Polar low le Cygne: Satellite observations and numerical simulations. *Quarterly Journal of the Royal Meteorological Society: A Journal of the Atmospheric Sciences, Applied Meteorology and Physical Oceanography*, 130(598), 1075-1102.

Claud, C., Duchiron, B., & Terray, P. (2007). Associations between large-scale atmospheric circulation and polar low developments over the North Atlantic during winter. *Journal of Geophysical Research: Atmospheres*, 112(D12).

Collin, A. E., & Dunbar, M. (1964). Physical oceanography in arctic Canada.

Cook, E. R., D'Arrigo, R. D., & Briffa, K. R. (1998). A reconstruction of the North Atlantic Oscillation using tree-ring chronologies from North America and Europe. *The Holocene*, 8(1), 9-17.

Copland, L., Mueller, D. R., & Weir, L. (2007). Rapid loss of the Ayles ice shelf, Ellesmere Island, Canada. *Geophysical Research Letters*, 34(21).

Craig, G., & Cho, H. R. (1988). Cumulus heating and CISK in the extratropical atmosphere. Part I: Polar lows and comma clouds. *Journal of the Atmospheric Sciences*, 45(19), 2622-2640.

Cullather, R. I., & Lynch, A. H. (2003). The annual cycle and interannual variability of atmospheric pressure in the vicinity of the North Pole. *International Journal of Climatology: A Journal of the Royal Meteorological Society*, 23(10), 1161-1183.

Cuny, J., Rhines, P. B., & Kwok, R. (2005). Davis Strait volume, freshwater and heat fluxes. *Deep Sea Research Part I: Oceanographic Research Papers*, 52(3), 519-542.

Curry, J. A., Schramm, J. L., Rossow, W. B., & Randall, D. (1996). Overview of Arctic cloud and radiation characteristics. *Journal of Climate*, 9(8), 1731-1764.

Danish Hydraulic Institute. (1979). Environmental conditions offshore West Greenland. Vol. 1. Summary. Greenland Technical Organization, Horsholm, Denmark.

Darby, M. S., Willmott, A. J., & Mysak, L. A. (1994). A nonlinear steady-state model of the North Water Polynya, Baffin Bay. *Journal of Physical Oceanography*, 24(5), 1011-1020.

Davis, C. A., & Emanuel, K. A. (1988). Observational evidence for the influence of surface heat fluxes on rapid maritime cyclogenesis. *Monthly Weather Review*, 116(12), 2649-2659.

Defant, F. R., & Taba, H. (1957). The threefold structure of the atmosphere and the characteristics of the tropopause. *Tellus A*, 9(3), 259-274.

de Lange Boom, B. R., MacNeill, M. R., & Buckley, J. R. (1982). Iceberg motion in Lancaster Sound and northwest Baffin Bay, summer 1978. *Arctic*, 219-233.

Deser, C. (2000). On the teleconnectivity of the "Arctic Oscillation". *Geophysical Research Letters*, 27(6), 779-782.

Deser, C., Magnusdottir, G., Saravanan, R., & Phillips, A. (2004). The effects of North Atlantic SST and sea ice anomalies on the winter circulation in CCM3. Part II: Direct and indirect components of the response. *Journal of Climate*, 17(5), 877-889.

Deveson, A. C. L., Browning, K. A., & Hewson, T. D. (2002). A classification of FASTEX cyclones using a height-attributable quasi-geostrophic vertical-motion diagnostic. *Quarterly Journal of the Royal Meteorological Society: A Journal of the Atmospheric Sciences, applied meteorology and physical oceanography*, 128(579), 93-117.

Dey, B. (1981). Monitoring winter sea ice dynamics in the Canadian Arctic with NOAA-TIR images. *Journal of Geophysical Research: Oceans*, 86(C4), 3223-3235.

Dickson, R. R., Meincke, J., Malmberg, S. A., & Lee, A. J. (1988). The "great salinity anomaly" in the northern North Atlantic 1968–1982. *Progress in Oceanography*, 20(2), 103-151.

Dickson, R., Lazier, J., Meincke, J., Rhines, P., & Swift, J. (1996). Long-term coordinated changes in the convective activity of the North Atlantic. *Progress in Oceanography*, 38(3), 241-295.

Dickson, R. R., Osborn, T. J., Hurrell, J. W., Meincke, J., Blindheim, J., Adlandsvik, B., ... & Maslowski, W. (2000). The Arctic ocean response to the North Atlantic oscillation. *Journal of Climate*, 13(15), 2671-2696.

Dickson, R. R., Curry, R., & Yashayaev, I. (2003). Recent changes in the North Atlantic. *Philosophical Transactions of the Royal Society of London. Series A: Mathematical, Physical and Engineering Sciences*, 361(1810), 1917-1934.

DiMego, G. J., & Bosart, L. F. (1982). The transformation of Tropical Storm Agnes into an extratropical cyclone. Part I: The observed fields and vertical motion computations. *Monthly Weather Review*, 110(5), 385-411.

Dole, R. M., & Black, R. X. (1990). Life cycles of persistent anomalies. Part II: The development of persistent negative height anomalies over the North Pacific Ocean. *Monthly Weather Review*, 118(4), 824-846.

Douglas, M. W., Shapiro, M. A., Fedor, L. S., & Saukkonen, L. (1995). Research aircraft observations of a polar low at the east Greenland ice edge. *Monthly Weather Review*, 123(1), 5-15.

Doyle, J. D., & Shapiro, M. A. (1999). Flow response to large-scale topography: The Greenland tip jet. *Tellus A*, 51(5), 728-748.

Doyle, J. D., Shapiro, M. A., Jiang, Q., & Bartels, D. L. (2005). Large-amplitude mountain wave breaking over Greenland. *Journal of the Atmospheric Sciences*, 62(9), 3106-3126.

Dukhovskoy, D. S., Johnson, M. A., & Proshutinsky, A. (2004). Arctic decadal variability: An auto-oscillatory system of heat and fresh water exchange. *Geophysical Research Letters*, 31(3).

Dunbar, M. J. (1951). Eastern arctic waters: a summary of our present knowledge of the physical oceanography of the eastern arctic area, from Hudson Bay to Cape Farewell and from Belle Isle to Smith Sound. Fisheries Research Board of Canada.

Dunbar, M., & Dunbar, M. J. (1972). 21.—The History of the North Water. *Proceedings of the Royal Society of Edinburgh, Section B: Biological Sciences*, 72(1), 231-241.

Dunbar, M. (1973). Winter regime of the North Water. Defence Research Establishment Ottawa (Ontario).

Duncan, C. N. (1977). A numerical investigation of polar lows. *Quarterly Journal of the Royal Meteorological Society*, 103(436), 255-267.

Dzerdzeevskii, B. L. (1945). Tsirkuliatsionnye skhemy v troposfere Tsentral'noi Arktiki. *Izdatel'stvo Akademii Nauk*, 28.

Egger, J., & Schilling, H. D. (1983). On the theory of the long-term variability of the atmosphere. *Journal of the Atmospheric Sciences*, 40(5), 1073-1085.

Eliassen, A., & Raustein, E. (1970). A numerical integration experiment with a six-level atmospheric model with isentropic information surface. *Aschehoug*.

Emanuel, K. A., Fantini, M., & Thorpe, A. J. (1987). Baroclinic instability in an environment of small stability to slantwise moist convection. Part I: Two-dimensional models. *Journal of the Atmospheric Sciences*, 44(12), 1559-1573.

Emanuel, K. A., & Rotunno, R. (1989). Polar lows as arctic hurricanes. *Tellus A: Dynamic Meteorology and Oceanography*, 41(1), 1-17.

Emile-Geay, J., Cane, M. A., Naik, N., Seager, R., Clement, A. C., & van Geen, A. (2003). Warren revisited: Atmospheric freshwater fluxes and "Why is no deep water formed in the North Pacific". *Journal of Geophysical Research: Oceans*, 108(C6).

The Editors of Encyclopedia Britannica. (2018). Davis Strait. In Encyclopedia Britannica. Encyclopedia Britannica, Inc. Retrieved from: https://www.britannica.com/place/Davis-Strait.

Evans, C., & Hart, R. E. (2008). Analysis of the wind field evolution associated with the extratropical transition of Bonnie (1998). *Monthly Weather Review*, 136(6), 2047-2065.

Environmental Working Group Joint U.S. Russian Sea Ice Atlas. (2000). *Sea Ice Atlas for the Arctic Ocean*. 1st edition. Boulder, CO: National Snow and Ice Data Center.

Exner, F. M. (1913). Uber monatliche Witterungs-anomalien auf der nordlichen Erdhalfte im Winter. Sitzb. *Mathematik der Natur*, Kaiserlichen Akademie der Wissenshaften, 1165-1240.

Fan, S. M., Harris, L. M., & Horowitz, L. W. (2015). Atmospheric energy transport to the Arctic 1979–2012. *Tellus A: Dynamic Meteorology and Oceanography*, 67(1), 25482.

Fantini, M. (1990). The influence of heat and moisture fluxes from the ocean on the development of baroclinic waves. *Journal of the Atmospheric Sciences*, 47(7), 840-855.

Feldstein, S. B. (2000). The timescale, power spectra, and climate noise properties of teleconnection patterns. *Journal of Climate*, 13(24), 4430-4440.

Feldstein, S. B. (2002). Fundamental mechanisms of the growth and decay of the PNA teleconnection pattern. *Quarterly Journal of the Royal Meteorological Society: A Journal of the Atmospheric Sciences, Applied Meteorology and Physical Oceanography*, 128(581), 775-796.

Fissel, D. B., Lemon, D. D., & Birch, J. R. (1982). Major features of the summer near-surface circulation of western Baffin Bay, 1978 and 1979. *Arctic*, 180-200.

Forbes, G. S., & Lottes, W. D. (1985). Classification of mesoscale vortices in polar airstreams and the influence of the large-scale environment on their evolutions. *Tellus A: Dynamic Meteorology and Oceanography*, 37(2), 132-155.

Føre, I., Kristjánsson, J. E., Saetra, Ø., Breivik, Ø., Røsting, B., & Shapiro, M. (2011). The full life cycle of a polar low over the Norwegian Sea observed by three research aircraft flights. *Quarterly Journal of the Royal Meteorological Society*, 137(660), 1659-1673.

Føre, I., Kristjánsson, J. E., Kolstad, E. W., Bracegirdle, T. J., Saetra, Ø., & Røsting, B. (2012). A 'hurricane-like'polar low fuelled by sensible heat flux: high-resolution numerical simulations. *Quarterly Journal of the Royal Meteorological Society*, 138(666), 1308-1324.

Francis, J. A., Chan, W., Leathers, D. J., Miller, J. R., & Veron, D. E. (2009). Winter Northern Hemisphere weather patterns remember summer Arctic sea-ice extent. *Geophysical Research Letters*, 36(7).

Franzke, C., Fraedrich, K., & Lunkeit, F. (2001). Teleconnections and low-frequency variability in idealized experiments with two storm tracks. *Quarterly Journal of the Royal Meteorological Society*, 127(574), 1321-1339.

Franzke, C., Feldstein, S. B., & Lee, S. (2011). Synoptic analysis of the Pacific–North American teleconnection pattern. *Quarterly Journal of the Royal Meteorological Society*, 137(655), 329-346.

Frederiksen, J. S. (1983). A unified three-dimensional instability theory of the onset of blocking and cyclogenesis. II. Teleconnection patterns. *Journal of the Atmospheric Sciences*, 40(11), 2593-2609.

Gadd, A. J., Hall, C. D., & Kruze, R. E. (1990). Operational numerical prediction of rapid cyclogenesis over the North Atlantic. *Tellus A: Dynamic Meteorology and Oceanography*, 42(1), 116-121.

Gall, R. (1976). The effects of released latent heat in growing baroclinic waves. *Journal of the Atmospheric Sciences*, 33(9), 1686-1701.

Geng, Q., & Sugi, M. (2001). Variability of the North Atlantic cyclone activity in winter analyzed from NCEP–NCAR reanalysis data. *Journal of Climate*, 14(18), 3863-3873.

Gershunov, A., & Barnett, T. P. (1998). Interdecadal modulation of ENSO teleconnections. *Bulletin of the American Meteorological Society*, 79(12), 2715-2726.

Giovinetto, M. B., & Zwally, H. J. (1995). Annual changes in sea ice extent and of accumulation on ice sheets: implications for sea level variability. *Journal of Glacial Science and Glacial Geology*, 31, 39-49.

Gloersen, P. (1995). Modulation of hemispheric sea-ice cover by ENSO events. *Nature*, 373(6514), 503.

Gong, G., Entekhabi, D., & Cohen, J. (2002). A large-ensemble model study of the wintertime AO–NAO and the role of interannual snow perturbations. *Journal of Climate*, 15(23), 3488-3499.

Goosse, H., Campin, J. M., Fichefet, T., & Deleersnijder, E. (1997). Sensitivity of a global ice–ocean model to the Bering Strait throughflow. *Climate Dynamics*, 13(5), 349-358.

Gray, S. L., & Dacre, H. F. (2006). Classifying dynamical forcing mechanisms using a climatology of extratropical cyclones. *Quarterly Journal of the Royal Meteorological Society: A Journal of the Atmospheric Sciences, Applied Meteorology and Physical Oceanography*, 132(617), 1119-1137.

Grønås, S. (1995). The seclusion intensification of the New Year's day storm 1992. *Tellus A*, 47(5), 733-746.

Grønås, S., & Kvamstø, N. G. (1995). Numerical simulations of the synoptic conditions and development of Arctic outbreak polar lows. *Tellus A*, 47(5), 797-814.

Gyakum, J. R. (1983a). On the evolution of the QE II storm. I: Synoptic aspects. *Monthly Weather Review*, 111(6), 1137-1155.

Gyakum, J. R. (1983b). On the evolution of the QE II storm. II: Dynamic and thermodynamic structure. *Monthly Weather Review*, 111(6), 1156-1173.

Gyakum, J. R., Anderson, J. R., Grumm, R. H., & Gruner, E. L. (1989). North Pacific cold-season surface cyclone activity: 1975–1983. *Monthly Weather Review*, 117(6), 1141-1155.

Gyakum, J. R., Kuo, Y. H., Guo, Z., & Guo, Y. R. (1995). A case of rapid continental mesoscale cyclogenesis. Part II: Model and observational diagnosis. *Monthly Weather Review*, 123(4), 998-1024.

Haas, C., Hendricks, S., & Doble, M. (2006). Comparison of the sea-ice thickness distribution in the Lincoln Sea and adjacent Arctic Ocean in 2004 and 2005. *Annals of Glaciology*, 44, 247-252.

Haishan, C., & Zhaobo, S. (2003). The effects of Eurasian snow cover anomaly on winter atmospheric general circulation Part I. observational studies. *Chinese Journal of Atmospheric Sciences-Chinese Edition*, 27(3), 304-316.

Hanson, C. E., Palutikof, J. P., & Davies, T. D. (2004). Objective cyclone climatologies of the North Atlantic–a comparison between the ECMWF and NCEP Reanalyses. *Climate Dynamics*, 22(6-7), 757-769.

Harold, J. M., Bigg, G. R., & Turner, J. (1999). Mesocyclone activity over the Northeast Atlantic. Part 2: An investigation of causal mechanisms. *International Journal of Climatology: A Journal of the Royal Meteorological Society*, 19(12), 1283-1299.

Harrold, T. W., & Browning, K. A. (1969). The polar low as a baroclinic disturbance. *Quarterly Journal of the Royal Meteorological Society*, 95(406), 710-723.

Hart, R. E., & Evans, J. L. (2001). A climatology of the extratropical transition of Atlantic tropical cyclones. *Journal of Climate*, 14(4), 546-564.

Hartmann, B., & Wendler, G. (2003). The significance of the 1976 Pacific climate shift in the climatology of Alaska. *Journal of Climate*, 18(22), 4824-4839.

Hayes, I. I. (1867). The Open Polar Sea: A Narrative of a Voyage of Discovery Towards the North Pole, in the Schooner" United States". London: Sampson Low, Son, and Marston.

Hedley, M., & Yau, M. K. (1991). Anelastic modeling of explosive cyclogenesis. *Journal of the Atmospheric Sciences*, 48(5), 711-727.

Heide-Jørgensen, M. P., Stern, H., & Laidre, K. L. (2007a). Dynamics of the sea ice edge in Davis Strait. *Journal of Marine Systems*, 67(1-2), 170-178.

Heide-Jørgensen, M. P., Laidre, K. L., Logsdon, M. L., & Nielsen, T. G. (2007b). Springtime coupling between chlorophyll a, sea ice and sea surface temperature in Disko Bay, West Greenland. *Progress in Oceanography*, 73(1), 79-95.

Heide-Jørgensen, M. P., Burt, L. M., Hansen, R. G., Nielsen, N. H., Rasmussen, M., Fossette, S., & Stern, H. (2013). The significance of the North Water polynya to Arctic top predators. *Ambio*, 42(5), 596-610.

Hewson, T. D., & Titley, H. A. (2010). Objective identification, typing and tracking of the complete life-cycles of cyclonic features at high spatial resolution. *Meteorological Applications*, 17(3), 355-381.

Higgins, R. W., & Mo, K. C. (1997). Persistent North Pacific circulation anomalies and the tropical intraseasonal oscillation. *Journal of Climate*, 10(2), 223-244.

Hirschberg, P. A., & Fritsch, J. M. (1991). Tropopause undulations and the development of extratropical cyclones. Part I. Overview and observations from a cyclone event. *Monthly Weather Review*, 119(2), 496-517.

Hoerling, M. P., Hurrell, J. W., & Xu, T. (2001). Tropical origins for recent North Atlantic climate change. *Science*, 292(5514), 90-92.

Hongbao, W. (1993). Relationships between Winter Temperature Anomalies in China and 500—HPA Teleconnection Patterns of the Atmospheric Circulation in the Northern Hemisphere. *Journal of Nanjing Institute of Meteorology*, 2.

Hoskins, B. J., & Karoly, D. J. (1981). The steady linear response of a spherical atmosphere to thermal and orographic forcing. *Journal of the Atmospheric Sciences*, 38(6), 1179-1196.

Hoskins, B. J., & Valdes, P. J. (1990). On the existence of storm-tracks. *Journal of the Atmospheric Sciences*, 47(15), 1854-1864.

Hoskins, B. J., & Ambrizzi, T. (1993). Rossby wave propagation on a realistic longitudinally varying flow. *Journal of the Atmospheric Sciences*, 50(12), 1661-1671.

Hurrell, J. W. (1995). Decadal trends in the North Atlantic Oscillation: regional temperatures and precipitation. *Science*, 269(5224), 676-679.

Hurrell, J. W. (1996). Influence of variations in extratropical wintertime teleconnections on Northern Hemisphere temperature. *Geophysical Research Letters*, 23(6), 665-668.

Hurrell, J. W., & Van Loon, H. (1997). Decadal variations in climate associated with the North Atlantic Oscillation. In *Climatic Change at High Elevation Sites* (pp. 69-94). Springer, Dordrecht.

Hurrell, J. W., Kushnir, Y., Ottersen, G., & Visbeck, M. (2003). An overview of the North Atlantic oscillation. *Geophysical Monograph-American Geophysical Union*, 134, 1-36.

International Hydrographic Organization. (1953). Limits of oceans and seas (No. 23). *International Hydrographic Organization*.

Ionita, M. (2014). The impact of the East Atlantic/Western Russia pattern on the hydroclimatology of Europe from mid-winter to late spring. *Climate*, 2(4), 296-309.

Ionita, M., Scholz, P., Lohmann, G., Dima, M., & Prange, M. (2016). Linkages between atmospheric blocking, sea ice export through Fram Strait and the Atlantic Meridional Overturning Circulation. *Scientific Reports*, 6, 32881.

Johnson, C. M. (1980). Wintertime Arctic sea ice extremes and the simultaneous atmospheric circulation. *Monthly Weather Review*, 108(11), 1782-1791.

Jones, E. P., Swift, J. H., Anderson, L. G., Lipizer, M., Civitarese, G., Falkner, K. K., ... & McLaughlin, F. (2003). Tracing Pacific water in the North Atlantic ocean. *Journal of Geophysical Research: Oceans*, 108(C4).

Jung, T., & Hilmer, M. (2001). The link between the North Atlantic Oscillation and Arctic sea ice export through Fram Strait. *Journal of Climate*, 14(19), 3932-3943.

Jung, T., & Rhines, P. B. (2007). Greenland's pressure drag and the Atlantic storm track. *Journal of the Atmospheric Sciences*, 64(11), 4004-4030.

Kang, I. S. (1990). Influence of zonal mean flow change on stationary wave fluctuations. *Journal of the Atmospheric Sciences*, 47(2), 141-147.

Keegan, T. J. (1958). Arctic synoptic activity in winter. *Journal of Meteorology*, 15(6), 513-521.

Kellogg, W. W. (1975). Climatic feedback mechanisms involving the polar regions. *Climate of the Arctic*, 111-116.

Khatiwala, S. P., Fairbanks, R. G., & Houghton, R. W. (1999). Freshwater sources to the coastal ocean off northeastern North America: Evidence from H2 18O/H2 16O. *Journal of Geophysical Research: Oceans*, 104(C8), 18241-18255.

Kiilerich, A. B. (1939). The Godthaab Expedition, 1928...: A Theoretical Treatment of the Hydrographical Observation Material. *CA Reitzel*.

Kocin, P. J., & Uccellini, L. W. (1985). A survey of major east coast snowstorms, 1960-1983. Part 2. Summary of Surface and Upperlevel Characteristics.

Kolstad, E. W. (2006). A new climatology of favourable conditions for reverse-shear polar lows. Tellus A: Dynamic Meteorology and Oceanography, 58(3), 344-354.

Koyama, T., Stroeve, J., Cassano, J., & Crawford, A. (2017). Sea ice loss and Arctic cyclone activity from 1979 to 2014. *Journal of Climate*, 30(12), 4735-4754.

Kristjánsson, J. E., & Thorsteinsson, S. (1995). The structure and evolution of an explosive cyclone near Iceland. *Tellus A*, 47(5), 656-670.

Kristjánsson, J. E., & McInnes, H. (1999). The impact of Greenland on cyclone evolution in the North Atlantic. *Quarterly Journal of the Royal Meteorological Society*, 125(560), 2819-2834.

Kuo, Y. H., Low-Nam, S., & Reed, R. J. (1991a). Effects of surface energy fluxes during the early development and rapid intensification stages of seven explosive cyclones in the western Atlantic. *Monthly Weather Review*, 119(2), 457-476.

Kuo, Y. H., Shapiro, M. A., & Donall, E. G. (1991b). The interaction between baroclinic and diabatic processes in a numerical simulation of a rapidly intensifying extratropical marine cyclone. *Monthly Weather Review*, 119(2), 368-384.

Kurz, M. (2004). On the dynamics of the splitting process of cyclones near southern Greenland. *Meteorologische Zeitschrift*, 13(2), 143-148.

Kutzbach, J. E. (1970). Large-scale features of monthly mean Northern Hemisphere anomaly maps of sea-level pressure. *Monthly Weather Review*, 98(9), 708-716.

Kutzbach, G. (2016). The thermal theory of cyclones: A history of meteorological thought in the nineteenth century. Springer.

Kwok, R., & Rothrock, D. A. (1999). Variability of Fram Strait ice flux and North Atlantic oscillation. *Journal of Geophysical Research: Oceans*, 104(C3), 5177-5189.

Kwok, R. (2004). Annual cycles of multiyear sea ice coverage of the Arctic Ocean: 1999–2003. *Journal of Geophysical Research: Oceans*, 109(C11).

Kwok, R. (2005). Variability of Nares Strait ice flux. *Geophysical Research Letters*, 32(24).

Kwok, R. (2006). Exchange of sea ice between the Arctic Ocean and the Canadian Arctic Archipelago. *Geophysical Research Letters*, 33(16).

Kwok, R. (2007). Baffin Bay ice drift and export: 2002–2007. *Geophysical Research Letters*, 34(19).

Kwok, R. (2009). Outflow of Arctic Ocean sea ice into the Greenland and Barents Seas: 1979–2007. *Journal of Climate*, 22(9), 2438-2457.

Kwok, R. (2015). Sea ice convergence along the Arctic coasts of Greenland and the Canadian Arctic Archipelago: Variability and extremes (1992–2014). *Geophysical Research Letters*, 42(18), 7598-7605.

Lamb, P. J., & Peppler, R. A. (1987). North Atlantic Oscillation: concept and an application. *Bulletin of the American Meteorological Society*, 68(10), 1218-1225.

Langehaug, H. R., Geyer, F., Smedsrud, L. H., & Gao, Y. (2013). Arctic sea ice decline and ice export in the CMIP5 historical simulations. *Ocean Modelling*, 71, 114-126.

Lau, N. C. (1988). Variability of the observed midlatitude storm tracks in relation to low-frequency changes in the circulation pattern. *Journal of the Atmospheric Sciences*, 45(19), 2718-2743.

Lazier, J. R. (1994). Observations in the northwest corner of the North Atlantic Current. *Journal of Physical Oceanography*, 24(7), 1449-1463.

Lazier, J. R. (1995). The salinity decrease in the Labrador Sea over the past thirty years (pp. 295-302). National Academy Press, Washington, DC.

LeDrew, E. F. (1984). The role of local heat sources in synoptic activity within the Polar Basin. *Atmosphere-Ocean*, 22(3), 309-327.

LeDrew, E. F. (1988). Development processes for five depression systems within the Polar Basin. *Journal of Climatology*, 8(2), 125-153.

Lique, C., Treguier, A. M., Scheinert, M., & Penduff, T. (2009). A model-based study of ice and freshwater transport variability along both sides of Greenland. *Climate Dynamics*, 33(5), 685-705.

Loder, J. W. (1998). The coastal ocean of northeastern North America (Cape Hatteras to Hudson Strait). *The Global Coastal Ocean: Regional Studies and Syntheses*.

Lorenz, E. N. (1951). Seasonal and irregular variations of the Northern Hemisphere sea-level pressure profile. *Journal of Meteorology*, 8(1), 52-59.

Lorenz, E. N. (1983). A history of prevailing ideas about the general circulation of the atmosphere. *Bulletin of the American Meteorological Society*, 730-734.

Lim, Y. K. (2015). The East Atlantic/West Russia (EA/WR) teleconnection in the North Atlantic: climate impact and relation to Rossby wave propagation. *Climate dynamics*, 44(11-12), 3211-3222.

Liu, Y. Y., & Chen, W. (2012). Variability of the Eurasian teleconnection pattern in the Northern Hemisphere winter and its influences on the climate in China. Chin. *Journal of the Atmospheric Sciences*, 36(2), 423-432.

Liu, Y., Wang, L., Zhou, W., & Chen, W. (2014). Three Eurasian teleconnection patterns: Spatial structures, temporal variability, and associated winter climate anomalies. *Climate Dynamics*, 42(11-12), 2817-2839.

Luo, D., Gong, T., Diao, Y., & Zhou, W. (2007). Storm tracks and annular modes. *Geophysical Research Letters*, 34(17).

Lupo, A. R., Smith, P. J., & Zwack, P. (1992). A diagnosis of the explosive development of two extratropical cyclones. *Monthly Weather Review*, 120(8), 1490-1523.

Macdonald, B. C., & Reiter, E. R. (1988). Explosive cyclogenesis over the eastern United States. *Monthly Weather Review*, 116(8), 1568-1586.

Madden, R. A., & Julian, P. R. (1971). Detection of a 40–50 day oscillation in the zonal wind in the tropical Pacific. *Journal of the Atmospheric Sciences*, 28(5), 702-708.

Madden, R. A., & Julian, P. R. (1972). Description of global-scale circulation cells in the tropics with a 40–50 day period. *Journal of the Atmospheric Sciences*, 29(6), 1109-1123.

Mallet, P. E., Claud, C., Cassou, C., Noer, G., & Kodera, K. (2013). Polar lows over the Nordic and Labrador Seas: Synoptic circulation patterns and associations with North Atlantic-Europe wintertime weather regimes. *Journal of Geophysical Research: Atmospheres*, 118(6), 2455-2472.

Mann, C. R. (1967). The termination of the Gulf Stream and the beginning of the North Atlantic Current. In *Deep Sea Research and Oceanographic Abstracts* (Vol. 14, No. 3, pp. 337-359). Elsevier.

Mann, K. H., & Drinkwater, K. F. (1994). Environmental influences on fish and shellfish production in the Northwest Atlantic. *Environmental Reviews*, 2(1), 16-32.

Mansfield, D. A. (1974). Polar lows: The development of baroclinic disturbances in cold air outbreaks. *Quarterly Journal of the Royal Meteorological Society*, 100(426), 541-554.

Mantua, N. J., Hare, S. R., Zhang, Y., Wallace, J. M., & Francis, R. C. (1997). A Pacific interdecadal climate oscillation with impacts on salmon production. *Bulletin of the American Meteorological Society*, 78(6), 1069-1080.

Mantua, N. J., & Hare, S. R. (2002). The Pacific decadal oscillation. *Journal of Oceanography*, 58(1), 35-44.

Martin, J. E., Grauman, R. D., & Marsili, N. (2001). Surface cyclolysis in the North Pacific Ocean. Part I: A synoptic climatology. *Monthly Weather Review*, 129(4), 748-765.

Maslanik, J. A., Serreze, M. C., & Barry, R. G. (1996). Recent decreases in Arctic summer ice cover and linkages to atmospheric circulation anomalies. *Geophysical Research Letters*, 23(13), 1677-1680.

McInnes, H., Kristiansen, J., Kristjánsson, J. E., & Schyberg, H. (2011). The role of horizontal resolution for polar low simulations. *Quarterly Journal of the Royal Meteorological Society*, 137(660), 1674-1687.

Melling, H. (2000). Exchanges of freshwater through the shallow straits of the North American Arctic. In *The Freshwater Budget of the Arctic Ocean* (pp. 479-502). Springer, Dordrecht.

Melling, H., Gratton, Y., & Ingram, G. (2001). Ocean circulation within the North Water polynya of Baffin Bay. *Atmosphere-Ocean*, 39(3), 301-325.

Melling, H., Agnew, T. A., Falkner, K. K., Greenberg, D. A., Lee, C. M., Münchow, A., ... & Woodgate, R. A. (2008). Fresh-water fluxes via Pacific and Arctic outflows across the Canadian polar shelf. In *Arctic–Subarctic Ocean Fluxes* (pp. 193-247). Springer, Dordrecht.

Miller, J. E. (1946). Cyclogenesis in the Atlantic coastal region of the United States. *Journal of Meteorology*, 3(2), 31-44.

Montgomery, M. T., & Farrell, B. F. (1992). Polar low dynamics. *Journal of the Atmospheric Sciences*, 49(24), 2484-2505.

Morris Jr, W. E., & Smith, P. J. (2001). Cyclolysis: A diagnosis of two extratropical cyclones. *Monthly Weather Review*, 129(11), 2714-2729.

Moses, T., Kiladis, G. N., Diaz, H. F., & Barry, R. G. (1987). Characteristics and frequency of reversals in mean sea level pressure in the North Atlantic sector and their relationship to long-term temperature trends. *Journal of Climatology*, 7(1), 13-30.

Muench, R. D. (1971). The Physical oceanography of the northern Baffin Bay region. The Baffin Bay–North Water Project. Arctic Institute of North America, *Science Report*, 1, 1-150.

Mullen, S. L., & Baumhefner, D. P. (1988). Sensitivity of numerical simulations of explosive oceanic cyclogenesis to changes in physical parameterizations. *Monthly Weather Review*, 116(11), 2289-2329.

Münchow, A., Melling, H., & Falkner, K. K. (2006). An observational estimate of volume and freshwater flux leaving the Arctic Ocean through Nares Strait. *Journal of Physical Oceanography*, 36(11), 2025-2041.

Murray, R. J., & Simmonds, I. (1995). Responses of climate and cyclones to reductions in Arctic winter sea ice. *Journal of Geophysical Research: Oceans*, 100(C3), 4791-4806.

Mysak, L. A., & Huang, F. (1992). A latent-and sensible-heat polynya model for the North Water, northern Baffin Bay. *Journal of Physical Oceanography*, 22(6), 596-608.

Mysak, L. A., Ingram, R. G., Wang, J., & Van Der Baaren, A. (1996). The anomalous sea-ice extent in Hudson Bay, Baffin Bay and the Labrador Sea during three simultaneous NAO and ENSO episodes. *Atmosphere-Ocean*, 34(2), 313-343.

Nakamura, H., Tanaka, M., & Wallace, J. M. (1987). Horizontal structure and energetics of Northern Hemisphere wintertime teleconnection patterns. *Journal of the Atmospheric Sciences*, 44(22), 3377-3391.

Namias, J. (1958). The general circulation of the lower troposphere over Arctic regions and its relation to the circulation elsewhere. In *Polar Atmosphere Symposium*, Pt (Vol. 1).

Newman, M., Sardeshmukh, P. D., & Penland, C. (1997). Stochastic forcing of the wintertime extratropical flow. *Journal of the Atmospheric Sciences*, 54(3), 435-455.

Nigam, S., & Lindzen, R. S. (1989). The sensitivity of stationary waves to variations in the basic state zonal flow. *Journal of the Atmospheric Sciences*, 46(12), 1746-1768.

Nordeng, T. E. (1987). The effect of vertical and slantwise convection on the simulation of polar lows. *Tellus A*, 39(4), 354-375.

Nordeng, T. E., & Rasmussen, E. A. (1992). A most beautiful polar low. A case study of a polar low development in the Bear Island region. *Tellus A*, 44(2), 81-99.

Notaro, M., Wang, W. C., & Gong, W. (2006). Model and observational analysis of the northeast US regional climate and its relationship to the PNA and NAO patterns during early winter. *Monthly Weather Review*, 134(11), 3479-3505.

Nuss, W. A., & Kamikawa, S. I. (1990). Dynamics and boundary layer processes in two Asian cyclones. Monthly Weather Review, 118(3), 755-771.

Nutt, D. C. (1966). The drift of ice island WH-5. *Arctic*, 244-262.

Ogi, M., Yamazaki, K., & Tachibana, Y. (2004). The summertime annular mode in the Northern Hemisphere and its linkage to the winter mode. *Journal of Geophysical Research: Atmospheres*, 109(D20).

Ogi, M., & Rigor, I. G. (2013). Trends in Arctic sea ice and the role of atmospheric circulation. *Atmospheric Science Letters*, 14(2), 97-101.

Ohhashi, Y., & Yamazaki, K. (1999). Variability of the Eurasian pattern and its interpretation by wave activity flux. *Journal of the Meteorological Society of Japan*. Ser. II, 77(2), 495-511.

Onarheim, I. H., Eldevik, T., Smedsrud, L. H., & Stroeve, J. C. (2018). Seasonal and regional manifestation of Arctic sea ice loss. *Journal of Climate*, 31(12), 4917-4932.

Orlanski, I. (1986). Localized baroclinicity- A source for meso-alpha cyclones. *Journal of the Atmospheric Sciences*, 43, 2857-2885.

Ortega, P., Robson, J., Sutton, R. T., & Andrews, M. B. (2017). Mechanisms of decadal variability in the Labrador Sea and the wider North Atlantic in a high-resolution climate model. *Climate Dynamics*, 49(7-8), 2625-2647.

Overland, J. E., & Pease, C. H. (1982). Cyclone climatology of the Bering Sea and its relation to sea ice extent. *Monthly Weather Review*, 110(1), 5-13.

Overland, J. E., & Turet, P. (1994). Variability of the atmospheric energy flux across 70 N computed from the GFDL data set. *Washington DC American Geophysical Union Geophysical Monograph Series*, 85, 313-325.

Overland, J. E., Turet, P., & Oort, A. H. (1996). Regional variations of moist static energy flux into the Arctic. *Journal of Climate*, 9(1), 54-65.

Overland, J. E., & Wang, M. (2010). Large-scale atmospheric circulation changes are associated with the recent loss of Arctic sea ice. *Tellus A*, 62(1), 1-9.

Palmén, E. (1951). The role of atmospheric disturbances in the general circulation. *Quarterly Journal of the Royal Meteorological Society*, 77(333), 337-354.

Palmén, E. H., & Newton, C. W. (1969). Atmospheric circulation systems: their structure and physical interpretation (Vol. 13). Academic press.

Park, T. W., Ho, C. H., Yang, S., & Jeong, J. H. (2010). Influences of Arctic Oscillation and Madden-Julian Oscillation on cold surges and heavy snowfalls over Korea: A case study for the winter of 2009–2010. *Journal of Geophysical Research: Atmospheres*, 115(D23).

Park, T. W., Ho, C. H., & Yang, S. (2011). Relationship between the Arctic Oscillation and cold surges over East Asia. *Journal of Climate*, 24(1), 68-83.

Parker, D. J. (1998). Secondary frontal waves in the North Atlantic region: A dynamical perspective of current ideas. *Quarterly Journal of the Royal Meteorological Society*, 124(547), 829-856.

Parkinson, C. L. (1995). Recent sea-ice advances in Baffin Bay/Davis Strait and retreats in the Bellingshausen Sea. *Annals of Glaciology*, 21, 348-352.

Parkinson, C. L., Cavalieri, D. J., Gloersen, P., Zwally, H. J., & Comiso, J. C. (1999). Arctic sea ice extents, areas, and trends, 1978–1996. *Journal of Geophysical Research: Oceans*, 104(C9), 20837-20856.

Parkinson, C. L., & Cavalieri, D. J. (2008). Arctic sea ice variability and trends, 1979–2006. *Journal of Geophysical Research: Oceans*, 113(C7).

Parsons, K. E., & Smith, P. J. (2004). An investigation of extratropical cyclone development using a scale-separation technique. *Monthly Weather Review*, 132(4), 956-974.

Partington, K., Flynn, T., Lamb, D., Bertoia, C., & Dedrick, K. (2003). Late twentieth century Northern Hemisphere sea-ice record from US National Ice Center ice charts. *Journal of Geophysical Research: Oceans*, 108(C11).

Petermann, A. (1867). Das Nordlichste Land der Erde. *PetermannÕs Geographische Mitteil*, (13).

Petersen, G. N., Ólafsson, H., & Kristjánsson, J. E. (2003). Flow in the lee of idealized mountains and Greenland. *Journal of the Atmospheric Sciences*, 60(17), 2183-2195.

Pettersson, O. (1900). Die Wasserzirkulation im Nordatlantischen Ozean.

Petterssen, S., Dunn, G. E., & Means, L. L. (1955). Report of an experiment in forecasting of cyclone development. *Journal of Meteorology*, 12(1), 58-67.

Petterssen, S., & Smebye, S. J. (1971). On the development of extratropical cyclones. *Quarterly Journal of the Royal Meteorological Society*, 97(414), 457-482.

Portis, D. H., Walsh, J. E., El Hamly, M., & Lamb, P. J. (2001). Seasonality of the North Atlantic oscillation. *Journal of Climate*, 14(9), 2069-2078.

Porter, D. F., Cassano, J. J., Serreze, M. C., & Kindig, D. N. (2010). New estimates of the large-scale Arctic atmospheric energy budget. *Journal of Geophysical Research: Atmospheres*, 115(D8).

Press, M. J., & Blais, R. (1993). A study of the North Water polynya using passive microwave and infrared imagery. *Canadian Journal of Remote Sensing*, 19(1), 092-101.

Prinsenberg, S. J., & Bennett, E. B. (1987). Mixing and transports in Barrow Strait, the central part of the Northwest Passage. *Continental Shelf Research*, 7(8), 913-935.

Raible, C. C., Della-Marta, P. M., Schwierz, C., Wernli, H., & Blender, R. (2008). Northern Hemisphere extratropical cyclones: A comparison of detection and tracking methods and different reanalyses. *Monthly Weather Review*, 136(3), 880-897.

Rasmussen, E. (1979). The polar low as an extratropical CISK disturbance. *Quarterly Journal of the Royal Meteorological Society*, 105(445), 531-549.

Rasmussen, E. (1981). An investigation of a polar low with a spiral cloud structure. *Journal of the Atmospheric Sciences*, 38(8), 1785-1792.

Rasmussen, E. A., Turner, J., & Thorpe, A. J. (2004). Polar lows: Mesoscale weather systems in the polar regions. *Quarterly Journal of the Royal Meteorological Society*, 130(596), 371-372.

Reed, R. J., & Kunkel, B. A. (1960). The Arctic circulation in summer. *Journal of Meteorology*, 17(5), 489-506.

Reader, M. C., & Moore, G. K. (1995). Stratosphere-troposphere interactions associated with a case of explosive cyclogenesis in the Labrador Sea. *Tellus A*, 47(5), 849-863.

Reed, R. J., & Duncan, C. N. (1987). Baroclinic instability as a mechanism for the serial development of polar lows: a case study. *Tellus A*, 39(4), 376-384.

Reed, R. J., Grell, G. A., & Kuo, Y. H. (1993). The ERICA IOP 5 storm. Part II: Sensitivity tests and further diagnosis based on model output. *Monthly Weather Review*, 121(6), 1595-1612.

Renfrew, I. A. (2003). Polar lows.

Reverdin, G., Niiler, P. P., & Valdimarsson, H. (2003). North Atlantic ocean surface currents. *Journal of Geophysical Research: Oceans*, 108(C1), 2-1.

Ricker, R., Girard-Ardhuin, F., Krumpen, T., & Lique, C. (2018). Satellite-derived sea ice export and its impact on Arctic ice mass balance. *The Cryosphere*, 12(9), 3017-3032.

Rigor, I. G., Wallace, J. M., & Colony, R. L. (2002). Response of sea ice to the Arctic Oscillation. *Journal of Climate*, 15(18), 2648-2663.

Rigor, I. G., & Wallace, J. M. (2004). Variations in the age of Arctic sea-ice and summer sea-ice extent. *Geophysical Research Letters*, 31(9).

Rignot, E., & Steffen, K. (2008). Channelized bottom melting and stability of floating ice shelves. *Geophysical Research Letters*, 35(2).

Riis-Carstenson, E. (1931). The GODTHAAB expedition 1928. Report on the Expedition. *Meddelelser om Grønland*, 78(1), 1-105.

Rodwell, M. J., Rowell, D. P., & Folland, C. K. (1999). Oceanic forcing of the wintertime North Atlantic Oscillation and European climate. *Nature*, 398(6725), 320.

Roebber, P. J. (1984). Statistical analysis and updated climatology of explosive cyclones. *Monthly Weather Review*, 112(8), 1577-1589.

Roebber, P. J. (1989). On the statistical analysis of cyclone deepening rates. *Monthly Weather Review*, 117(10), 2293-2298.

Rogers, J. C. (1984). The association between the North Atlantic Oscillation and the Southern Oscillation in the northern hemisphere. *Monthly Weather Review*, 112(10), 1999-2015.

Rogers, E., & Bosart, L. F. (1986). An investigation of explosively deepening oceanic cyclones. *Monthly Weather Review*, 114(4), 702-718.

Rogers, E., & Bosart, L. F. (1991). A diagnostic study of two intense oceanic cyclones. *Monthly Weather Review*, 119(4), 965-996.

Rogers, J. C. (1990). Patterns of low-frequency monthly sea level pressure variability (1899–1986) and associated wave cyclone frequencies. *Journal of Climate*, 3(12), 1364-1379.

Rogers, J. C., & Mosley-Thompson, E. (1995). Atlantic Arctic cyclones and the mild Siberian winters of the 1980s. *Geophysical Research Letters*, 22(7), 799-802.

Rogers, J. C. (1997). North Atlantic storm track variability and its association to the North Atlantic Oscillation and climate variability of northern Europe. *Journal of Climate*, 10(7), 1635-1647.

Rolfson, D. M., & Smith, P. J. (1996). A composite diagnosis of synoptic-scale extratropical cyclone development over the United States. *Monthly Weather Review*, 124(6), 1084-1099.

Romero, R. (2008). A method for quantifying the impacts and interactions of potential-vorticity anomalies in extratropical cyclones. *Quarterly Journal of the Royal Meteorological Society: A Journal of the Atmospheric Sciences, Applied Meteorology and Physical Oceanography*, 134(631), 385-402.

Romero, R., & Emanuel, K. (2017). Climate change and Hurricane-like extratropical cyclones: Projections for North Atlantic polar lows and medicanes based on CMIP5 models. *Journal of Climate*, 30(1), 279-299.

Ross, C. K. (1990a). Currents and Temperature Data from Northwestern Baffin Bay, September, 1983-September, 1984. Bedford Institute of Oceanography.

Ross, C. K. (1990b). Currents and Temperature Data from Southwestern Baffin Bay, October, 1984-October, 1985. Bedford Institute of Oceanography.

Ross, C. K. (1991). Currents, Temperature and Salinity Data from Northern Baffin Bay, October 1985-August 1986. Fisheries and Oceans, Canada.

Ross, C. K. (1993). Currents, Temperature and Salinity Data from Eastern Baffin Bay, August 1986-September 1987. Bedford Institute of Oceanography.

Rossby, C. G. (1939). Relation between variations in the intensity of the zonal circulation of the atmosphere and the displacements of the semi-permanent centers of action. *Journal of Marine Research*, 2, 38-55.

Sadler, H. E. (1976). Water, heat, and salt transports through Nares Strait, Ellesmere Island. *Journal of the Fisheries Board of Canada*, 33(10), 2286-2295.

Saltzman, B., & Tang, C. M. (1972). Analytical study of the evolution of an amplifying baroclinic wave. *Journal of the Atmospheric Sciences*, 29(3), 427-444.

Saltzman, B., & Tang, C. M. (1974). Mid-tropospheric frontogenesis in an amplifying baroclinic wave. *Journal of the Atmospheric Sciences*, 31(3), 835-839.

Samelson, R. M., Agnew, T., Melling, H., & Münchow, A. (2006). Evidence for atmospheric control of sea-ice motion through Nares Strait. *Geophysical Research Letters*, 33(2).

Sanders, F., & Gyakum, J. R. (1980). Synoptic-dynamic climatology of the "bomb". *Monthly Weather Review*, 108(10), 1589-1606.

Sanders, F. (1986). Explosive cyclogenesis in the west-central North Atlantic Ocean, 1981–84. Part I: Composite structure and mean behavior. *Monthly Weather Review*, 114(10), 1781-1794.

Sanders, F. (1987). Skill of NMC operational dynamical models in prediction of explosive cyclogenesis. *Weather and Forecasting*, 2(4), 322-336.

Sanders, F., & Auciello, E. P. (1989). Skill in prediction of explosive cyclogenesis over the western North Atlantic Ocean, 1987/88: A forecast checklist and NMC dynamical models. *Weather and Forecasting*, 4(2), 157-172.

Sanderson, B. G., & LeBlond, P. H. (1984). The cross-channel flow at the entrance of Lancaster Sound. *Atmosphere-Ocean*, 22(4), 484-497.

Sardeshmukh, P. D., Newman, M., & Borges, M. D. (1997). Free barotropic Rossby wave dynamics of the wintertime low-frequency flow. *Journal of the Atmospheric Sciences*, 54(1), 5-23.

Sardie, J. M., & Warner, T. T. (1983). On the Mechanism for the, Development of Polar Lows. *Journal of the Atmospheric Sciences*, 40(4), 869-881.

Sardie, J. M., & Warner, T. T. (1985). A numerical study of the development mechanisms of polar lows. *Tellus A*, 37(5), 460-477.

Sawyer, J. S. (1950). Formation of secondary depressions in relation to the thickness pattern. *The Meteorology Magazine*, 79, 1-5.

Schuenemann, K. C., Cassano, J. J., & Finnis, J. (2009). Synoptic forcing of precipitation over Greenland: Climatology for 1961–99. *Journal of Hydrometeorology*, 10(1), 60-78.

Scherhag, R. (1934). Zur theorie der hoch-und tiefdruckgebiete. *Meteorologische Zeitschrift*, 51, 129-138.

Schultz, D. M., & Vaughan, G. (2011). Occluded fronts and the occlusion process: A fresh look at conventional wisdom. *Bulletin of the American Meteorological Society*, 92(4), 443-466.

Scott, F., & Feltham, D. L. (2010). A model of the three-dimensional evolution of Arctic melt ponds on first-year and multiyear sea ice. *Journal of Geophysical Research: Oceans*, 115(C12).

Screen, J. A., & Francis, J. A. (2016). Contribution of sea-ice loss to Arctic amplification is regulated by Pacific Ocean decadal variability. *Nature Climate Change*, 6(9), 856.

Serreze, M. C., & Barry, R. G. (1988). Synoptic activity in the Arctic Basin, 1979–85. *Journal of Climate*, 1(12), 1276-1295.

Serreze, M. C., Box, J. E., Barry, R. G., & Walsh, J. E. (1993). Characteristics of Arctic synoptic activity, 1952–1989. *Meteorology and Atmospheric Physics*, 51(3-4), 147-164.

Serreze, M. C. (1995). Climatological aspects of cyclone development and decay in the Arctic. *Atmosphere-Ocean*, 33(1), 1-23.

Serreze, M. C., Carse, F., Barry, R. G., & Rogers, J. C. (1997). Icelandic low cyclone activity: Climatological features, linkages with the NAO, and relationships with recent changes in the Northern Hemisphere circulation. *Journal of Climate*, 10(3), 453-464.

Serreze, M. C., Barrett, A. P., Slater, A. G., Woodgate, R. A., Aagaard, K., Lammers, R. B., ... & Lee, C. M. (2006). The large-scale freshwater cycle of the Arctic. *Journal of Geophysical Research: Oceans*, 111(C11).

Serreze, M. C., Barrett, A. P., Slater, A. G., Steele, M., Zhang, J., & Trenberth, K. E. (2007a). The large-scale energy budget of the Arctic. *Journal of Geophysical Research: Atmospheres*, 112(D11).

Serreze, M. C., Holland, M. M., & Stroeve, J. (2007b). Perspectives on the Arctic's shrinking sea-ice cover. *Science*, 315(5818), 1533-1536.

Serreze, M. C., & Barrett, A. P. (2011). Characteristics of the Beaufort Sea high. *Journal of Climate*, 24(1), 159-182.

Serreze, M. C., & Barry, R. G. (2014). The Arctic climate system. Cambridge University Press.

Shaffrey, L., & Sutton, R. (2004). The interannual variability of energy transports within and over the Atlantic Ocean in a coupled climate model. *Journal of Climate*, 17(7), 1433-1448.

Shapiro, M. A. (1975). Simulation of upper-level frontogenesis with a 20-level isentropic coordinate primitive equation model. *Monthly Weather Review*, 103(7), 591-604.

Shapiro, M. A., Fedor, L. S., & Hampel, T. (1987). Research aircraft measurements of a polar low over the Norwegian Sea. *Tellus A: Dynamic Meteorology and Oceanography*, 39(4), 272-306.

Shapiro, M. A., & Keyser, D. (1990). Fronts, jet streams, and the tropopause. *Extratropical Cyclones, The Erik Palmen Memorial Volume*, CW Newton and E. Holopainen, Eds. American Meteorological Society, 167.

Silberberg, S. R., & Bosart, L. F. (1982). An analysis of systematic cyclone errors in the NMC LFM-II model during the 1978–79 cool season. *Monthly Weather Review*, 110(4), 254-271.

Simmons, A. J., Wallace, J., & Branstator, G. W. (1983). Barotropic wave propagation and instability, and atmospheric teleconnection patterns. *Journal of the Atmospheric Sciences*, 40(6), 1363-1392.

Simmons, A. J., Mureau, R., & Petroliagis, T. (1995). Error growth and estimates of predictability from the ECMWF forecasting system. *Quarterly Journal of the Royal Meteorological Society*, 121(527), 1739-1771.

Simmonds, I., Burke, C., & Keay, K. (2008). Arctic climate change as manifest in cyclone behavior. *Journal of Climate*, 21(22), 5777-5796.

Smethie, W. M., Fine, R. A., Putzka, A., & Jones, E. P. (2000). Tracing the flow of North Atlantic Deep Water using chlorofluorocarbons. *Journal of Geophysical Research: Oceans*, 105(C6), 14297-14323.

Smith, E. H., Soule, F. M., & Mosby, O. (1937). The Marion and General Greene expeditions to Davis Strait and Labrador Sea. *Bulletin of the US Coast Guard*, 19(2), 1-259.

Solberg, H. (1928). Integrations of the Atmospheric Flow Equations. *Geofysiske Publikasjoner*, 5(9).

Solberg, H. (1931). The Cyclone Problem. Proceedings of the 3rd International Congress for Applied Mechanics, Stockholm, 1, 121-131.

Steele, M., & Boyd, T. (1998). Retreat of the cold halocline layer in the Arctic Ocean. *Journal of Geophysical Research: Oceans*, 103(C5), 10419-10435.

Steffen, K. (1985). Warm water cells in the North Water, northern Baffin Bay during winter. *Journal of Geophysical Research: Oceans*, 90(C5), 9129-9136.

Stern, H. L., & Heide-Jørgensen, M. P. (2003). Trends and variability of sea ice in Baffin Bay and Davis Strait, 1953–2001. *Polar Research*, 22(1), 11-18.

Stirling, I. (1980). The biological importance of polynyas in the Canadian Arctic. *Arctic*, 303-315.

Stirling, I., Cleator, H., & Boyd, H. (1981). Polynyas in the Canadian Arctic (No. 45). Environment Canada.

Sun, Y., Fu, G., Sun, J., & Zhang, S. (2018). Spatial Distribution and Seasonal Variation of Explosive Cyclones over the North Atlantic. *Journal of Ocean University of China*, 17(5), 1000-1010.

Sung, M. K., Lim, G. H., Kwon, W. T., Boo, K. O., & Kug, J. S. (2009). Short-term variation of Eurasian pattern and its relation to winter weather over East Asia. *International Journal of Climatology: A Journal of the Royal Meteorological Society*, 29(5), 771-775.

Sutcliffe, R. C. (1939). Cyclonic and anticyclonic development. *Quarterly Journal of the Royal Meteorological Society*, 65(282), 518-524.

Sutcliffe, R. C. (1947). A contribution to the problem of development. *Quarterly Journal of the Royal Meteorological Society*, 73(317-318), 370-383.

Tachibana, Y., Oshima, K., & Ogi, M. (2008). Seasonal and interannual variations of Amur River discharge and their relationships to large-scale atmospheric patterns and moisture fluxes. *Journal of Geophysical Research: Atmospheres*, 113(D16).

Talley, L. D., & McCartney, M. S. (1982). Distribution and circulation of Labrador Sea water. *Journal of Physical Oceanography*, 12(11), 1189-1205.

Tang, C. C., Ross, C. K., Yao, T., Petrie, B., DeTracey, B. M., & Dunlap, E. (2004). The circulation, water masses and sea-ice of Baffin Bay. *Progress in Oceanography*, 63(4), 183-228.

Terpstra, A., Spengler, T., & Moore, R. W. (2015). Idealised simulations of polar low development in an Arctic moist-baroclinic environment. *Quarterly Journal of the Royal Meteorological Society*, 141(691), 1987-1996.

Thompson, D. W., & Wallace, J. M. (1998). The Arctic Oscillation signature in the wintertime geopotential height and temperature fields. *Geophysical Research Letters*, 25(9), 1297-1300.

Thompson, D. W., & Wallace, J. M. (2000a). Annular modes in the extratropical circulation. Part I: Month-to-month variability. *Journal of Climate*, 13(5), 1000-1016.

Thompson, D. W., Wallace, J. M., & Hegerl, G. C. (2000). Annular modes in the extratropical circulation. Part II: Trends. *Journal of Climate*, 13(5), 1018-1036.

Ting, M., & Lau, N. C. (1993). A diagnostic and modeling study of the monthly mean wintertime anomalies appearing in a 100-year GCM experiment. *Journal of the Atmospheric Sciences*, 50(17), 2845-2867.

Trenberth, K. E., & Paolino Jr, D. A. (1980). The Northern Hemisphere sea-level pressure data set: Trends, errors and discontinuities. *Monthly Weather Review*, 108(7), 855-872.

Tsukernik, M., Kindig, D. N., & Serreze, M. C. (2007). Characteristics of winter cyclone activity in the northern North Atlantic: Insights from observations and regional modeling. *Journal of Geophysical Research: Atmospheres*, 112(D3).

Uccellini, L. W., Keyser, D., Brill, K. F., & Wash, C. H. (1985). The Presidents' Day cyclone of 18–19 February 1979: Influence of upstream trough amplification and associated tropopause folding on rapid cyclogenesis. *Monthly Weather Review*, 113(6), 962-988.

Uccellini, L. W. (1990). Processes contributing to the rapid development of extratropical cyclones. In *Extratropical Cyclones* (pp. 81-105). American Meteorological Society, Boston, MA.

Ulbrich, U., & Christoph, M. (1999). A shift of the NAO and increasing storm track activity over Europe due to anthropogenic greenhouse gas forcing. *Climate Dynamics*, 15(7), 551-559.

United Kingdom Meteorological Office. (1964). The Northern Seas, Part I. Weather in Home Fleet Waters, 1.

Valeur, H. H. (1996). Weather, sea and ice conditions in eastern Baffin Bay, offshore Northwest Greenland. A review. Danish Meteorological Institute.

Van den Dool, H., & Cpc, P. S. (2007). Empirical methods in short-term climate prediction. Oxford University Press.

Van Loon, H., & Rogers, J. C. (1978). The seesaw in winter temperatures between Greenland and northern Europe. Part I: General description. *Monthly Weather Review*, 106(3), 296-310.

Vihma, T., Tisler, P., & Uotila, P. (2012). Atmospheric forcing on the drift of Arctic sea ice in 1989–2009. *Geophysical Research Letters*, 39(2).

Wagner, A. J. (1979). Weather and circulation of January 1979: widespread record cold with heavy snowfall in the Midwest. *Monthly Weather Review*, 107(4), 499-506.

Walker, G. T. (1923). Correlation in seasonal variation of weather. VIII: A preliminary study of world weather. *Memoirs of the Indian Meteorological Department*, 24, 75-131.

Walker, G. T. Y EW Bliss, 1932. World Weather V, Men. *Royal Meteorological Society*, 4, 53-84.

Wallace, J. M., & Gutzler, D. S. (1981). Teleconnections in the geopotential height field during the Northern Hemisphere winter. *Monthly Weather Review*, 109(4), 784-812.

Walsh, J. E., & Chapman, W. L. (1990). Short-term climatic variability of the Arctic. *Journal of Climate*, 3(2), 237-250.

Wang, J., Mysak, L. A., & Ingram, R. G. (1994). Interannual variability of sea-ice cover in Hudson Bay, Baffin Bay and the Labrador Sea. *Atmosphere-Ocean*, 32(2), 421-447.

Wang, C. C., & Rogers, J. C. (2001). A composite study of explosive cyclogenesis in different sectors of the North Atlantic. Part I: Cyclone structure and evolution. *Monthly Weather Review*, 129(6), 1481-1499.

Wang, N., & Zhang, Y. (2015). Evolution of Eurasian teleconnection pattern and its relationship to climate anomalies in China. *Climate Dynamics*, 44(3-4), 1017-1028.

Wang, X. L., Wan, H., & Swail, V. R. (2006). Observed changes in cyclone activity in Canada and their relationships to major circulation regimes. *Journal of Climate*, 19(6), 896-915.

Watanabe, M., & Nitta, T. (1999). Decadal changes in the atmospheric circulation and associated surface climate variations in the Northern Hemisphere winter. *Journal of Climate*, 12(2), 494-510.

Warren, B. A. (1983). Why is no deep water formed in the North Pacific?. *Journal of Marine Research*, 41(2), 327-347.

Wei, L., Qin, T., & Li, C. (2017). Seasonal and inter-annual variations of Arctic cyclones and their linkage with Arctic sea ice and atmospheric teleconnections. *Acta Oceanologica Sinica*, 36(10), 1-7.

White, D., Hinzman, L., Alessa, L., Cassano, J., Chambers, M., Falkner, K., ... & Huntington, H. (2007). The arctic freshwater system: Changes and impacts. *Journal of Geophysical Research: Biogeosciences*, 112(G4).

Whitaker, J. S., & Davis, C. A. (1994). Cyclogenesis in a saturated environment. *Journal of the Atmospheric Sciences*, 51(6), 889-908.

Whittaker, L. M., & Horn, L. H. (1982). Atlas of Northern Hemisphere extratropical cyclone activity, 1958-1977.

Willmott, A. J., Maqueda, M. M., & Darby, M. S. (1997). A model for the influence of wind and oceanic currents on the size of a steady-state latent heat coastal polynya. *Journal of Physical Oceanography*, 27(10), 2256-2275.

Wilson, K. J., Barber, D. G., & King, D. J. (2001). Validation and production of RADARSAT-1 derived ice-motion maps in the North Water (NOW) polynya, January-December 1998. *Atmosphere-Ocean*, 39(3), 257-278.

Woodgate, R. A., & Aagaard, K. (2005). Revising the Bering Strait freshwater flux into the Arctic Ocean. *Geophysical Research Letters*, 32(2).

Yanase, W., & Niino, H. (2005). Effects of baroclinicity on the cloud pattern and structure of polar lows: A high-resolution numerical experiment. *Geophysical Research Letters*, 32(2).

Yanase, W., & Niino, H. (2007). Dependence of polar low development on baroclinicity and physical processes: An idealized high-resolution numerical experiment. *Journal of the Atmospheric Sciences*, 64(9), 3044-3067.

Yang, J., Comiso, J., Walsh, D., Krishfield, R., & Honjo, S. (2004). Storm-driven mixing and potential impact on the Arctic Ocean. *Journal of Geophysical Research: Oceans*, 109(C4).

Yu, L., Zhong, S., Winkler, J. A., Zhou, M., Lenschow, D. H., Li, B., ... & Yang, Q. (2017). Possible connections of the opposite trends in Arctic and Antarctic sea-ice cover. *Scientific Reports*, 7, 45804.

Zehnder, J. A., & Keyser, D. (1991). The influence of interior gradients of potential vorticity on rapid cyclogenesis. *Tellus A*, 43(3), 198-212.

Zhang, Y., Wallace, J. M., & Battisti, D. S. (1997). ENSO-like interdecadal variability: 1900–93. *Journal of Climate*, 10(5), 1004-1020.

Zhang, T., Hoerling, M. P., Perlwitz, J., & Xu, T. (2016). Forced atmospheric teleconnections during 1979–2014. *Journal of Climate*, 29(7), 2333-2357.

Zhang, S., Fu, G., Lu, C., & Liu, J. (2017). Characteristics of explosive cyclones over the Northern Pacific. *Journal of Applied Meteorology and Climatology*, 56(12), 3187-3210.

Zishka, K. M., & Smith, P. J. (1980). The climatology of cyclones and anticyclones over North America and surrounding ocean environs for January and July, 1950–77. *Monthly Weather Review*, 108(4), 387-401.

Zveryaev, I. I. (2006). Seasonally varying modes in long-term variability of European precipitation during the 20th century. *Journal of Geophysical Research: Atmospheres*, 111(D21).

Zweng, M. M., & Münchow, A. (2006). Warming and freshening of Baffin Bay, 1916–2003. *Journal of Geophysical Research: Oceans*, 111(C7).

APPENDIX A

INDIVIDUAL MONTHLY CYCLONE FREQUENCY HISTOGRAMS

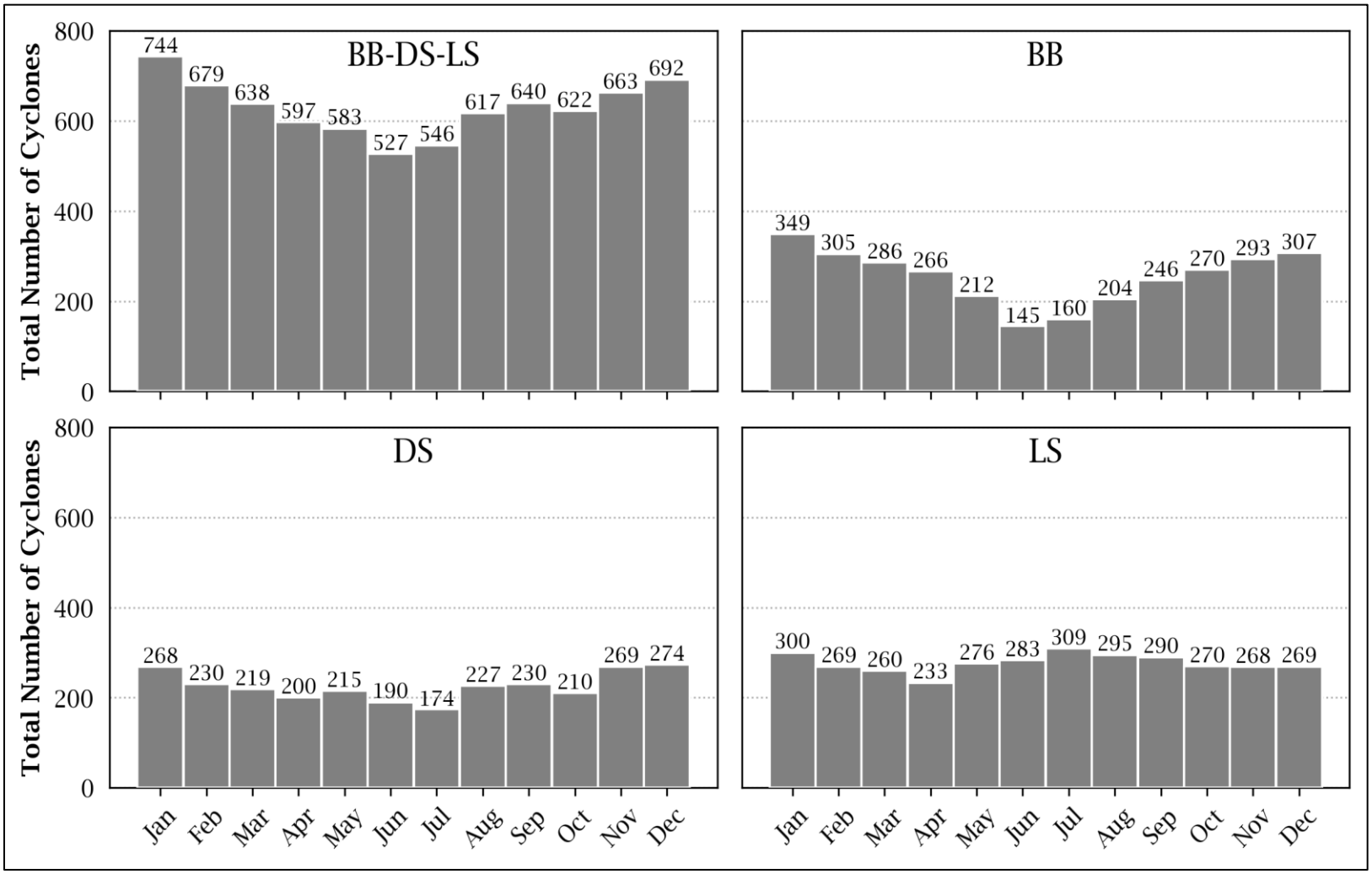

Figure A1: Total number of cyclones in each subregion summed from 1980-2015 for each individual month.